UNIVERSITÀ DEGLI STUDI FIRENZE

DOTTORATO DI RICERCA
INTERNATIONAL DOCTORATE IN STRUCTURAL BIOLOGY

CICLO XXX

COORDINATORE Prof. Claudio Luchinat

Development of novel sample preparation strategies for in-cell NMR

Settore Scientifico Disciplinare CHIM/03

Dottorando
Dott. *Eleonora Mercatelli*

Tutore
Prof. *Lucia Banci*

Coordinatore
Prof. *Claudio Luchinat*

Novembre 2014 - 2017

This thesis has been approved by the University of Florence, the University of Frankfurt and the Utrecht University

Universiteit Utrecht

CERM Firenze

FRANKFURT AM MAIN

Ai miei cari

TABLE OF CONTENTS

φύσις κρύπτεσθαι φιλεῖ

Eraclito

1. INTRODUCTION

1.1. In-cell NMR

Structural Biology is a field of Life Sciences that determines and analyzes structural information of biological macromolecules at atomic level, in particular throughout techniques such as X-ray crystallography and nuclear magnetic resonance (NMR). Despite the fact that the majority of protein structures come from X-ray crystallography data, NMR is the technique of choice when it comes to study protein-protein interactions, folding, affinity constants, kinetics and thermodynamics in solution. The structural characterization is the first step to get towards functional information, relation and interaction with partners, physiological responses to environment changes or site-specific mutations. Most – if not all – intracellular proteins exert their function by interacting with specific partners.

To date, the structural characterization of such interactions is mostly carried out with isolated proteins *in vitro.* Nowadays the interest of characterizing macromolecular functions inside the complex cellular environment is rising. To achieve this ambitious purpose, high resolution imaging and high-resolution structural tools are required. In the last fifteen years, in-cell NMR spectroscopy has been established as a method to investigate biological macromolecules in their physiological environment (Figure 1). In-cell NMR allows us to study several physiological processes such as protein folding [1], interactions with other proteins [2], metal ions binding [3], and drug screening [4]. The information obtained has a high biological significance, as the proteins are closer to their physiological conditions in terms of components present in the cell and of other

aspects such as pH, redox potential and macromolecular crowding.

A first series of successful in-cell NMR applications relied initially on living *E. coli* cells to study macromolecular crowding, protein structure and folding, and interaction with other molecules such as proteins, drugs, nucleic acids, or other cellular components [5, 6]. More recently, the technique has been further extended to the investigation of eukaryotic proteins in eukaryotic cells, which could provide higher biological significance when studying structure and function [7]. Several methods rely on recombinant protein production in *E. coli*, followed by protein insertion inside eukaryotic cells. Different insertion techniques were developed such as microinjection [8] in oocytes, fusion with a cell-penetrating peptides [9], the use of pore-forming toxins [10] and protein electroporation [11, 12] in cultured cells. A conceptually different approach relies on transient protein expression directly in mammalian cells [13]. This approach is especially suited for monitoring protein folding and maturation events occurring right after protein synthesis [14] and to co-translationally deliver proteins to specific organelles, allowing *in organello* NMR approaches [15].

Furthermore, recent works showed that a protein structure (GB1 domain)

Figure 1. Overview of the existing sample preparation approaches for in-cell NMR. A) isotopically labeled proteins can be expressed (*green*) in bacterial cells, yeast cells, insect and mammalian cells by introducing an expression vector(s) encoding the protein(s) of interest; Isotopically enriched nutrients are provided after induction/transfection. *B)* purified labeled proteins (*blue*) can be delivered in *X. laevis* oocytes by microinjection or in human cells by CPP-mediated, or by permeabilizing the cells either with pore-forming toxins or via electroporation [6].

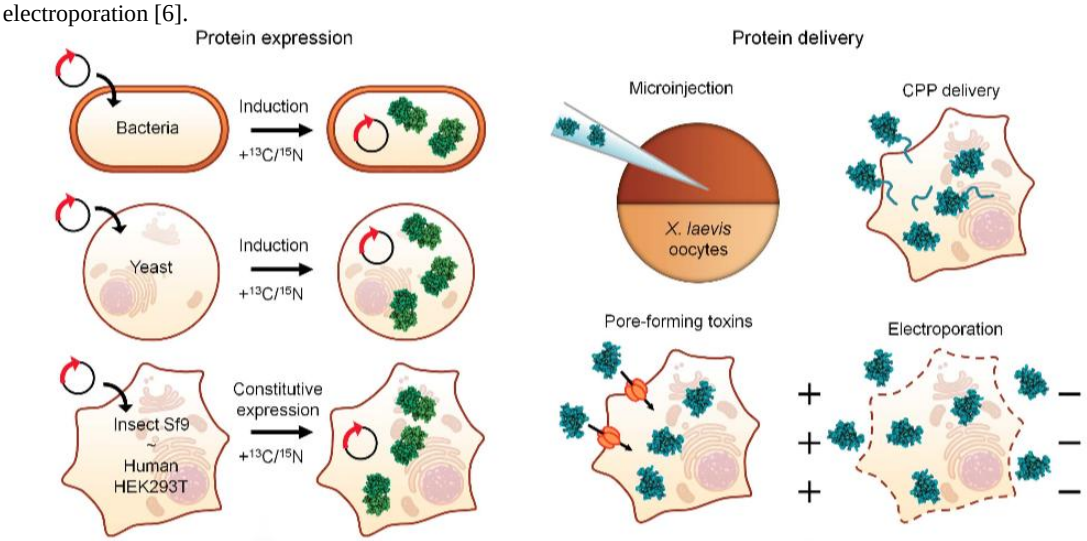

could be resolved inside eukaryotic cells by in-cell NMR thanks to the introduction of a paramagnetic lanthanide-binding tag, which allowed measuring paramagnetic-based structural constraints, protein backbone PCSs and RDCs, in *Xenopus laevis* oocytes [16, 17].

In this PhD research work, I addressed a number of aspects both at methodological and at application level. We successfully applied solution in-cell NMR to investigate the redox-state of soluble disulfide-containing proteins inside different living systems (bacterial and human cells). We determined the protein redox-state distribution when cofactors or redox partners are supplied. We showed how in-cell NMR is a promising sensitive and direct technique for investigating protein redox distributions inside cells, exploitable also in addition or as a valuable alternative to GSH-fluorescence probes and chemical essays on cell extracts.

Furthermore, we showed how in-cell NMR can shed light on the effects of potential drugs on a target protein within the cellular context. Such strategy will be beneficial for evaluating candidate drugs for treating neurodegenerative diseases, such as amyotrophic lateral sclerosis.

When investigating proteins in the cellular context, many challenges arise, as a consequence of its intrinsic complexity. In particular, to increase the opportunities of in-cell NMR applications, practical limitations need to be overcome: on one hand sample preparation issues must be addressed to ensure that the physiological conditions of macromolecules inside the living cells are maintained during the measurements (cell viability and stability over time, proper amount of oxygen and nutrients, Temperature, pH); on the other hand, although there have been considerable advances in the sensitivity of the NMR technique throughout consistent hardware improvements, the short sample lifetime still

imposes limits on the type and length of the NMR experiments that can be recorded.

To widen the range of in-cell NMR applications and to overcome some of the practical limitations from a sample preparation perspective, our primary focus has been to enable the detection of intracellular soluble proteins that are not detectable with canonical solution NMR experiments. Within the cells, complex phenomena such as intermolecular interactions take place that might affect the relaxation properties of proteins. In particular, specific and nonspecific interactions with other cellular components can increase the rotational correlation time and cause line broadening beyond detection. Such protein-specific effects are therefore a limiting factor for in-cell NMR in solution. Cellular solid-state NMR in principle has the chance to overcome such limitations allowing the characterization of proteins involved in molecular complexes in the cellular environment [18].

In parallel, we sought to expand the existing solution in-cell NMR methods to study protein-protein interactions with atomic detail in living cells. To this aim, our strategy relied on the combination of DNA transfection with protein delivery techniques in order to maximize protein labeling selectivity inside the cells and minimizing cellular background signals in the NMR spectra. Among the various protein mediated delivery techniques suitable for in cell NMR sample preparation, we focused on protein electroporation, which has several advantages: it does not require specific protein modifying targeting sequences (such as cell-penetrating peptides) and it does not imply any cell treatment with toxic and harmful compounds (such as pore-forming toxins).

1.2. Cellular redox systems and oxidative stress

Sulfur is among the six most abundant elements in Life. Indeed it is present in

many cellular components, such as small metabolites and proteins. Thanks to its chemical reactivity, sulfur is strongly involved in the redox biochemistry of living organisms. In proteins, methionine and cysteine are the only amino acid that can undergo reversible oxidation in a biological environment. In particular, the thiol group (-SH) of cysteine is the main character of many oxidative reactions and modifications that are involved in gene regulation, signalling and protein function [19,20]. A change in the redox state of thiol/disulfide couples affect protein conformation [21], transporter activity, enzymatic activity, ligand binding [22], protein-protein interactions, protein trafficking, protein-DNA interactions [23], and protein degradation.

In order to maintain physiological conditions, redox homeostasis plays a key role, from bioenergetics to functional processes and metabolism, and it is controlled by sophisticated oxidation-reduction processes. Like most biological processes, intracellular redox reactions do not reach the thermodynamic equilibrium but are kept in non-equilibrium steady states [24]. Whenever in a cell there is an imbalance between redox systems operating concurrently, deviations from physiological conditions arise, which are often linked to the insurgence of pathologies. In particular, oxidative stress has been linked to a high intracellular levels of aerobic metabolism products that cause damage. A wide definition of oxidative stress is “an imbalance between oxidants and antioxidants in a cell, in favor of the oxidants” [25]. A large number of oxidants is represented by reactive oxygen species (ROS), which cover a variety of radicals derived from oxygen such as the superoxide anion O_2^{-2}, hydroxyl ($HO^{\bullet}$), peroxyl ($RO_2^{\bullet}$) and alkoxyl radicals ($RO^{\bullet}$), as well as non radical species such as hydrogen peroxide (H_2O_2). In addition to ROS, reactive nitrogen species (RNS), reactive sulfur species (RSS) and reactive carbonyl species (RCS) also have notable effects on redox biology

and oxidative stress [26, 27].

Despite the large amount of knowledge, the current understanding of the mechanisms of ROS-induced toxicity is still incomplete. There are studies showing that some ROS can act as signaling molecules promoting physiological functions, high level of ROS show evidences of promoting irreversible oxidative changes of DNA, lipid and proteins, promote protein disfunction, trigger cell death [28], regulate signaling pathways [29], and are involved in tumor progression [30].

As a defense against ROS, cells have developed several antioxidant systems [31, 32]. Eukaryotic cells have several ways to protect themselves from oxidative damage: the glutathione system, superoxide dismutase, the thioredoxin/peroxiredoxin system and catalase.

Oxidative stress has also been associated with the onset of long-term neurodegenerative diseases such as Alzheimer disease, Parkinson disease and multiple sclerosis. Among them, Amyotrophic Lateral Sclerosis (ALS) is a fatal degenerative disease that cause the death of motor neurons [REF 33]. Several variants of ALS are known, which have been associated to different genes. Despite the large amount of knowledge, the pathogenesis of ALS is not yet fully understood. A subset of ALS cases, both sporadic and familial, are linked to the antioxidant enzyme superoxide dismutase 1 (SOD1) The hallmark of SOD-linked ALS is a toxic gain-of-function, which causes the misfolding and aggregation of SOD1 within motor neurons. Indeed, several mutations of the SOD1 gene have been identified in familial-ALS patients, which impair SOD1 folding and/or maturation and ultimately lead to its aggregation.

1.2.1. The glutathione system

The tripeptide glutathione (GSH, reduced form, and GSSG, oxidized form) is the

most abundant thiol-containing molecule inside cells. It has indeed a crucial role in redox homeostasis and in maintaining the proper intracellular redox environment for optimal cellular protein functions. Both GSH and proteins exert their thiol redox reactivity throughout the amino acid cysteine, that can undergo reversible thiol oxidation forming a disulfide bond. GSH is one of the molecules that mitigates the effects of ROS by reacting with disulfide bonds of cytoplasmic proteins, reducing them to cysteines and producing glutathione disulfide (GSSG). However, such process does not occur spontaneously and need enzymatic regulation [34]. The glutathione system includes GSH, glutathione reductase, glutathione peroxidases (GPX) and glutathione S-transferases (GST). Glutathione peroxidases (GPX) catalyze the decomposition of hydrogen peroxide and organic hydroperoxides. Glutathione reductase reduces GSSG and restores the GSH pool. Glutathione S-transferases are detoxification enzymes that catalyze the conjugation of GSH to a variety of exogenous and endogenous electrophilic compounds [35].

GSH is present in all cellular compartments, including the cytosol, the mitochondria, the nucleus and the endoplasmic reticulum, and acts as a distinct redox pool in each. Due to its high abundance, the redox couple GSH/GSSG is considered to be the primary cellular redox buffer, hence its redox potential is often used as an indicator for the redox environment of the cell [36].

The intracellular environment is generally reducing with respect to the extracellular environment. However, inside a cell the redox status is compartment-dependent: the endoplasmic reticulum (ER), the Golgi apparatus and the mitochondrial intermembrane space (IMS) have a less reducing environment compared to the one found in the cytoplasm and the nucleus [37]. Typically, this difference in the redox pool is reflected by the higher abundance of disulfide

bonds found in proteins of the ER/Golgi and of the IMS, compared to cytosolic proteins.

1.2.2. The thioredoxin system

In cells there are two main pathways in charge of keeping the protein thiols reduced: the thioredoxin-thioredoxin reductase pathway and the glutaredoxin-glutathione reductase one, which are both linked to NADPH as electron donor.
Thioredoxins are ubiquitous enzymes in all living organisms, which exert a central role in many physiological functions such as thiol-based redox system catalysis [38], iron-sulfur proteins biogenesis [39], redox sensing and redox environment maintenance and antioxidant activity [40].

Thioredoxins (Trx) are small proteins that share a common folding, the so called 'thioredoxin fold' constituted by a barrel core of five β-strands surrounded by four α-helices; their active site contains a highly conserved cysteines pattern, usually a CXXC motif, that is cycled between an active (reduced) dithiol form and an oxidized disulfide form [41]. In its active state, thioredoxin scavenges reactive oxygen species and keeps proteins in their reduced state [42].

Like GSH in mammalian cells, members of the thioredoxin family are compartmentalized: inside the cytosol there are thioredoxin 1 (Trx1) and glutaredoxin 1 (Grx1), that interact with copious cytosolic substrates and catalyze protein dithiol/disulfide exchange reactions. The mechanism through which Trx1 interacts with its substrates consists in the reduction of the protein-protein disulfide bond throughout a dithiol reaction ending up in a intramolecular disulfide bond formation between the two thiols of the active site. Thioredoxin reductase restores reduced Trx1 through reducing equivalents provided by NADPH [43]. Grx1 instead has a highly specificity for glutathione and has a stronger tendency to reduce glutathionylated proteins. The mechanism of

reduction relies on a thiol-disulfide exchange mechanism resulting in the formation of glutathionylated Grx1 intermediate, regenerated to reduced Grx1 by GSH forming GSSG. In turn, glutathione reductase catalyzes GSSG reduction to 2 GSH through NADPH.

Among the various partners, Grx1 and Trx1 play a key role in keeping reduced some mitochondrial CHCH proteins while they are synthesized inside the cytoplasm so that they can translocate inside the intermembrane mitochondrial space [44, 45].

1.2.3. Superoxide dismutase

Superoxide dismutases (SODs) are metalloenzymes which catalyze the disproportionation of superoxide anion to oxygen and hydrogen peroxide:

$$(2\ O_2^{-2} + 2\ H^{+} \rightarrow O_2 + H_2O_2)$$

Superoxide dismutases ubiquitously exist in eukaryotes and prokaryotes. Different SOD enzymes exist, located in different cellular compartments, and rely on metal ions such as copper (Cu^{2+}), manganese (Mn^{2+}) or iron (Fe^{2+}) as cofactors. Copper-zinc superoxide dismutase 1 (SOD1) is a 32 kDa homo-dimer where each monomer is a folded greek-key β-barrel. SOD1 is ubiquitously expressed in all eukaryotic cells, and it is present at high concentration inside the cytoplasm, as well as inside the mitochondrial intermembrane space (IMS). It also translocates into the nucleus as a response to oxidative stress [46]. To reach the functional form and exert the catalytic activity, SOD1 needs to undergo a series of maturation events: dimerization, zinc and copper binding, and the formation of an intramolecular disulfide bond. In the case of human SOD1, two activation pathways have been identified to date: one requiring the copper chaperone for SOD1 (CCS) to bring copper and activate SOD1 through oxidation and one that works independently from CCS. The SOD1 maturation pathway has been

recapitulated in cultured human cells with atomic resolution by in-cell NMR [47]. In human cells, zinc binding occurs spontaneously, while copper-binding and disulfide formation occur when CCS is co-expressed together with SOD1, suggesting that increased levels of CCS are required to efficiently deliver copper to SOD1 when the latter is overexpressed, and for disulfide-bond formation [48]. CCS could promote disulfide formation even in the absence of copper, suggesting an alternative copper-independent mechanism for the oxidation of SOD1 cysteines [45].

Mutations in the hSOD1 gene have been associated to a familial form of Amyotrophic Lateral Sclerosis (fALS), a progressive debilitating neurodegenerative disease consisting in a selective progressive loss of motor neurons (primary motor cortex, brain stem and spinal), causing a progressive muscle atrophy, spasticity, paralysis and ultimately death. To date, more than 150 familial fALS-linked sequence mutations have been reported [49]. Most of these mutations do not affect SOD1 enzymatic function. Instead, the pathogenic activity of SOD1 mutants stems from a gain of toxic function, which is correlated to the formation of aberrant SOD1 oligomers or fibrillar aggregates. Still, the exact mechanism of SOD1-linked fALS pathogenesis remains unclear [50, 51, 52]. Notably, these mutations have been shown not to be strictly necessary for triggering toxic aggregation of SOD1 [53]. Indeed, wild-type SOD1 has been shown to have a similar toxic gain of function due to a fibrillation behavior analogous to SOD1 mutants [54]. In particular, it has been shown that the metal-binding deficiency and the reduced disulfide bond promote structural instability and protein aggregation, also for wild-type SOD1 [55, 56, 57]. Therefore, understanding which factors negatively affect the SOD1 maturation pathway within a cell is critical to develop novel fALS therapeutic strategies.

2. RESULTS

2.1. Direct structural evidence of protein redox regulation obtained by in-cell NMR

In-cell NMR analysis was applied to study the folding and to the redox state of three human proteins in the cytoplasm of human and bacterial cells. These are two small proteins of the mitochondrial IMS, human Cox17 and Mia40, which are encoded by nuclear DNA and therefore are present in the cytoplasm before they enter mitochondria. The redox state of human SOD1 was also investigated. Through in-cell NMR we can probe directly the structural properties of the proteins in different redox states in each cellular environments. Thanks to these structural information, we could determine the distribution of proteins redox states, which was then compared to the one predicted from the midpoint reduction potential, assuming the thermodynamic equilibrium with GSH. In human cells, the distributions were not at the equilibrium, while co-expression of redox-regulating protein partners of Cox17 and Mia40 (Grx1 and Trx1) shifted their distributions closer to the equilibrium. In bacterial cells (BL21) the proteins were mostly reduced, despite the less reducing cellular environment, while in the absence of the disulfide reduction pathways (in Origami B cells) the oxidized state of each protein was observed despite the predicted $E^{o'}$. These results show that in-cell NMR is a suitable method to directly observe the redox state of a soluble disulfide-containing protein. They also showed that the oxidation state of some proteins is controlled by specific proteins and pathways, which are not directly linked to the GSH pool, as is the case for the SOD1-CCS pathway.

Biochimica et Biophysica Acta (Published, 2016)

Direct structural evidence of protein redox regulation obtained by in-cell NMR

Eleonora Mercatelli[1], Letizia Barbieri[1,2], Enrico Luchinat[1,3], Lucia Banci[1,2]

Affiliations

1. Magnetic Resonance Centre (CERM), University of Florence, 50019 Sesto Fiorentino, Italy.
2. Department of Chemistry, University of Florence, 50019 Sesto Fiorentino, Florence, Italy.
3. Department of Biomedical, Clinical and Experimental Sciences, University of Florence, 50134 Florence, Italy.

Biochimica et Biophysica Acta 1863 (2016) 198–204

Contents lists available at ScienceDirect

Biochimica et Biophysica Acta

journal homepage: www.elsevier.com/locate/bbamcr

Direct structural evidence of protein redox regulation obtained by in-cell NMR

Eleonora Mercatelli [a], Letizia Barbieri [a,b], Enrico Luchinat [a,c], Lucia Banci [a,b,*]

[a] Magnetic Resonance Center — CERM, University of Florence, Via Luigi Sacconi 6, 50019 Sesto Fiorentino, Florence, Italy
[b] Department of Chemistry, University of Florence, Via della Lastruccia 3, 50019 Sesto Fiorentino, Florence, Italy
[c] Department of Biomedical, Clinical and Experimental Sciences, University of Florence, Viale Morgagni 50, 50134 Florence, Italy

ARTICLE INFO

Article history:
Received 7 October 2015
Received in revised form 4 November 2015
Accepted 7 November 2015
Available online 14 November 2015

Keywords:
In-cell NMR
Glutathione
Redox regulation
Nuclear magnetic resonance
Disulfide bond

ABSTRACT

The redox properties of cellular environments are critical to many functional processes, and are strictly controlled in all living organisms. The glutathione-glutathione disulfide (GSH-GSSG) couple is the most abundant intracellular redox couple. A GSH redox potential can be calculated for each cellular compartment, which reflects the redox properties of that environment. This redox potential is often used to predict the redox state of a disulfide-containing protein, based on thermodynamic considerations. However, thiol-disulfide exchange reactions are often catalyzed by specific partners, and the distribution of the redox states of a protein may not correspond to the thermodynamic equilibrium with the GSH pool. Ideally, the protein redox state should be measured directly, bypassing the need to extrapolate from the GSH. Here, by in-cell NMR, we directly observe the redox state of three human proteins, Cox17, Mia40 and SOD1, in the cytoplasm of human and bacterial cells. We compare the observed distributions of redox states with those predicted by the GSH redox potential, and our results partially agree with the predictions. Discrepancies likely arise from the fact that the redox state of SOD1 is controlled by a specific partner, its copper chaperone (CCS), in a pathway which is not linked to the GSH redox potential. In principle, in-cell NMR allows determining whether redox proteins are at the equilibrium with GSH, or they are kinetically regulated. Such approach does not need assumptions on the redox potential of the environment, and provides a way to characterize each redox-regulating pathway separately.

1. Introduction

Living systems have developed a strict control of the redox cellular environment. In most prokaryotes and all eukaryotes, the most abundant redox couple in the cell is the glutathione–glutathione disulfide (GSH–GSSG) couple [1,2]. The redox potential of the glutathione pool (E'_{GSH}) in a given cellular compartment, which is dependent on the $[GSH]^2/[GSSG]$ ratio, is therefore a critical parameter to understand the redox properties of the environment [1,3]. Consequently, numerous methods have been developed to quantitatively measure the absolute and relative concentrations of both GSH and GSSG, either by chemical assays on cell extracts [4,5] or, more recently, by using GSH-sensitive intracellular fluorescent probes [6–8]. These methods have contributed much to understand how the intracellular E'_{GSH} is influenced under physiological and oxidative stress conditions, and have shown that some cellular compartments have a less reducing environment with respect to the cytoplasm, such as the endoplasmic reticulum (ER) and the mitochondrial intermembrane space (IMS) [3,5,9,10]. In principle, from the E'_{GSH} of the various cellular compartments, the redox state of disulfide-containing proteins can be predicted, provided that the midpoint reduction potential ($E^{\circ\prime}$) of each protein is known, and such capability has allowed a deeper understanding of the many redox-dependent mechanisms of protein maturation, such as the PDI-mediated folding in the ER and the disulfide-relay system of the mitochondrial IMS [3,11–13].

Despite these remarkable examples, sometimes glutathione alone is not sufficient to understand intracellular redox processes. In order for the difference (ΔE) between $E^{\circ\prime}$ of a protein and E'_{GSH} to act as a driving force for thiol-disulfide redox reactions, allowing the system to move towards the thermodynamic equilibrium (given by the Nernst equation), there needs to be a direct reaction between the protein and GSH/GSSG. In biological systems, this is usually not the case, as thiol-disulfide reactions would occur on timescales many orders of magnitude slower, if they were not catalyzed by specific enzymes [14,15]. Consequently, the actual protein redox states cannot always be inferred from E'_{GSH}, as they also depend on the kinetics of the catalyzed reactions. In fact, it has been even suggested that under some circumstances the redox properties of an intracellular environment may not depend on E'_{GSH} at all [14,16]. Moreover, the measure of E'_{GSH} itself poses some challenges, as the result can vary considerably depending on which method is used [17,18].

Ideally, when studying redox-regulated pathways, the redox state of the proteins involved should be monitored directly inside the cells, thus

* Corresponding author at: Magnetic Resonance Center — CERM, University of Florence, Via Luigi Sacconi 6, 50019 Sesto Fiorentino, Florence, Italy.
E-mail address: banci@cerm.unifi.it (L. Banci).

http://dx.doi.org/10.1016/j.bbamcr.2015.11.009
0167-4889/

bypassing all the assumptions required by the use of E'_{GSH}. For this purpose, Nuclear Magnetic Resonance applied to observe proteins in living cells (in-cell NMR) is a promising approach. In-cell NMR has been successfully applied to obtain atomic-level information on protein structure, dynamics and interactions in both bacterial and eukaryotic cells [19–22]. In particular, in-cell NMR can be applied to monitor protein maturation pathways involving the formation of one or more disulfide bonds [23–26]. NMR is extremely sensitive to changes in protein structure and dynamics, thus it easily detects the formation of disulfide bonds as they affect the protein structure and consequently the chemical shifts.

In this work, we report the direct observation of the redox state of three soluble proteins expressed in the cytoplasm of both human (HEK293T) and bacterial cells (*E. coli* BL21 and Origami B strains). By integrating the obtained data with previously reported findings, we determined the actual distributions of redox states of each protein in different cell types, and we compared them with those calculated from the reported $E^{\circ\prime}$ of the protein and cytoplasmic E'_{GSH} of each cell type. Due to the broad range of reported E'_{GSH} values, the redox state distributions predicted from the Nernst equation can change considerably. Despite this, our data is not always compatible with the range of E'_{GSH} values, suggesting that the observed proteins are not at the thermodynamic equilibrium with the environment. We also analyzed how the redox state distribution of the observed proteins changes in response of supplemented cofactors or increased levels of redox partners. In principle, with a more accurate estimate of E'_{GSH} in our experimental conditions, this method could be used to determine how far the steady-state distribution of redox sates of a protein is from the equilibrium with the E'_{GSH} of the environment in each cell type.

2. Materials and methods

2.1. Gene cloning

cDNA encoding full-length human Cox17 (amino acids 1–63, GenBank: NP_005685) was amplified by PCR and cloned into the pHLsec [27] vector between EcoRI and XhoI restriction enzyme sites to generate the mammalian expression plasmid and into the pET16b plasmid between NdeI and XhoI restriction enzyme sites to generate the bacterial expression plasmid. cDNA encoding full-length human Mia40 (amino acids 1–142, GenBank: NP_001091972.1) was amplified by PCR and cloned into the pET21a between NdeI and XhoI restriction enzyme sites to generate the bacterial expression plasmid. All clones were verified by DNA sequencing. SOD1 in pET28a, pET21a and pHLsec, and Mia40, Grx1 and Trx1 in pHLsec were cloned as previously reported [23–25].

2.2. Human cell culture and transfection

HEK293T cells were maintained in DMEM (high glucose, D6546, Sigma) supplemented with L-glutamine, antibiotics (penicillin and streptomycin) and 10% FBS (Gibco) in uncoated 75 cm^2 plastic flasks and incubated at 37 °C, 5% CO_2 in a humidified atmosphere.

HEK293T cells were transiently transfected with the pHLsec plasmid containing the gene of interest using polyethylenimine (PEI), as previously described [24]. Different DNA:PEI ratios were tested for maximizing protein expression (PEI was kept constant at 50 μg/flask), and an optimal ratio of 1:1 was used (50 μg/flask DNA, 50 μg/flask PEI). For co-expression of Cox17 and Grx1 or Cox17 and Trx1, cells were transfected with plasmids containing the constructs in different amounts and ratios. The ratios were chosen in order to obtain similar expression levels of Cox17, specifically 1.9:0.1:2 was used for Cox17:Grx1:PEI and 1.5:0.5:2 for Cox17:Trx1:PEI. To ensure complete activation of Trx1, sodium selenite was supplemented to the cell culture media to a final concentration of 100 nM, starting 24 h before transfection.

During protein expression, commercial DMEM medium was used to prepare unlabeled in-cell NMR samples; BioExpress6000 medium (CIL) was used for U–^{15}N labeling; for selective [^{15}N]cysteine labeling a reconstituted medium was prepared following the DMEM (Sigma) reported composition, in which [^{15}N]cysteine was added together with all the other unlabelled components. The expression media were supplemented with 2% FBS and antibiotics.

2.3. Western Blot analysis

Cox17 expression levels were determined on cell extracts by Western Blot analysis, by using a sample of purified Cox17 at increasing dilutions as a reference; Grx1 and Trx1 concentrations in the cell extracts were determined as above, by using samples of purified Grx1 and Trx1 as references. Cox17 was stained with a rabbit polyclonal anti-Cox17 antibody (Abcam: ab69611, diluted to 0.5 μg/ml); Grx1 with a rabbit polyclonal anti-glutaredoxin 1 antibody (Abcam: ab45953, 1.0 μg/ml); Trx1 with a rabbit polyclonal anti-thioredoxin/TRX antibody (Abcam: ab26320, 0.4 μg/ml). Goat anti-rabbit IgG (whole molecule)-peroxidase secondary antibody (Sigma: A0545) was used for detection, diluted at 1:80,000.

2.4. Protein expression and purification

Pure Cox17 sample was produced following a previously described protocol [28]. Briefly, the pETG-30A vector containing the hCox17 gene was transformed in *E. coli* Origami B (DE3) cells (Novagen). Cells were induced with 0.5 mM IPTG for 16 h at 25 °C. Cox17 was purified by affinity chromatography using a nickel chelating HisTrap (GE Healthcare) column. After digestion with AcTEV protease (Invitrogen) O/N at 25 °C the protein was separated from the affinity tag in a HisTrap column. The sample buffer was then exchanged with 50 mM potassium phosphate, 0.5 mM EDTA, pH = 7. Grx1 for reference in the WB analysis was produced as previously described [25]. Briefly, the pTH34 vector containing the human Grx1 gene was transformed in *E. coli* BL21(DE3) Gold competent cells. Cells were grown at 37 °C in minimal medium until O.D. 0.6 and then induced with 0.5 mM IPTG for 16 h at 25 °C. Grx1 was purified by affinity chromatography using a nickel chelating HisTrap (GE Healthcare) column. After digestion with AcTEV protease (Invitrogen) O/N at 25 °C the protein was separated from the affinity tag in a HisTrap column. The sample buffer was then exchanged with 50 mM potassium phosphate, 0.5 mM EDTA, pH = 7. Pure Trx1 for WB analysis was prepared from HEK293T cells overexpressing Trx1 as previously described [25]. Cells were lysed in 20 mM potassium phosphate buffer (pH 7) and the cleared extract was incubated at 70 °C for 4 min. After centrifugation (30 min at 16,000 g), Trx1 was purified by anionic exchange chromatography using a HiTrap™ DEAE FF (Amersham Biosciences) column applying a linear gradient of potassium phosphate buffer (10 to 100 mM, pH 7).

2.5. In-cell NMR sample preparation (human cells)

HEK293T cells for in-cell NMR samples were collected as previously reported [24]. Briefly, cells from a 75 cm^2 flask were detached by trypsin treatment and suspended in one cell pellet volume of DMEM medium supplemented with 90 mM glucose, 70 mM HEPES buffer and 20% D_2O. The cell suspension was transferred to a 3 mm Shigemi tube; cells were spun down at the bottom of the tube. Cell viability before and after NMR experiments remained above 90%, as determined by trypan blue staining. Cleared cell lysates were prepared as follows: cells were suspended in one pellet volume of PBS buffer supplemented with 0.5 mM EDTA and 4-(2-aminoethyl)-benzenesulfonyl fluoride hydrochloride (AEBSF, Sigma) and lysed by freeze-thaw cycles with liquid N_2 and warm water. The cell lysate was centrifuged (60 min at 16,000 g, 4 °C) and the cleared supernatant was recovered for NMR analysis in a 3 mm standard tube.

2.6. In-cell NMR sample preparation (bacterial cells)

U–^{15}N samples for in-cell NMR in *E. Coli* cells were prepared as follows: a cell culture of BL21 (DE3) Gold (Agilent Technologies) or Origami B (DE3) (Novagen) transformed with the plasmid containing the gene of interest was grown overnight at 30 °C in 35 mL of LB medium. After gentle centrifugation (3000 g) for 20 min, the cells were re-suspended in 50 mL of M9 minimal medium [M9 buffer (7 g/L K_2HPO_4, 3 g/L KH_2PO_4, 0.5 g/L NaCl, pH 7.4), 2 mM $MgSO_4$, 0.1 mM $CaCl_2$, 1 mg/L biotin, 1 mg/L thiamine, antibiotic] containing 1 g/L $(^{15}NH_4)_2SO_4$ and 3 g/L of unlabelled glucose to obtain an OD_{600} of ~1.6. After 10-min recovery time, overexpression was induced with 0.5 mM IPTG, and carried out at 30 °C for 4 h. The cells were washed once with 50 mL of M9 buffer in order to remove nutrients, metal ions and any excreted by-product, and they were harvested through gentle centrifugation. The pellet was then re-suspended in M9 buffer until 500 μL of a ~ 50% v./v. cell slurry were obtained. 50 μL of D_2O were added, and the final volume was put in a 5 mm NMR tube. The cleared cell lysates for NMR experiments were prepared as follows: the cell pellet was re-suspended in an equal volume of M9 buffer and lysed by ultrasonication. The cell lysate was centrifuged (40 min at 18,000 g, 4 °C), the supernatant was collected and its volume was brought to 500 μL with M9 buffer; 50 μL of D_2O were added. The sample was placed into a standard 5 mm tube for NMR analysis.

2.7. In-cell NMR experiments

NMR experiments on human cells and lysates were acquired at a 950 MHz Bruker Avance III spectrometer equipped with a CP TCI Cryo-Probe. NMR experiments on bacterial cells and lysates were acquired at a 900 MHz Bruker Avance spectrometer equipped with a TCI Cryoprobe. 1D ^{1}H and 2D ^{1}H–^{15}N SOFAST-HMQC [29] spectra were acquired at 307 K. The total acquisition time for each cell sample was ~1 h. The supernatant of each cell sample was checked in the same experimental conditions to exclude the presence of any signal arising from protein leaked out of the cells. The same NMR spectra were also acquired on the cell lysates. The NMR spectra were processed with Bruker Topspin software. The 2D NMR spectra acquired on U–^{15}N labeled human cells and lysates were further processed by subtracting a spectrum of untransfected cells/cell lysate acquired in the same experimental conditions and identically processed, to eliminate the signals arising from partial ^{15}N labeling of other cellular components.

2.8. Analysis of the redox state distribution

The ratio of oxidized vs. total protein was calculated as follows: for Cox17, the ratio was obtained by integrating crosspeaks in the 2D NMR spectra corresponding to the oxidized and the reduced species (2D NMR spectra of [^{15}N]cysteine-labeled cells were used for human cells, of U–^{15}N labeled lysates for bacteria); for Mia40 in human cells, the values previously reported were used [25]; for Mia40 in bacteria, the 2D NMR spectra of the lysates were used; for SOD1 in human cells, the ratio was obtained by integrating crosspeaks in the 2D in-cell NMR spectra corresponding to the oxidized and the reduced species (from a U–^{15}N labeled sample for E,Zn–SOD1; from a [^{15}N]cysteine-labeled sample for Cu,Zn–SOD1); for SOD1 in bacteria, 2D NMR spectra of U–^{15}N labeled cells were used. The error bars were obtained by taking the standard deviation of the spectral noise as the error of the integrals, followed by error propagation.

2.9. Redox species plots

The redox species curves for each protein as a function of the GSH redox potential were calculated from the Nernst equation applied to the reaction between the oxidized protein and 2 GSH molecules:

$$P_{ox} + 2GSH \rightleftharpoons P_{red} + GSSG \tag{1}$$

where P_{ox} and P_{red} indicate the protein in the oxidized and reduced state, respectively. The corresponding Nernst equation at the equilibrium is:

$$0 = E^{\circ\prime}{}_P - E^{\circ\prime}{}_{GSH} - \frac{RT}{zF}\ln\frac{[GSSG][P_{red}]}{[GSH]^2[P_{ox}]} \tag{2}$$

where $E^{\circ\prime}{}_P$ is the protein midpoint potential at pH = 7; $E^{\circ\prime}{}_{GSH}$ is the reduction potential of GSH at pH = 7; R = 8.314 J K^{-1} mol^{-1}; T = 310 K; z = 2; F = 96,485 C mol^{-1}. The GSH reduction potential (E'_{GSH}) in each cellular environment is given by:

$$E'_{GSH} = E^{\circ\prime}{}_{GSH} - \frac{RT}{zF}\ln\frac{[GSH]^2}{[GSSG]}. \tag{3}$$

Combining Eq. (3) with Eq. (2) gives:

$$0 = E^{\circ\prime}{}_P - E'_{GSH} - \frac{RT}{zF}\ln\frac{[P_{red}]}{[P_{ox}]}. \tag{4}$$

Which is rearranged to give the fraction of oxidized protein (ox. fraction) as a function of E'_{GSH}:

$$ox.fraction = \frac{[P_{ox}]}{[P_{ox}]+[P_{red}]} = \frac{1}{1+e^{-\frac{RT}{zF}(E'_{GSH}-E^{\circ\prime}{}_P)}}. \tag{5}$$

The oxidized fraction vs. E'_{GSH} plots were obtained using the reported midpoint potentials for each protein (corrected for pH = 7.0): $E^{\circ\prime}{}_{Cox17} = -305$ mV [30]; $E^{\circ\prime}{}_{Mia40} \leq E^{\circ\prime}{}_{Cox17}$ [31]; $E^{\circ\prime}{}_{E,Zn-SOD1} = -320$ mV [32]; $E^{\circ\prime}{}_{Cu,Zn-SOD1} = -305$ mV [32,33]. In the case of Cox17 and Mia40 two disulfide bonds are formed, requiring the oxidation of four GSH molecules. However, the redox curve of Cox17 had been previously determined experimentally in vitro, and had been fitted with parameters compatible with the oxidation of two GSH molecules (i.e. the formation of one disulfide bond, see Eq. (1)) [30]. Therefore, Eq. (5) was also used to calculate the redox curves of Cox17 and Mia40.

3. Results

3.1. Mitochondrial CHCH proteins

We analyzed the folding and redox state of two small proteins of the mitochondrial IMS, human Cox17 and Mia40, in the cytoplasm of human and bacterial cells [28,31]. Like most mitochondrial proteins, Cox17 and Mia40 are synthesized in the cytoplasm, and have to translocate to the mitochondria [13,34]. Both proteins are constituted by a coiled-coil helix coiled-coil helix (CHCH) domain, consisting of two alpha helices stabilized through two structural disulfide bonds [35]. In order to reach the IMS, these small CHCH proteins can only cross the outer mitochondrial membrane in an unfolded state, therefore with the four cysteines of the CHCH motif reduced. ^{15}N-labeled Cox17 and Mia40 were overexpressed in the cytoplasm of human cells (E'_{GSH} ranging from −300 mV to −320 mV [36–39]), and the backbone amide signals of the folded CHCH domain were detected for both proteins (Fig. 1A,B), with their chemical shifts matching those of the in vitro NMR spectra of the folded, oxidized proteins [28,31]. This observation is further confirmed by the in-cell NMR spectra of [^{15}N]cysteine-labeled proteins (Fig. 1C,D). The ratio of folded Cox17 over total Cox17 was determined from the intensities of cysteine crosspeaks corresponding to the oxidized and reduced protein (Fig. 1D–F), while the ratio of folded Mia40 over total Mia40 was determined from the intensities of a set of crosspeaks in the in-cell NMR spectra of the ^{15} N-labeled protein (Fig. 1G–I). For Mia40,

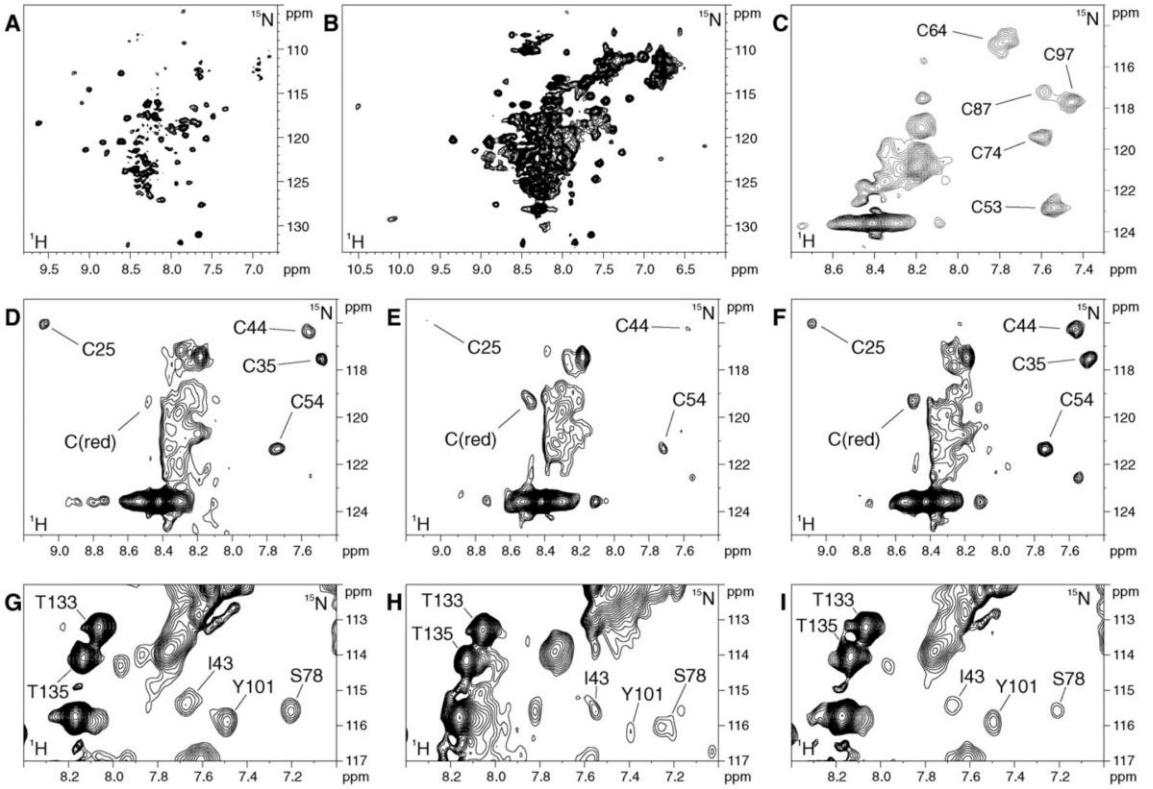

Fig. 1. In-cell NMR spectra of human cells expressing Cox17 and Mia40. (A–C) ^{1}H–^{15}N SOFAST-HMQC spectra of human cells expressing (A) [U–^{15}N]-labeled Cox17, (B) [U–^{15}N]-labeled Mia40, (C) [^{15}N]cysteine-labeled Mia40. (D–F) ^{1}H–^{15}N SOFAST-HMQC spectra of human cells expressing [^{15}N]cysteine-labeled Cox17 either alone (D) or in presence of increased levels of Grx1 (E) and Trx1 (F). (G–I) Selected region of ^{1}H–^{15}N SOFAST-HMQC spectra of human cells expressing [U–^{15}N]-labeled Mia40 either alone (G) or in presence of increased levels of Grx1 (H) and Trx1 (I). In (C–F), the amide crosspeaks corresponding to the cysteine residues in the oxidized, folded conformation are indicated. For Cox17, the crosspeak corresponding to a cysteine of the reduced conformation [C(red)] is indicated. In (G–I), the amide crosspeaks used to determine the redox state distribution are indicated.

this method yielded results consistent with previous measurements [25]. This analysis revealed that in the human cytoplasm ~70% of Cox17 and ~75% of Mia40 are folded and therefore oxidized (Fig. 2A,B), and consequently unable to enter mitochondria. The values obtained were somewhat higher that those predicted from the Nernst equation (ranging between 25% and 60% oxidized over total protein) using the reported E'_{GSH} values. As we had previously shown [25], the folding state of Mia40 in the human cytoplasm is dependent on the levels of the cytoplasmic proteins thioredoxin 1 (Trx1) and glutaredoxin 1 (Grx1): when Grx1 or Trx1 were co-expressed with Mia40, the latter shifted towards the unfolded, reduced state as a function of Grx1/Trx1 levels (Fig. 2B). A similar, albeit moderate effect on the folding state of Cox17 was observed when Grx1 was co-expressed, while co-expression of Trx1 had a smaller effect (Figs. 1E,F, 2A and Fig. S1).

When Cox17 and Mia40 were expressed in *E. coli* BL21 cells ($E'_{GSH} = -259/-261$ mV [40,41]) both proteins were mostly unfolded and in the reduced state, and no folded protein was detected in either intact cells or lysates despite the apparently less reducing environment (Fig. 2A,B and S2). Only when the Origami B strain of *E. coli* was used, which lacks the genes encoding glutathione reductase and thioredoxin reductase, and is even less reducing ($E'_{GSH} = -235$ mV [41]), the folded conformation was observed again: ~45% of Cox17 was folded, and Mia40 was completely folded (estimated from the cell lysate due to severe signal broadening of the folded domain of both proteins in bacterial cells) (Fig. 2A,B and Fig. S3).

3.2. Superoxide dismutase 1 and its copper chaperone

Unlike Cox17 and Mia40, which need to be reduced in the cytoplasm in order to reach their functional compartment, the cytoplasmic enzyme superoxide dismutase 1 (SOD1) in its active form harbors an intramolecular disulfide bond. We had previously characterized the SOD1 maturation process both in bacterial and human cells [23,24,26]. SOD1 sequentially binds one zinc ion, dimerizes, and binds one copper ion per subunit with simultaneous formation of the disulfide bond. The copper binding step requires the interaction with a specific copper chaperone for SOD1 (CCS). CCS also catalyzes the formation of the SOD1 intramolecular disulfide bond through an intermolecular thiol-disulfide exchange reaction with its C-terminal unfolded domain [32,42]. When SOD1 is expressed in human cells it readily binds zinc and dimerizes, and the zinc-bound form is observed by in-cell NMR (E,Zn–SOD1, Fig. 3A,B). In these conditions ~85% of E,Zn–SOD1 is found in the reduced state, as the endogenous CCS is apparently not sufficient to allow copper binding and disulfide bond formation (Fig. 2C). If CCS is co-expressed with SOD1 at similar levels, disulfide formation is partial in defect of copper, but almost reaches completion if excess copper is supplemented (~80% oxidized SOD1), and the mature protein Cu,Zn–SOD1 is formed (Figs. 2C and 3C,D).

Zinc binding and dimerization of SOD1 are known to occur spontaneously in bacterial cells, and Cu,Zn–SOD1 is formed when bacteria are treated with excess copper after protein expression, without the

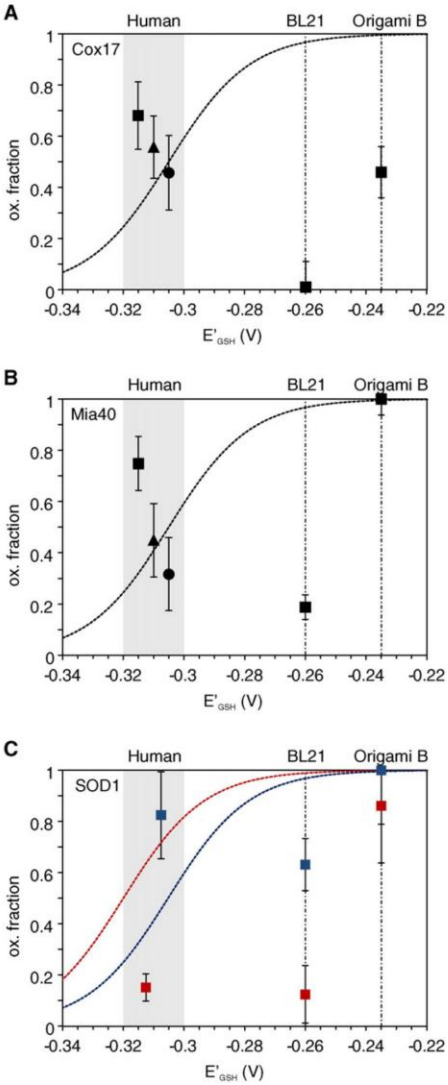

Fig. 2. Protein redox state distributions measured by NMR in different cellular environments. Fraction of oxidized Cox17 (A), Mia40 (B) and SOD1 (C), experimentally measured through in-cell NMR in human HEK293T, *E. coli* BL21 and *E. coli* Origami B cells, plotted against the redox potential of the cytoplasmic glutathione pool reported for each cell type (E'_{GSH}, range shown as gray area, single values as dot-dashed lines). The oxidized fractions of Cox17 and Mia40 alone are shown as black squares, in presence of overexpressed Grx1 and Trx1 as black circles and triangles, respectively. E,Zn–SOD1 fractions are shown as red squares; Cu,Zn–SOD1 fractions as blue squares. Error bars are calculated from standard errors. The curves represent the predicted fraction of oxidized protein calculated from the Nernst equation for Cox17 (black), Mia40 (black), E,Zn–SOD1 (red) and Cu,Zn–SOD1 (blue).

need of co-expressed CCS [23,24]. In *E. coli* BL21 cells E,Zn–SOD1 was mostly observed in the reduced state, whereas Cu,Zn–SOD1 was partially oxidized (~60%, Fig. 2C and Fig. S4A,B). In *E. coli* Origami B cells E,Zn–SOD1 had already reached the oxidized state (~85%), and after copper supplementation fully oxidized Cu,Zn–SOD1 was observed (Fig. 2C and Fig. S4C,D).

4. Discussion

If a disulfide-containing protein is assumed to be at the equilibrium with the environment, the distribution of its redox states can be calculated from the difference between $E^{\circ\prime}$ of the protein and E'_{GSH} measured in the cellular compartment of interest, using the Nernst equation. When considering some uncertainty in the actual E'_{GSH} of the cytoplasm (as shown from the previously reported values), the redox state distribution of each observed protein can be expected to fall within a certain range (Fig. 2). In the case of Cox17 and Mia40 expressed in human cells, our data show that the redox states observed by in-cell NMR fall slightly out of the predicted range, towards the oxidized state (Fig. 2A, B). Interestingly, when the levels of redox-regulating proteins Grx1/Trx1 are increased, our data agree with the E'_{GSH} values previously reported, indicating that those proteins contribute to establish the thermodynamic equilibrium between Cox17/Mia40 and the GSH pool. Unlike for Cox17 and Mia40, the data obtained on SOD1 in human cells are not in agreement with the predicted redox state distributions: E,Zn–SOD1 is mostly reduced while Cu,Zn–SOD1 is mostly oxidized, while in both metallation states SOD1 is expected to populate both states (Fig. 2C). This discrepancy suggests that SOD1 never reaches the thermodynamic equilibrium with the GSH pool, and its redox state is determined by different factors, e.g. CCS. Indeed the interaction with CCS, which affected dramatically the redox state of SOD1, is known to catalyze the formation of SOD1 disulfide bond together with copper transfer [43], moving the final distribution of SOD1 redox states further away from the equilibrium with the GSH pool. These results suggest that the disulfide exchange between SOD1 and CCS is uncoupled from the glutathione pool, and that the redox pathway of CCS is not driven by the glutathione redox potential. On the contrary, the Grx1 pathway is expected to be dependent on the glutathione redox potential, as glutaredoxins catalyze thiol-disulfide exchange reactions between protein thiols and glutathione [44].

The data obtained in *E. coli* has a larger discrepancy from the predicted distribution of redox states (Fig. 2). Indeed, all three proteins are almost completely in the reduced state in *E. coli* BL21 cells, despite E'_{GSH} being less reducing compared to that of the mammalian cell cytoplasm. SOD1 in copper-treated BL21 cells is the only exception, as it is partially oxidized upon copper treatment. Only when the proteins are expressed in the Origami B strain, which is purposely designed to facilitate the folding of disulfide-containing proteins, all three proteins are observed in the oxidized state (either partially in the case Cox17, or completely in the case of Mia40 and SOD1). Given these discrepancies, one may speculate that in bacterial cells the distribution of oxidation states of our proteins does not reach the equilibrium with the GSH pool, and is mainly controlled by the thioredoxin system (which is non-functional in the Origami B strain). Alternatively, our data could be compatible with a lower E'_{GSH} of *E. coli* cells (both BL21 and Origami B) than the reported values.

Lastly, discrepancies may also be introduced by macromolecular crowding, a property of the intracellular environment, which has been recently shown to affect the stability of protein folding [45–47]. If the change in redox state has a large effect on the folding state of a protein, the reduction potential measured in vitro may differ from the actual reduction potential in-cell. That would be especially true for Cox17 and Mia40, as the CHCH fold is strictly dependent on the disulfide bond formation, while the structure of SOD1 is not as much affected. While this effect may explain some discrepancies between the expected protein redox states and those actually observed by in-cell NMR, it does not justify the significant changes that occur in the same cellular environment when a redox partner is co-expressed at similar levels. Therefore, the observed changes are the result of specific redox-regulating processes.

5. Conclusions

The link between the intracellular glutathione and the redox state of the cell is an established property of living organisms. However, analysis

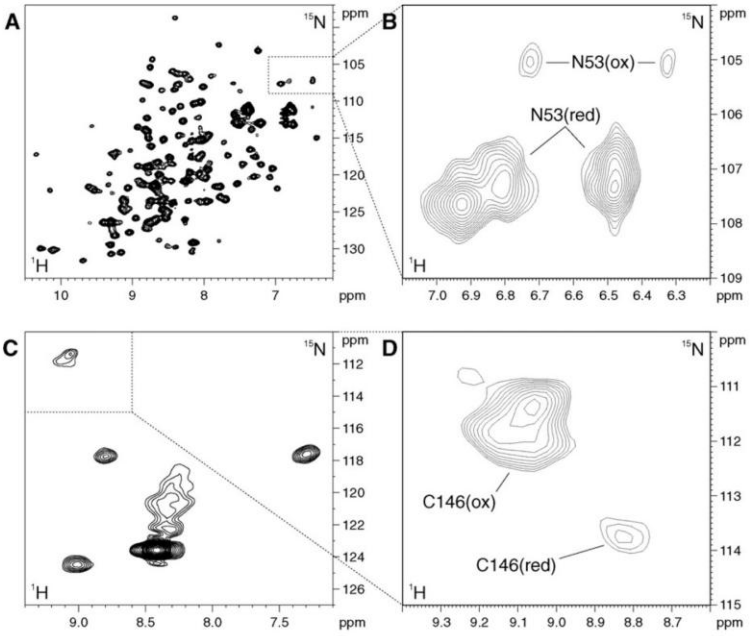

Fig. 3. In-cell NMR spectra of human cells expressing SOD1. (A) ^{1}H–^{15}N SOFAST-HMQC spectrum of human cells expressing [U–^{15}N]-labeled SOD1 in presence of excess zinc, corresponding to the zinc-bound protein (E,Zn–SOD1); (B) detail of the NMR spectrum (A) with lower contour levels showing the crosspeaks arising from the Asn53 HNδ1, HNδ2 of E,Zn–SOD1^{SS} (ox) and E,Zn–SOD1^{SH} (red); (C) ^{1}H–^{15}N SOFAST-HMQC spectrum of human cells expressing [^{15}N]cysteine-labeled SOD1 in presence of excess zinc and copper, and increased levels of CCS, in which Cu,Zn–SOD1 is observed; (D) detail of the NMR spectrum (E) with lower contour levels showing the crosspeaks arising from Cys146 of Cu,Zn–SOD1^{SS} (ox) and Cu,Zn–SOD1^{SH} (red).

at the molecular level reveals that the oxidation state of disulfide-containing proteins cannot be always predicted from the glutathione redox potential of the cellular compartment. By in-cell NMR analysis, we observed the redox state of three human proteins in the cytoplasm of human and bacterial cells. By obtaining direct information on the conformational properties of each protein in different redox states, we could directly obtain the distribution of redox states, which was then compared to the one predicted by assuming the thermodynamic equilibrium with GSH. In human cells, co-expression of redox-regulating protein partners altered the distribution of redox states. In bacterial cells (BL21) the proteins were mostly reduced, despite the less reducing cellular environment, while in the absence of the disulfide reduction pathways (in Origami B cells) the oxidized state of each protein was observed. Our results show that in-cell NMR is a suitable method to directly observe the redox state of a soluble disulfide-containing protein, and suggest that the oxidation state of some proteins is controlled by a specific pathway, which may not be linked to the GSH pool. Understanding such specific redox pathways would require focusing on the interactions between the various partners (e.g. SOD1 and CCS) irrespective of the GSH pool, similarly to how kinase signaling cascades are studied.

Author contribution

Lu.B., Le.B. and E.L. conceived the work; Le.B., E.L. and E.M. designed the experiments; Le.B and E.M. cloned the genes, produced the in-cell NMR samples and performed the Western Blot analysis; E.L. performed the in-cell NMR experiments and analyzed the data; Lu.B., Le.B., E.L. and E.M. wrote the manuscript.

Transparency document

The Transparency document associated with this article can be found, in online version.

Acknowledgements

This work has been supported by "MEDINTECH: Tecnologie convergenti per aumentare la sicurezza e l'efficacia di farmaci e vaccini" (grant number CTN01_00177_962865) and by Instruct, part of the European Strategy Forum on Research Infrastructures (ESFRI) and supported by national member subscriptions. Specifically, we thank the EU ESFRI Instruct Core Centre CERM-Italy.

Appendix A. Supplementary data

Supplementary data to this article can be found online at http://dx.doi.org/10.1016/j.bbamcr.2015.11.009.

References

[1] F.Q. Schafer, G.R. Buettner, Redox environment of the cell as viewed through the redox state of the glutathione disulfide/glutathione couple, Free Radic. Biol. Med. 30 (2001) 1191–1212.
[2] J.B. Owen, D.A. Butterfield, Measurement of oxidized/reduced glutathione ratio, Methods Mol. Biol. Clifton NJ 648 (2010) 269–277.
[3] C. Hwang, A.J. Sinskey, H.F. Lodish, Oxidized redox state of glutathione in the endoplasmic reticulum, Science 257 (1992) 1496–1502.
[4] W.G. Kirlin, J. Cai, S.A. Thompson, D. Diaz, T.J. Kavanagh, D.P. Jones, Glutathione redox potential in response to differentiation and enzyme inducers, Free Radic. Biol. Med. 27 (1999) 1208–1218.
[5] B.M. Dixon, S.-H.D. Heath, R. Kim, J.H. Suh, T.M. Hagen, Assessment of endoplasmic reticulum glutathione redox status is confounded by extensive ex vivo oxidation, Antioxid. Redox Signal. 10 (2008) 963–972.
[6] H. Østergaard, C. Tachibana, J.R. Winther, Monitoring disulfide bond formation in the eukaryotic cytosol, J. Cell Biol. 166 (2004) 337–345.
[7] M. Gutscher, A.-L. Pauleau, L. Marty, T. Brach, G.H. Wabnitz, Y. Samstag, A.J. Meyer, T.P. Dick, Real-time imaging of the intracellular glutathione redox potential, Nat. Methods 5 (2008) 553–559.
[8] B. Morgan, M.C. Sobotta, T.P. Dick, Measuring E(GSH) and H2O2 with roGFP2-based redox probes, Free Radic. Biol. Med. 51 (2011) 1943–1951.

[9] J. Hu, L. Dong, C.E. Outten, The redox environment in the mitochondrial intermembrane space is maintained separately from the cytosol and matrix, J. Biol. Chem. 283 (2008) 29126–29134.
[10] K. Kojer, M. Bien, H. Gangel, B. Morgan, T.P. Dick, J. Riemer, Glutathione redox potential in the mitochondrial intermembrane space is linked to the cytosol and impacts the Mia40 redox state, EMBO J. 31 (2012) 3169–3182.
[11] D.A. Hudson, S.A. Gannon, C. Thorpe, Oxidative protein folding: from thiol-disulfide exchange reactions to the redox poise of the endoplasmic reticulum, Free Radic. Biol. Med. 80 (2015) 171–182.
[12] H. Lu, S. Allen, L. Wardleworth, P. Savory, K. Tokatlidis, Functional TIM10 chaperone assembly is redox-regulated in vivo, J. Biol. Chem. 279 (2004) 18952–18958.
[13] N. Mesecke, N. Terziyska, C. Kozany, F. Baumann, W. Neupert, K. Hell, J.M. Herrmann, A disulfide relay system in the intermembrane space of mitochondria that mediates protein import, Cell 121 (2005) 1059–1069.
[14] L. Flohé, The fairytale of the GSSG/GSH redox potential, Biochim. Biophys. Acta 1830 (2013) 3139–3142.
[15] C. Berndt, C.H. Lillig, L. Flohé, Redox regulation by glutathione needs enzymes, Front. Pharmacol. 5 (2014) 168.
[16] B. Morgan, Reassessing cellular glutathione homoeostasis: novel insights revealed by genetically encoded redox probes, Biochem. Soc. Trans. 42 (2014) 979–984.
[17] J. Birk, M. Meyer, I. Aller, H.G. Hansen, A. Odermatt, T.P. Dick, A.J. Meyer, C. Appenzeller-Herzog, Endoplasmic reticulum: reduced and oxidized glutathione revisited, J. Cell Sci. 126 (2013) 1604–1617.
[18] B. Morgan, D. Ezeriņa, T.N.E. Amoako, J. Riemer, M. Seedorf, T.P. Dick, Multiple glutathione disulfide removal pathways mediate cytosolic redox homeostasis, Nat. Chem. Biol. 9 (2013) 119–125.
[19] D.I. Freedberg, P. Selenko, Live cell NMR, Annu. Rev. Biophys. 43 (2014) 171–192.
[20] R. Hänsel, L.M. Luh, I. Corbeski, L. Trantirek, V. Dötsch, In-cell NMR and EPR spectroscopy of biomacromolecules, Angew. Chem. Int. Ed. Engl. 53 (2014) 10300–10314.
[21] A.E. Smith, Z. Zhang, G.J. Pielak, C. Li, NMR studies of protein folding and binding in cells and cell-like environments, Curr. Opin. Struct. Biol. 30 (2015) 7–16.
[22] L. Barbieri, E. Luchinat, L. Banci, Protein interaction patterns in different cellular environments are revealed by in-cell NMR, Sci. Rep. 5 (2015) 14456.
[23] L. Banci, L. Barbieri, I. Bertini, F. Cantini, E. Luchinat, In-cell NMR in E. coli to monitor maturation steps of hSOD1, PLoS One 6 (2011), e23561.
[24] L. Banci, L. Barbieri, I. Bertini, E. Luchinat, E. Secci, Y. Zhao, A.R. Aricescu, Atomic-resolution monitoring of protein maturation in live human cells by NMR, Nat. Chem. Biol. 9 (2013) 297–299.
[25] L. Banci, L. Barbieri, E. Luchinat, E. Secci, Visualization of redox-controlled protein fold in living cells, Chem. Biol. 20 (2013) 747–752.
[26] E. Luchinat, L. Barbieri, J.T. Rubino, T. Kozyreva, F. Cantini, L. Banci, In-cell NMR reveals potential precursor of toxic species from SOD1 fALS mutants, Nat. Commun. 5 (2014) 5502.
[27] A.R. Aricescu, W. Lu, E.Y. Jones, A time- and cost-efficient system for high-level protein production in mammalian cells, Acta Crystallogr. D Biol. Crystallogr. 62 (2006) 1243–1250.
[28] L. Banci, I. Bertini, S. Ciofi-Baffoni, A. Janicka, M. Martinelli, H. Kozlowski, P. Palumaa, A structural-dynamical characterization of human Cox17, J. Biol. Chem. 283 (2008) 7912–7920.
[29] P. Schanda, B. Brutscher, Very fast two-dimensional NMR spectroscopy for real-time investigation of dynamic events in proteins on the time scale of seconds, J. Am. Chem. Soc. 127 (2005) 8014–8015.
[30] A. Voronova, W. Meyer-Klaucke, T. Meyer, A. Rompel, B. Krebs, J. Kazantseva, R. Sillard, P. Palumaa, Oxidative switches in functioning of mammalian copper chaperone Cox17, Biochem. J. 408 (2007) 139–148.
[31] L. Banci, I. Bertini, C. Cefaro, S. Ciofi-Baffoni, A. Gallo, M. Martinelli, D.P. Sideris, N. Katrakili, K. Tokatlidis, MIA40 is an oxidoreductase that catalyzes oxidative protein folding in mitochondria, Nat. Struct. Mol. Biol. 16 (2009) 198–206.
[32] L. Banci, I. Bertini, F. Cantini, T. Kozyreva, C. Massagni, P. Palumaa, J.T. Rubino, K. Zovo, Human superoxide dismutase 1 (hSOD1) maturation through interaction with human copper chaperone for SOD1 (hCCS), Proc. Natl. Acad. Sci. U. S. A. 109 (2012) 13555–13560.
[33] S.D. Bouldin, M.A. Darch, P.J. Hart, C.E. Outten, Redox properties of the disulfide bond of human Cu,Zn superoxide dismutase and the effects of human glutaredoxin 1, Biochem. J. 446 (2012) 59–67.
[34] W. Neupert, J.M. Herrmann, Translocation of proteins into mitochondria, Annu. Rev. Biochem. 76 (2007) 723–749.
[35] L. Banci, I. Bertini, S. Ciofi-Baffoni, K. Tokatlidis, The coiled coil-helix-coiled coil-helix proteins may be redox proteins, FEBS Lett. 583 (2009) 1699–1702.
[36] C.T. Dooley, T.M. Dore, G.T. Hanson, W.C. Jackson, S.J. Remington, R.Y. Tsien, Imaging dynamic redox changes in mammalian cells with green fluorescent protein indicators, J. Biol. Chem. 279 (2004) 22284–22293.
[37] C. Schwarzer, B. Illek, J.H. Suh, S.J. Remington, H. Fischer, T.E. Machen, Organelle redox of CF and CFTR-corrected airway epithelia, Free Radic. Biol. Med. 43 (2007) 300–316.
[38] A.J. Meyer, T.P. Dick, Fluorescent protein-based redox probes, Antioxid. Redox Signal. 13 (2010) 621–650.
[39] M. Schwarzländer, T.P. Dick, A.J. Meye, B. Morgan, Dissecting redox biology using fluorescent protein sensors, Antioxid. Redox Signal. (2015).
[40] H. Ostergaard, A. Henriksen, F.G. Hansen, J.R. Winther, Shedding light on disulfide bond formation: engineering a redox switch in green fluorescent protein, EMBO J. 20 (2001) 5853–5862.
[41] W. Zhang, W. Zheng, M. Mao, Y. Yang, Highly efficient folding of multi-disulfide proteins in superoxidizing Escherichia coli cytoplasm, Biotechnol. Bioeng. 111 (2014) 2520–2527.
[42] Y. Furukawa, A.S. Torres, T.V. O'Halloran, Oxygen-induced maturation of SOD1: a key role for disulfide formation by the copper chaperone CCS, EMBO J. 23 (2004) 2872–2881.
[43] M.C. Carroll, J.B. Girouard, J.L. Ulloa, J.R. Subramaniam, P.C. Wong, J.S. Valentine, V.C. Culotta, Mechanisms for activating Cu- and Zn-containing superoxide dismutase in the absence of the CCS Cu chaperone, Proc. Natl. Acad. Sci. U. S. A. 101 (2004) 5964–5969.
[44] A.P. Fernandes, A. Holmgren, Glutaredoxins: glutathione-dependent redox enzymes with functions far beyond a simple thioredoxin backup system, Antioxid. Redox Signal. 6 (2004) 63–74.
[45] W.B. Monteith, G.J. Pielak, Residue level quantification of protein stability in living cells, Proc. Natl. Acad. Sci. U. S. A. 111 (2014) 11335–11340.
[46] W.B. Monteith, R.D. Cohen, A.E. Smith, E. Guzman-Cisneros, G.J. Pielak, Quinary structure modulates protein stability in cells, Proc. Natl. Acad. Sci. U. S. A. 112 (2015) 1739–1742.
[47] S. Majumder, J. Xue, C.M. DeMott, S. Reverdatto, D.S. Burz, A. Shekhtman, Probing protein quinary interactions by in-cell nuclear magnetic resonance spectroscopy, Biochemistry (Mosc) 54 (2015) 2727–2738.

2.2. The antioxidant molecule ebselen rescues the toxic characteristics of mutant SOD1

Oxidative stress has been linked to a countless amount of pathologies, including ALS and asthma. The main pathological hallmark of ALS is the formation of protein aggregates mainly in degenerating motor neurons and surrounding oligodendrocytes [58]. About 20% of familial ALS cases are caused by mutations in the hSOD1 gene. There are evidences that mutated SOD1 can form cytotoxic protein aggregates alone or with other proteins that possibly lead to a loss of the enzymatic function or to acquiring toxic properties [59]. In this work, we studied the interaction of the small antioxidant molecule ebselen with disease-related SOD1 mutants. Intrestingly we found that in cells ebselen restores the correct folding of destabilized SOD1 mutants by promoting disulfide formation and zinc binding. *In vitro*, ebselen was found to covalently bind SOD1 near the dimer interface, thereby restoring the strength of dimerization towards the proper maturation pathway. Ebselen, therefore, contributes to restore SOD1 physiological maturation and prevents its unfolding and aggregation. In addition to its already known anti-inflammatory pharmacological properties, ebselen could be exploited as a drug precursor for translation into the clinical trials.

(Submitted)

The antioxidant molecule ebselen rescues the toxic characteristics of mutant SOD1

Michael J. Capper[1], Gareth S. A. Wright[1], Letizia Barbieri[2,3], Enrico Luchinat[2,4], Eleonora Mercatelli[2], Luke McAlary[5], Justin J. Yerbury[6], Paul M. O'Neill[7], Svetlana V. Antonyuk[1], Lucia Banci[2,8], S. Samar Hasnain[1]

Affiliations

1. Molecular Biophysics Group, Institute of Integrative Biology, Faculty of Health and Life Sciences, University of Liverpool, L69 7ZB UK.
2. Magnetic Resonance Centre (CERM), University of Florence, 50019 Sesto Fiorentino, Italy.
3. Interuniversity Consortium for Magnetic Resonance of Metallo Proteins (CIRMMP), 50019 Sesto Fiorentino, Italy.
4. Department of Biomedical, Clinical and Experimental Sciences, University of Florence, 50134 Florence, Italy.
5. Department of Physics & Astronomy, University of British Columbia, Vancouver, British Columbia, Canada.
6. llawarra Health and Medical Research Institute, University of Wollongong, Wollongong, Australia.
7. Department of Chemistry, University of Liverpool, Liverpool, L69 7ZD UK.
8. Department of Chemistry, University of Florence, 50019 Sesto Fiorentino, Florence, Italy.

The antioxidant molecule ebselen rescues the toxic characteristics of mutant SOD1

Michael J. Capper[1*], Gareth S. A. Wright[1*], Letizia Barbieri[2,3*], Enrico Luchinat[2,4*], Eleonora Mercatelli[2], Luke McAlary[5], Justin J. Yerbury[6], Paul M. O'Neill[7], Svetlana V. Antonyuk[1], Lucia Banci[2,8,§], S. Samar Hasnain[1,§].

* These authors contributed equally, § Corresponding authors

1. Molecular Biophysics Group, Institute of Integrative Biology, Faculty of Health and Life Sciences, University of Liverpool, L69 7ZB UK.
2. Magnetic Resonance Centre (CERM), University of Florence, 50019 Sesto Fiorentino, Italy.
3. Interuniversity Consortium for Magnetic Resonance of Metallo Proteins (CIRMMP), 50019 Sesto Fiorentino, Italy.
4. Department of Biomedical, Clinical and Experimental Sciences, University of Florence, 50134 Florence, Italy.
5. Department of Physics & Astronomy, University of British Columbia, Vancouver, British Columbia, Canada.
6. llawarra Health and Medical Research Institute, University of Wollongong, Wollongong, Australia.
7. Department of Chemistry, University of Liverpool, Liverpool, L69 7ZD UK.
8. Department of Chemistry, University of Florence, 50019 Sesto Fiorentino, Florence, Italy.

Significance Statement

Chronic lung and neurodegenerative diseases are not often causally linked. However oxidative stress and the propensity for the antioxidant protein SOD1 to become disulphide reduced are common to asthma and amyotrophic lateral sclerosis. Here we show that ebselen, a small molecule which is known to combat oxidative stress, can change the molecular characteristics of SOD1 associated with disease through a direct interaction. Ebselen promotes SOD1 disulphide bonding, zinc binding and folding. It can also covalently attach to SOD1 at the dimer interface and restore the strength of dimerization. Ebselen's direct and indirect pharmacological properties mark it as very good candidate for translation into the clinic.

Key words: Small molecules; neurodegenerative disease; asthma; oxidative stress.

Abstract

Superoxide dismutase-1 (SOD1) is an important part of human oxidative stress defence

but point mutations in its primary sequence cause the neurodegenerative disease (ND) amyotrophic lateral sclerosis (ALS). ALS mutations reduce the ability of SOD1 to fold, metalate, dimerize and form an intra-subunit disulphide bond. Ultimately this leads to neuronal death through the accumulation of large insoluble aggregates or small oligomers. Loss of the disulphide bond from wild-type SOD1 is also seen in asthma where dismutase activity is decreased as a result. The role of oxidative stress in the pathogenesis of ND prompted us to investigate the small molecule antioxidant compound, ebselen, and its effect on the molecular characteristics of SOD1 associated with ALS and asthma. Within the cell, ebselen very efficiently catalyzes SOD1 intra-subunit disulphide bond formation through a selenylsulphide/selenol-thiol exchange mechanism. This directs correct SOD1 folding and zinc binding which depopulates the globally unfolded precursor associated with mutant SOD1 toxicity. Aggregate formation and the propensity of mutant SOD1 for premature degradation are diminished as a result. This demonstrates that exogenous promotion of SOD1 disulphide bonding is a viable therapeutic approach for ALS. In less reducing environments, ebselen forms a selenylsulphide bond with Cys111 and restores the monomer-dimer equilibrium of A4V SOD1 to wild-type through non-covalent reinforcement of the dimer interface. Ebselen is therefore a potent, bi-modal SOD1 pharmacological chaperone which combines properties of the copper chaperone for SOD1 and the antioxidant edaravone, which recently became only the second ALS therapeutic to be licenced in the United States.

Introduction

Amyotrophic lateral sclerosis (ALS) is a fatal motor system neurodegenerative disease. Mutations to the superoxide dismutase-1 gene were the first identified genetic link with ALS (1). Histopathology on tissues from humans and mutant superoxide dismutase-1 (SOD1) animal models has shown how SOD1 protein accumulates in Lewy-like bodies within the cytoplasm and the mitochondria of motor neurons and support cells. These insoluble inclusions are replete with misfolded SOD1 which has not been cleared by the protein degradation pathways (2).

Pioneering work on the catalytic activity of SOD1 and subsequent exploration of its structure proved that a host of post-translational modifications are necessary for stability and function (3). While zinc binding and an intra-subunit disulphide are not directly involved in catalysis they hold the molecule's tertiary and quaternary structure (4–6). ALS-related mutations reduce the ability of SOD1 to bind necessary metal cofactors and predispose it to disulphide reduction. Activity loss through disulphide bond reduction is also characteristic of SOD1 in asthma sufferers where elevation of intracellular reduced glutathione increases the reduction potential of the cytoplasm (7, 8). In ALS, an inability

to undergo these post-translational modifications shifts the oligomer equilibria in favour of the monomer and a portion of cellular SOD1 is forced to reside in a persistently misfolded state (9, 10). Exposure of normally internalized hydrophobic motifs leads to aberrant oligomerization which manifests as disulphide reduced, metal-free, insoluble SOD1 inclusions in cell and animal models (11, 12). In a corollary with β-amyloid accumulation in Alzheimer's Disease, it seems that non-native SOD1 monomers or small oligomers are the toxic species rather than large insoluble amyloid fibrils (13). Crystallographic structures have shown how these toxic seeds can be assembled (14, 15). The unfolding and aggregation propensity of SOD1 have been shown to correlate with life expectancy, post-diagnosis in humans and transgenic mouse models (9, 16–18). Consequentially, promoting normal folding and post-translational modification has the potential to divert mutant SOD1 away from the toxic pathway and, at the very least, extend the disease's clinical duration. Non-covalent ligand interactions have been demonstrated on the SOD1 β-barrel surface but each failed to change mutant thermal stability or inhibit aggregation *in vitro* possibly due to low binding affinity (19). Conversely, addition of cisplatin to the reactive Cys111 residues or covalently cross-linking them across the dimer interface groove with bis-maleimide analogues have been proven to modulate disease related characteristics. Both bismaleimidoethane (BMOE) and cisplatin increase SOD1 thermal stability, while the latter also inhibits *in vitro* and in-cell aggregation (20, 21). However, both interactions have been shown to inhibit heterodimer formation with the copper chaperone for SOD1 (hCCS) (22).

Ebselen is an organoselenium compound with broad antioxidant properties (23). It is also an anti-inflammatory and has been tested as a treatment for a variety of illnesses including stroke (24), bipolar disorder (25) and aneurysmal subarachnoid haemorrhage (26). It is well tolerated in humans can be formulated for oral administration and is neuroprotective. Interestingly, it has also been shown to reduce the cytotoxic burden of mutant SOD1 mitochondrial pathology (27). Ebselen has strong pharmacological and structural similarities with edaravone, which very recently became only the second drug licensed for the treatment of ALS in the United States. Both drugs are antioxidants and have been used in the treatment of stroke.

Here we demonstrate that ebselen and its analogue ebsulphur bind to SOD1 at the Cys111 site *in vitro*. This interaction shifts the SOD1 monomer-dimer equilibrium in favour of the dimer and returns the affinity of the A4V dimer to that of wild-type. This occurs without covalent tethering of monomer subunits within the SOD1 dimer. Importantly the increased dimer stability does not prevent heterodimer formation with hCCS. This proof of principle is important as Cys111 targeted drug compounds could bind the free

sulphydryl of both mutant or wild-type SOD1 and should not prevent hCCS catalysed activation. Furthermore, we show by in-cell and *in vitro* NMR that ebselen reacts with disulphide-reduced SOD1 in the human cell cytosol causing formation of the intra-subunit disulphide bond. In doing so, it promotes correct SOD1 folding and zinc binding. Directing the nascent protein down the correct post-translational modification pathway prevents accumulation of unfolded species, thought to be the precursor of mutant SOD1 toxicity, premature degradation and formation of insoluble aggregates (9, 10). Thus, Ebselen rescues the toxic characteristics of mutant SOD1 through two independent disulphide formation and dimer stabilization mechanisms deployment of which is dependent on the nature of the environment. Ebselen's on-target SOD1 pharmacological chaperone activity, in combination with its usage history and positive secondary pharmacology reminiscent of edaravone, indicate it is a very promising lead not only in the search for therapeutics which can modulate pathogenic SOD1 behaviour in ALS, but also, asthma.

Results

Ebselen and ebsulphur form a covalent bond with SOD1 at Cys111

Screening libraries of existing drugs, those that are no longer used or drugs that were not successful in the final stages of clinical trials, is an increasingly popular approach for therapeutic discovery. Drug repurposing offers a cheaper and faster route through early clinical trials as ADMET information is available, creating a major advantage for 'orphan diseases' such as ALS. This approach has resulted in historic as well as recent successes (see review (28)), including the licensing of edaravone in Japan and the US to slow ALS progression (29). Given the susceptibility of Cys111 to oxidative modifications in SOD1-ALS and previous work on cisplatin and BMOE we undertook a crystallographic screen of a small library of cysteine-reactive compounds known to have favourable antioxidant properties (Supplementary Fig. 1). Ebselen and ebsulphur were found to bind SOD1 Cys111 while derivatives with a benzyl substitution on the benzoisoselenazole or benzoisothiazolone nitrogen did not, possibly due to altered reactivity or steric hindrance in the dimer groove.

The 1.3 and 1.5 Å resolution structures of wild-type, zinc metalated, disulphide intact SOD1 bound to ebselen or ebsulphur allowed for the unambiguous placement of the compounds in the SOD1 dimer groove (Fig. 1*A* and *B*). They show the formation of a selenylsulphide or mixed disulphide covalent bond, respectively, between ligand and Cys111 created by nucleophilic attack of the free Cys111 sulphydryl at the electrophilic Se-N and S-N centres contained within each respective heterocycle. Electron density is

clear for both ligands except for a small part of one of the ebsulphur phenyl rings which projects into solvent. This indicates some rotational freedom in this group (Figs. 1*C* and *D*). No ligand conjugation was observed at Cys6 and the intramolecular disulphide bond between Cys57 and Cys146 remained intact. No large structural changes were seen between the amino acid backbone or side chains of ebselen-conjugated SOD1 compared to unbound SOD1 crystallized under the same conditions (RMSD 0.242 Å, Supplementary Fig. 2). Ebselen and ebsulphur form tight interactions within the SOD1 dimer groove and a hydrogen bond is formed between the ligand carbonyl and a highly coordinated water molecule situated, on average, 2.55 Å away. Through this bond, the ligand is integrated into the crystallographic water network forming an indirect link to the Gly108 backbone amide of one SOD1 monomer. This reflects the asymmetry of ligand binding to each monomer. Ebselen and ebsulphur form an additional inter-dimer contact through planar stacking of their benzylamine groups. Analysis of the four dimer interface hydrogen bonds which contribute to SOD1 dimer affinity indicates bond shortening. The hydrogen bond between Gly51 N and Ile151 O is reduced from 2.81 Å in the atomic resolution model of SOD1 (PDB ID 2V0A) to 2.74 and 2.72 Å in the ebselen and ebsulphur models. The bond between Gly114O and Ile151N is also reduced, from 2.92 Å to 2.78 Å and 2.83 Å. Ile151 is located just 3.8 Å away from ebselen in chain A (Supplementary Fig. 3).

Ebselen and ebsulphur potentiate SOD1 dimer formation without hindering complex formation between SOD1 and hCCS

The propensity for mutant SOD1 to exist as a monomer is a key contributory factor in the pathology of SOD1-ALS. Indeed, preventing dimer dissociation has been shown to increase SOD1 thermal stability and inhibit aggregation *in vitro* (20, 30). Native mass spectrometry (MS) preserves non-covalent interactions and allows quantification of tight homo-oligomer dissociation constants without reverting to chaotropic unfolding as well as the ability to resolve differentially modified protein species (Supplementary Fig. 4) (18, 31). As such we determined the effect of ebselen and ebsulphur on the SOD1 monomer-dimer equilibrium. Wild-type zinc metalated, disulphide intact SOD1 was found to have a dimer dissociation constant (K_d) of 24 ± 4 nM and the strength of dimerization is increased slightly by the addition of ebselen and ebsulphur (Fig. 2*A*). A4V SOD1, which leads to an highly aggressive form of ALS, has a much weakened dimer interaction resulting in partial monomerization at low micromolar concentrations (30). This is reflected in an increased dimer K_d, 957 ± 30 nM. However, ebselen and ebsulphur completely restore dimer affinity to a wild-type level, K_d 16 ± 3 and 23 ± 4 nM respectively (Fig. 2*A*). A strengthening of the dimer interaction is also observed for ALS mutants G93A and I149T (Fig. 2*A*). The H46R/H48Q SOD1 artificial copper site mutant

displays caricature disease-related characteristics including a very strong propensity to exist in the disulphide reduced state and weakened affinity for zinc(32) that leads to complete monomerization at micromolar concentrations (Supplementary Fig. 5). Even in this extreme case, ebselen increases the strength of the dimer, K_d, 5.3 ± 0.4 μM to 220 ± 27 nM, with ebsulphur having a similar but less pronounced effect (Fig. 2*A*). Overall, mutant SOD1 shows better dimer stabilization when bound to ebselen than ebsulphur and A4V SOD1 benefitted from the largest stabilization; a 60-fold increase (Fig. 2*B*).

The copper chaperone for SOD1 (hCCS) is an important part of the cellular machinery that prepares SOD1 for its role in oxidant defence. Modifications to Cys111 that promote SOD1 thermal stability have previously been shown to prevent heterodimer formation between hCCS and SOD1, thus preventing hCCS-catalysed SOD1 copper acquisition and disulphide formation (22). In contrast to BMOE and cisplatin, and despite increasing the dimer affinity of SOD1, ebselen does not hinder complex formation between SOD1 and hCCS; the heterodimer readily forms under normal conditions (Fig. 3).

Ebselen promotes formation of the SOD1 intra-subunit disulphide bond in living cells

To determine whether ebselen exerts a protective role against SOD1 in the cytosol, its effect on intracellular SOD1 maturation was investigated in live human cells by in-cell NMR (33, 34). The pathway leading to SOD1 maturation has been recently recapitulated through in-cell NMR studies (35, 36). Beginning with monomeric, disulphide-reduced apo-SOD1, zinc binding occurs spontaneously leading to the formation of reduced E,Zn-SOD1. Copper binding and disulphide bond formation occur subsequently, upon interaction with hCCS (36, 37). Disulphide-reduced E,Zn-SOD1 becomes a stable intermediate species in the cytosol if hCCS is not present in sufficient amount (38). In human cells treated with ebselen, intracellular E,Zn-SOD1 was fully oxidized, showing that ebselen efficiently promotes the formation of the SOD1 intramolecular disulphide bond (between Cys57 and Cys146). In contrast, >95% of the total E,Zn-SOD1 is found in the disulphide reduced state in untreated cells (Fig. 4*A*). This effect could be reproduced *in vitro* by treating reduced E,Zn-SOD1 with 1 equivalent per monomer of ebselen in an anaerobic environment (Fig. 4*B*), indicating that a redox reaction occurs directly between ebselen and the reduced Cys57 and Cys146 of SOD1. This mechanism is consistent with the known thiol oxidase activity of ebselen (39) and would function through the formation of a transient selenylsuphide bond which is then rearranged by selenyl-thiol exchange to yield the SOD1 disulphide and free ebselen selenol (2-hydroseleno-N-phenylbenzamide). Interestingly, the ebselen selenol is a potent reducer of hydrogen peroxide and the ultimate product of this reaction is ebselen (40). Increased oxidative

stress could therefore promote ebselen recycling.

Ebselen was not found to stably bind Cys111 of either disulphide oxidized or reduced SOD1 within the cytosol (Supplementary Figs. 6*A* and *B*) likely due to reduction of the selenylsulphide bond by glutathione, free cysteine or other cellular thiols. This was verified *in vitro*; treatment of ebselen-SOD1 with thiols at low concentrations (1 mM glutathione or dithiothreitol) at neutral pH resulted in the complete loss of conjugation (Supplementary Fig. 6*C*).

Ebselen very effectively stabilizes mutant SOD1 in living cells

Several ALS-linked SOD1 mutants fail to bind zinc in the human cytosol, and accumulate as unstructured species that may act as precursors in the pathogenic aggregation of SOD1 (9, 10). Given that the intramolecular disulphide bond is known to increase the structural stability of wild-type and mutant SOD1, we reasoned that the oxidizing effect of ebselen could stabilize intracellular SOD1 mutants. Indeed, treatment with ebselen caused the oxidation of ALS-linked SOD1 mutants G93A and A4V in human living cells, and efficiently stabilized both proteins. This striking effect is evident when comparing the NMR spectra of treated and untreated cells (Fig. 5*A* and *B*). In cells treated with ebselen, disulphide intact E,Zn-SOD1 is detected at levels comparable to those of wild-type SOD1, whereas in untreated cells the SOD1 mutants are either largely accumulated as unfolded species (G93A, see Fig. 5*A*) or barely detected (A4V, possibly due to severe aggregation or degradation, see Fig. 5*B*). This stabilizing effect was further confirmed by western blot analysis of cell lysates, where the expression level of SOD1 mutants was markedly increased upon treatment with ebselen (Fig. 5*C*). Overall, these data indicate that the action of ebselen in stabilizing intracellular SOD1 occurs through a thiol exchange mechanism similar to that deployed by hCCS. The two modes of action targeting disulphide intact and disulphide reduced SOD1 (Fig. 6) are however not mutually exclusive and both could be exploited in future drug developments against ALS.

Discussion

Cellular oxidative stress is a common theme in the pathogenesis of neurodegenerative and lung inflammation diseases (41–43). In both asthma and ALS, the antioxidant SOD1 is found to be disulphide reduced. Dimerization, disulphide bond formation and metal ion acquisition are the canonical SOD1 post-translation modification (PTMs) steps on route to forming a stable and active enzyme (4–6). Each PTM contributes to both stability and activity. The inability of ALS-related SOD1 mutants to complete these steps is the central tenet of SOD1 pathogenesis dogma. This appears to extend to the bronchial inflammation disease asthma, where wild-type SOD1 is found to be disulphide is reduced as a result of

an imbalanced oxidized/reduced glutathione ratio. SOD1 dismutase activity is reduced as a result in both ALS and asthma however in ALS SOD1 accumulates into amorphous and fibrillar aggregates within the cytoplasm and mitochondria of neurons and astroglia (11, 12, 44). Here we have shown that ebselen has astonishing capacities for correcting several aspects of aberrant SOD1 maturation with implications for the treatment of ALS and asthma.

We have quantified the dimer dissociation constants of wild-type SOD1, and several disease related mutants, in non-denaturing conditions using native MS. While A4V and the artificial copper site mutant H46R/H48Q have a 40-fold and 220-fold reduction in their ability to form a dimer respectively, G93A and I149T have wild-type-like dimer interactions. This highlights the likelihood that SOD1 monomerization acts in concert with reduced copper or zinc affinity, thermal instability and local or global unfolding as the toxic cue. Using a combination of protein crystallography and native MS we have determined both the binding site and pose of two novel ligands, directly quantifying their effect on SOD1 dimerization and predicting their mode of action. We conclude that ebselen binding to Cys111 restores the dimer affinity of A4V SOD1 to that of wild-type. The effect is mediated by π-π stacking between ebselen or ebsulphur aromatic rings and increases the dimer binding energy by exclusion of water together with strengthening of native hydrogen bonding across the dimer interface. SOD1 dimer affinity is increased by both ebselen and ebsulphur binding irrespective of the SOD1 variant involved. As is the case for cisplatin and bis-maleimide derivatives, ebselen and ebsulphur are promiscuous thiol oxidases and form conjugates with a variety of proteins. However, the reaction with the target cysteine is reversible and likely to be stripped by cellular reductants such as glutathione. Indeed, our in-cell and *in vitro* NMR observations show that ebselen is not stably bonded to Cys111 in the reducing environment of the cytosol. Nevertheless, such reversible conjugation constitutes a novel means to modulate a behaviour of SOD1 associated with ALS, and may become useful if the target is in less reducing environments at the point of intervention, such as the extracellular matrix or the mitochondrial inter-membrane space. Moreover, ebselen and ebsulphur are a more amenable scaffold from which to grow into the SOD1 dimer groove and engineer specificity than cisplatin or BMOE, whose mode of action is unclear or require covalent dimer tethering respectively.

In recent years, the toxicity of large, insoluble SOD1 aggregates has been questioned. Monomers which are unable to bind zinc, fold and dimerize or small oligomers with non-native interface regions are now thought to be the origin of SOD1 toxicity. In most cases these inherently unstable species are cleared by the cellular degradation machinery

leading to a reduction in the abundance and activity of mutant SOD1. Reduction in the amount of erythrocyte SOD1 is in fact strongly associated with ALS mutations (45–47). However, a fraction of mutant SOD1 does not undergo controlled degradation. Instead it sequesters and inhibits the proteasome and chaperone mediated folding pathways. Ultimately these species go on to form large insoluble aggregates but the damage has already been done and cell death ensues. While ebselen does not appear to form a stable covalent bond with SOD1 Cys111 in the reducing environment of the cytosol it does very efficiently redirect the fate of these small toxic species. We have shown, based on our in-cell NMR characterization, that ebselen restores the mutant SOD1 post-translational modification pathway by promoting the formation of the intra-subunit disulphide bond. The mode of action of ebselen in cells has three possibilities: 1) An indirect effect on intracellular redox which promotes disulphide formation. 2) Increased activity of the SOD1 disulphide conferring chaperone protein hCCS. 3) Direct redox reaction between ebselen and SOD1 cysteines involved in the intra-subunit disulphide bond. While the first two hypotheses cannot be ruled out, we have shown the latter to occur spontaneously *in vitro*, in the absence of additional thiol-containing molecules. Therefore, ebselen likely reacts with one of the free Cys57 or Cys146 sulphydryls on SOD1, forming a transient selenyl-sulphide which is then easily rearranged by selenyl-thiol exchange to form the intra-subunit disulphide bond with the release of ebselen selenol. Disulphide bond formation greatly enhances the folding stability of mutant SOD1 and improves zinc binding affinity. Thus, the level of soluble mutant protein, which is constituted by SOD1 not swiftly degraded or aggregated, is increased. In summary, by strongly promoting SOD1 disulphide formation, ebselen facilitates correct folding and zinc acquisition of mutant SOD1 in the cytosol, while in less reducing environments it greatly enhances the SOD1 dimer affinity (Fig. 6). Ebselen can therefore be considered a true pharmacological chaperone for SOD1. These positive effects are important milestones in SOD1-ALS drug development.

To date, rational drug development for SOD1 has been impeded by insufficiently robust *in vitro* assays. This means drug screening has not effectively translated into clinical drugs. Two of the assay techniques used here, native mass-spectrometry and in-cell NMR, are novel in their application to SOD1 drug development. The insight we have gained through the combined use of multiple, highly complementary structural techniques has offered a new avenue for SOD1 drug discovery, promotion of disulphide formation, and new possibilities for analysis of drug molecules' effect on characteristics pertinent to ALS. This has obvious benefits to the drug optimization process.

The role of SOD1 in antioxidant defence cannot by understated. Indeed, nitroxidative

stress is elevated in ALS through the reaction of nitric oxide and superoxide to produce peroxynitrite. This can lead to tyrosine nitrosylation and glutamate excitotoxicity (48). Ebselen is known to inhibit inducible nitric oxide synthase, detoxify peroxynitrite and combat glutamate-induced excitotoxicity (49–51). This antioxidant behaviour, together with the pharmacological similarities with edaravone, indicate ebselen is likely to have positive secondary pharmacology as well as the primary pharmacological chaperone role investigated here. Several other drug-like molecules have shown negative on-target effects on the SOD1 interaction with hCCS (22). For SOD1 to perform its function it must be copper metalated and disulphide oxidized; a function largely performed by hCCS which takes E,Zn-SOD1$^{S\text{-}H}$ as a substrate and yields active and highly stable SOD1. While cisplatin and BMOE inhibit or completely prevent the interaction with hCCS respectively, ebselen-bound SOD1 is free to heterodimerize with its protein chaperone *in vitro* despite the increased dimer affinity engendered by ebselen binding. If the reversibility and specificity of ebselen binding can be fine-tuned through rational, structurally-informed design, the implication is that SOD1's toxic characteristics could be modulated *in vivo* over long time-courses for the treatment of ALS and asthma without damaging our response to oxidative stress.

Materials & Methods

Expression and purification of SOD1

Recombinant wild-type and mutant SOD1 were expressed in BL21 (DE3) *Escherichia coli* as previously described (19). Apo-SOD1 variants were produced by dialysis against 10 mM EDTA at pH 3.8 in sodium acetate buffer. Ebselen bound SOD1 was produced by adding the compound from a DMSO stock. Excess compound was removed by dialysis. H46R/H48Q SOD1 was analysed by SEC as described previously (22). Disulphide-reduced E,Zn-SOD1 was obtained by adding 50 mM DTT to apo-SOD1 in phosphate-buffered saline (PBS) and incubating for 40 min at 37°C. DTT was subsequently removed under anaerobic conditions and 1 equivalent of zinc was added.

Crystallization and structure solution

Crystals of as-isolated Zn bound SOD1 were produced using previously identified conditions with protein pre-conjugated with the ligand. Crystals were frozen in 3.2 M $(NH_4)_2SO_4$ as a cryoprotectant and data were collected on I02 at Diamond Light Source and Proxima1 at SOLEIL for ebsulphur and ebselen bound SOD1 respectively. Diffraction images were indexed using iMosflm (52) and data was processed using the CCP4 suite (53). Models were manually refined using Coot (54) followed by cycles of restrained refinement in Refmac5 (55). Restraints for both ebselen and ebsulphur were produced using JLigand (56). Crystallographic statistics are shown in **Table 1**. The

structures of ebselen- and ebsulphur- bound SOD1 are deposited in the PDB with ascension numbers 5O40 and 5O3Y.

Native mass spectrometry

Native mass spectrometry analysis was performed using a SYNAPT G1 HDMS (Waters, UK) with parameters set according to previous work (31). Briefly, purified recombinant SOD1 protein was buffer exchanged into 200 mM NH_4OAc (pH 6.8) using centrifugal concentrators with a 10 kDa molecular weight cut-off. Buffer exchanged SOD1 was diluted to working concentrations in NH_4OAc, loaded into gold-coated borosilicate capillaries (made in-house), and subjected to nano-electrospray ionization (n=3 electrosprays per dilution). All spectra were externally calibrated using 1 mg/mL caesium-iodide in 50% n-propanol, and were processed using Masslynx 4.1 software. Dissociation constants were determined according to Rose *et al* (57).

Size-exclusion chromatography

We used the artificial disulphide knock-out SOD1 mutant C57A/C146A to assay heterodimer formation with hCCS. This allowed us to bind ebselen to Cys111 only while maintaining the conditions necessary for complexation. 25 μM SOD1 was incubated with 100 μM ebselen dissolved in 100 % DMSO for 3 hours at 20 ^oC. hCCS was desalted into nitrogen purged buffer. The complex was formed with 250 pmoles of both SOD1 and hCCS and was observed as described previously (22). Ebselen-free SOD1 was also treated with DMSO.

Human cell culture and transfection

HEK293T (ATCC CRL-3216) cells were maintained in DMEM high glucose (Life Technologies) supplemented with L-glutamine, antibiotics (penicillin and streptomycin) and 10% FBS (Gibco) in uncoated 75 cm^2 plastic flasks, and were grown at 37°C, 5% CO_2 in a humidified atmosphere. Cells were transiently transfected with SOD1 cDNA (either wild-type or mutant) cloned in the pHLsec plasmid(58) using polyethylenimine (PEI), as described previously[4], with a DNA:PEI ratio of 1:1 (50 μg/flask DNA, 50 μg/flask PEI). For wild-type SOD1, 25 μg/flask of cDNA was used (mixed with an equal amount of empty DNA vector) to compensate for the lower expression level of the mutants. [U-^{15}N]-BioExpress6000 medium (Cambridge Isotope Laboratories) was used for in-cell NMR samples, supplemented with 2% FBS, antibiotics and 10 μM of $ZnSO_4$. Ebselen treatment was performed by adding 200 μM ebselen to the external medium 24 h before collecting the cells. 200 μM was the highest concentration of ebselen which preserved cell viability and protein expression, chosen within a 10 μM – 1 mM range.

In-cell NMR sample preparation

Samples for in-cell NMR were prepared following a reported protocol (59). Briefly, transfected cells were detached with trypsin, suspended in DMEM + 10% FBS, washed once with PBS and re-suspended in one pellet volume of DMEM supplemented with 90 mM glucose, 70 mM HEPES and 20% D_2O. The cell suspension was transferred in a 3 mm Shigemi NMR tube, which was gently spun to sediment the cells. Cell viability before and after NMR experiments was assessed by trypan blue staining. After the NMR experiments, the cells were collected and the supernatant was checked for protein leakage by NMR.

NMR experiments

NMR spectra, both in-cell and *in vitro*, were collected at 308 K at a 950 MHz Bruker Avance III spectrometer, equipped with a CP TCI CryoProbe. For cell samples, 2D ^{1}H-^{15}N SOFAST HMQC (60) spectra (~1 h) were recorded with 64 scans, 2048 points, 128 increments and a 0.3 s recycle delay. For *in vitro* NMR, samples of 130 µM E,Zn-SOD1 in PBS, pH 7.4 were analyzed in 3 mm NMR tubes. 2D ^{1}H-^{15}N SOFAST HMQC spectra (~40 m) were recorded with 32 scans, 2048 points, 192 increments and a 0.3 s recycle delay.

The NMR spectra collected were processed with Topspin NMR data-processing software. The in-cell NMR spectra were further processed by subtracting a spectrum of cells transfected with empty vector, acquired in the same experimental conditions, to eliminate the signals arising from partial ^{15}N labelling of other cellular components.

Western Blot analysis

Cell lysates were prepared by freeze-thaw cycles in PBS buffer followed by centrifugation to remove the insoluble fraction. SOD1 (both wild-type and mutants) was stained with a rabbit polyclonal anti-superoxide dismutase 1 antibody (Abcam: ab16831, diluted 1:2000 to 0.5 mg/mL); a goat anti-rabbit IgG (whole molecule)-peroxidase secondary antibody (Sigma:A0545) was used, diluted at 1:80,000. SOD1 expression levels were normalized to GAPDH, which was stained with a rabbit polyclonal anti-GAPDH antibody (Abcam: ab9485, diluted at 1:2000). LiteAblot EXTEND chemiluminescent substrate (EuroClone) was used for detection.

Acknowledgments:

This work was funded by the Motor Neurone Disease Association and the MRC-MRF, grant numbers Hasnain/Apr15/833-791 and MRF-060-0002-RG-HASNA respectively awarded to SSH, SVA & GSAW. We would like to thank the beamline staff on I02 at Diamond Light Source and Proxima1 at SOLEIL. Access to the mammalian expression

for in-cell NMR and solution NMR at CERM/CIRMMP (PID: 1940) was funded by Instruct, part of the European Strategy Forum on Research Infrastructures (ESFRI) and supported by national member subscriptions. Specifically, we thank the EU ESFRI Instruct Core Centre CERM-Italy.

Author Contributions:

MJC determined ebselen binding, produced the crystal structure and wrote the paper. **GSAW** conceived the work, designed a number of experiments, performed the CCS binding assay, interpreted the results and wrote the paper. **LeB** grew and transfected the human cells, performed the western blot analysis, analyzed the data and wrote the paper. **EL** designed and performed the NMR experiments, analyzed the data and wrote the paper. **EM** grew and transfected the human cells and analyzed the data. **LM** designed, performed and analysed mass spectrometry experiments and edited the manuscript. **JY** analysed mass spectrometry experiments and edited the manuscript. **PMO** conceived the idea that ebselen and ebsulphur could engage SOD1 Cys111 and provided a small array of cysteine reactive molecules for bioanalysis. **SVA** conceived the work, designed the crystallographic work and wrote the paper. **LuB** conceived the work, designed the NMR experiments and wrote the paper. **SSH** conceived and planned the project, and wrote the paper.

Competing financial interests

The authors declare no competing financial interests

References:

1. Rosen DR et al. (1993) Mutations in Cu/Zn superoxide dismutase gene are associated with familial amyotrophic lateral sclerosis. *Nature* 362:59–62.
2. Yerbury JJ et al. (2016) Walking the tightrope: proteostasis and neurodegenerative disease. *J Neurochem* 137:489–505.
3. McCord JM, Fridovich I (1969) Superoxide Dismutate An enzymic function for erthrocuprein (Hemocurprein). *J Biol Chem* 244:6049–6055.
4. Carrico RJ, Deutsch HF (1970) The Presence of Zinc in Human Cytocuprein and Some Properties of the Apoprotein. *J Biol Chem* 245:723–727.
5. Wood E, Dalgleish D, Bannister W (1971) Bovine Erythrocyte Cupro-Zinc Protein. *Eur J Biochem* 18:187–193.
6. Forman HJ, Fridovich I (1973) On the Stability of Bovine Superoxide Dismutase: Thef Effects of Metals. *J Biol Chem* 248:2645–2650.
7. De Raeve H et al. (1997) Decreased Cu,Zn-SOD activity in asthmatic airway epithelium: correction by inhaled corticosteroid in vivo. *Am J Physiol* 272:L148–L154.
8. Ghosh S et al. (2013) Disulfide Bond As a Switch for Copper-Zinc Superoxide Dismutase Activity in Asthma. *Antioxid Redox Signal* 18:412–423.
9. Lang L et al. (2015) SOD1 aggregation in ALS mice shows simplistic test tube behavior. *Proc Natl Acad Sci U S A* 112:9878–9883.
10. Luchinat E et al. (2014) In-cell NMR reveals potential precursor of toxic species from SOD1 fALS mutants. *Nat Commun* 5.

11. Jonsson PA et al. (2006) Disulphide-reduced superoxide dismutase-1 in CNS of transgenic amyotrophic lateral sclerosis models. *Brain* 129:451–464.
12. Bourassa MW, Brown HH, Borchelt DR, Vogt S, Miller LM (2014) Metal-deficient aggregates and diminished copper found in cells expressing SOD1 mutations that cause ALS. *Front Aging Neurosci* 6:1–6.
13. Proctor EA et al. (2016) Nonnative SOD1 trimer is toxic to motor neurons in a model of amyotrophic lateral sclerosis. *Proc Natl Acad Sci* 113:614–619.
14. Antonyuk S et al. (2005) Structural consequences of the familial amyotrophic lateral sclerosis SOD1 mutant His46Arg. *Protein Sci* 14:1201–1213.
15. Banci L et al. (2009) Structural and dynamic aspects related to oligomerization of apo SOD1 and its mutants. *Proc Natl Acad Sci U S A* 106:6980–6985.
16. Wang Q, Johnson JL, Agar NYR, Agar JN (2008) Protein Aggregation and Protein Instability Govern Familial Amyotrophic Lateral Sclerosis Patient Survival. *PLoS Biol* 6:1508–1526.
17. Pratt AJ et al. (2014) Aggregation propensities of superoxide dismutase G93 hotspot mutants mirror ALS clinical phenotypes. *Proc Natl Acad Sci U S A* 111:E4568–E4576.
18. McAlary L, Aquilina JA, Yerbury JJ (2016) Susceptibility of Mutant SOD1 to Form a Destabilized Monomer Predicts Cellular Aggregation and Toxicity but Not In vitro Aggregation Propensity. *Front Neurosci* 10:499.
19. Wright GSA, Antonyuk S V., Kershaw NM, Strange RW, Hasnain SS (2013) Ligand binding and aggregation of pathogenic SOD1. *Nat Commun* 4:1–10.
20. Auclair JR, Boggio KJ, Petsko GA, Ringe D, Agar JN (2010) Strategies for stabilizing superoxide dismutase (SOD1), the protein destabilized in the most common form of familial amyotrophic lateral sclerosis. *Proc Natl Acad Sci U S A* 107:21394–21399.
21. Banci L et al. (2012) Interaction of Cisplatin with Human Superoxide Dismutase. *J Am Chem Soc* 134:7009–7014.
22. Wright GSA, Antonyuk S V., Hasnain SS (2016) A faulty interaction between SOD1 and hCCS in neurodegenerative disease. *Sci Rep* 6:1–9.
23. Schewe T (1995) Molecular Actions of Ebselen - an Antiinflammatory Antioxidant. *Gen Pharmacol* 26:1153–1169.
24. Yamaguchi T et al. (1998) Ebselen in Acute Ischemic Stroke: A Placebo-Controlled, Double-blind Clinical Trial. *Stroke* 29:12–17.
25. Singh N et al. (2013) A safe lithium mimetic for bipolar disorder. *Nat Commun* 4:1–14.
26. Saito I et al. (1998) Neuroprotective Effect of an Antioxidant, Ebselen, in Patients with Delayed Neurological Deficits after Aneurysmal Subarachnoid Hemorrhage. *Neurosurgery* 42:269–277.
27. Wood-Allum CA et al. (2006) Impairment of mitochondrial anti-oxidant defence in SOD1-related motor neuron injury and amelioration by ebselen. *Brain* 129:1693–1709.
28. Shim JS, Liu JO (2014) Recent advances in drug repositioning for the discovery of new anticancer drugs. *Int J Biol Sci* 10:654–663.
29. Ito H et al. (2008) Treatment with edaravone, initiated at symptom onset, slows motor decline and decreases SOD1 deposition in ALS mice. *Exp Neurol* 213:448–455.
30. Ray SS et al. (2004) An Intersubunit Disulfide Bond Prevents in Vitro Aggregation of a Superoxide Dismutase-1 Mutant Linked to Familial Amytrophic Lateral Sclerosis. *Biochem* 43:4899–4905.
31. McAlary L, Yerbury JJ, Aquilina JA (2013) Glutathionylation potentiates benign superoxide dismutase 1 variants to the toxic forms associated with amyotrophic lateral sclerosis. *Sci Rep* 3:1–6.
32. Winkler DD et al. (2009) Structural and Biophysical Properties of the Pathogenic SOD1 Variant H46R/H48Q. *Biochem* 48:3436–3447.
33. Freedberg DI, Selenko P (2014) Live Cell NMR. *Annu Rev Biophys* 43:171–192.
34. Luchinat E, Banci L (2017) In-cell NMR: a topical review. *IUCrJ* 4:108–118.

35. Banci L, Barbieri L, Bertini I, Cantini F, Luchinat E (2011) In-cell NMR in E. coli to Monitor Maturation Steps of hSOD1. *PLoS One* 6:e23561.
36. Banci L et al. (2013) Atomic-resolution monitoring of protein maturation in live human cells by NMR. *Nat Chem Biol* 9:297–299.
37. Banci L et al. (2012) Human superoxide dismutase 1 (hSOD1) maturation through interaction with human copper chaperone for SOD1 (hCCS). *Proc Natl Acad Sci U S A* 109:13555–13560.
38. Mercatelli E, Barbieri L, Luchinat E, Banci L (2016) Direct structural evidence of protein redox regulation obtained by in-cell NMR. *Biochim Biophys Acta* 1863:198–204.
39. Sakurai T et al. (2006) Ebselen, a seleno-organic antioxidant, as an electrophile. *Chem Res Toxicol* 19:1196–1204.
40. Zhao R, Holmgren A (2002) A Novel Antioxidant Mechanism of Ebselen Involving Ebselen Diselenide, a Substrate of Mammalian Thioredoxin and Thioredoxin Reductase. *J Biol Chem* 277:39456–39462.
41. Rahman I, MacNee W (2000) Oxidative stress and regulation of glutathione in lung inflammation. *Eur Respir Jounal* 16:534–554.
42. Lin MT, Beal MF (2006) Mitochondrial dysfunction and oxidative stress in neurodegenerative diseases. *Nature* 443:787–795.
43. Sahiner UM, Birben E, Erzurum SC, Sacksen C, Kalayci O (2011) Oxidative Stress in Asthma. *World Allergy Organ J* 4:151–158.
44. Karch CM, Prudencio M, Winkler DD, Hart PJ, Borchelt DR (2009) Role of mutant SOD1 disulfide oxidation and aggregation in the pathogenesis of familial ALS. *Proc Natl Acad Sci U S A* 106:7774–7779.
45. Deng H-X et al. (1993) Amyotrophic lateral sclerosis and structural defects in Cu, Zn superoxide dismutase. *Science (80-)* 261:1047–1051.
46. Borchelt DR et al. (1995) Superoxide Dismutase 1 Subunits with Mutations Linked to Familial Amyotrophic Lateral Sclerosis Do Not Affect Wild Type Subunit Function. *J Biol Chem* 270:3234–3238.
47. Sato T et al. (2005) Rapid disease progression correlates with instability of mutant SOD1 in familial ALS. *Neurology* 65:1954–1957.
48. Beal MF et al. (1997) Increased 3-Nitrotyrosine in Both Sporadic and Familial Amyotrophic Lateral Sclerosis. *Ann Neurol* 42:644–654.
49. Zembowicz A, Hatchett RJ, Radziszewski W, Gryglewski RJ (1993) Inhibition of Endothelial Nitric Oxide Synthase by Ebselen. Prevention by Thiols Suggests the Inactivation by Ebselen of a Critical Thiol Essential for the Catalytic Activity of Nitric Oxide. *J Pharmacol Exp Ther* 267:1112–1118.
50. Masumoto H, Sies H (1996) The reaction of Ebselen with peroxynitrite. *Chem Res Toxicol* 9:262–267.
51. Porciúncula LO, Rocha JBT, Boeck CR, Vendite D, Souza DO (2001) Ebselen prevents excitotoxicity provoked by glutamate in rat cerebellar granule neurons. *Neurosci Lett* 299:217–220.
52. Battye TGG, Kontogiannis L, Johnson O, Powell HR, Leslie AGW (2011) iMOSFLM: a new graphical interface for diffraction-image processing with MOSFLM. *Acta Crystallogr Sect D Biol Crystallogr* D67:271–81.
53. Number 4 CCP (1994) The CCP4 suite: Programs for protein crystallography. *Acta Crystallogr Sect D Biol Crystallogr* D50:760–763.
54. Emsley P, Lohkamp B, Scott WG, Cowtan K (2010) Features and development of Coot. *Acta Crystallogr Sect D Biol Crystallogr* D66:486–501.
55. Murshudov GN et al. (2011) REFMAC5 for the refinement of macromolecular crystal structures. *Acta Crystallogr Sect D Biol Crystallogr* D67:355–367.
56. Lebedev AA et al. (2012) JLigand: a graphical tool for the CCP4 template-restraint library. *Acta Crystallogr Sect D Biol Crystallogr* D68:431–440.
57. Rose RJ et al. (2011) Quantitative analysis of the interaction strength and dynamics of human IgG4 half molecules by native mass spectrometry. *Structure* 19:1274–1282.
58. Aricescu AR, Lu W, Jones EY (2006) A time- and cost-efficient system for high-

level protein production in mammalian cells. *Acta Crystallogr D Biol Crystallogr* 62:1243–1250.
59. Barbieri L, Luchinat E, Banci L (2016) Characterization of proteins by in-cell NMR spectroscopy in cultured mammalian cells. *Nat Protoc* 11:1101–1111.
60. Schanda P, Brutscher B (2005) Very Fast Two-Dimensional NMR Spectroscopy for Real-Time Investigation of Dynamic Events in Proteins on the Time Scale of Seconds. *J Am Chem Soc* 127:8014–8015.

Figures & Tables

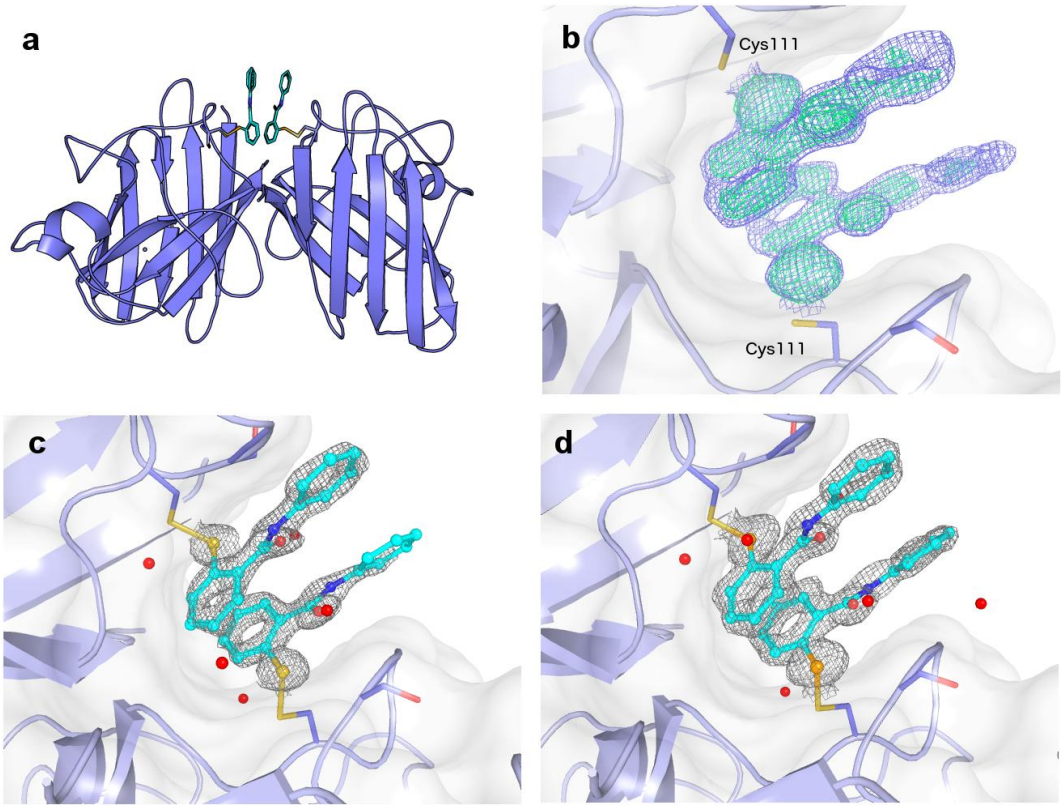

Fig. 1: The structure of ebselen and ebsulphur bound to SOD1. (**a**) Cartoon representation of the SOD1 dimer with ebselen or ebsulphur molecules shown as ball and stick and bound to Cys111 residues at the dimer interface. (**b**) Omit map revealing the electron density of the missing ebselen compound before modelling. 2Fo-Fc contoured at 1 σ in blue and Fo-Fc map contoured at 3 σ in green. (**c** and **d**) Electron density maps 2Fo-Fc contoured at 1 σ of (**c**) ebselen and (**d**) ebsulphur showing details of binding at Cys111 and proximal crystallographic waters.

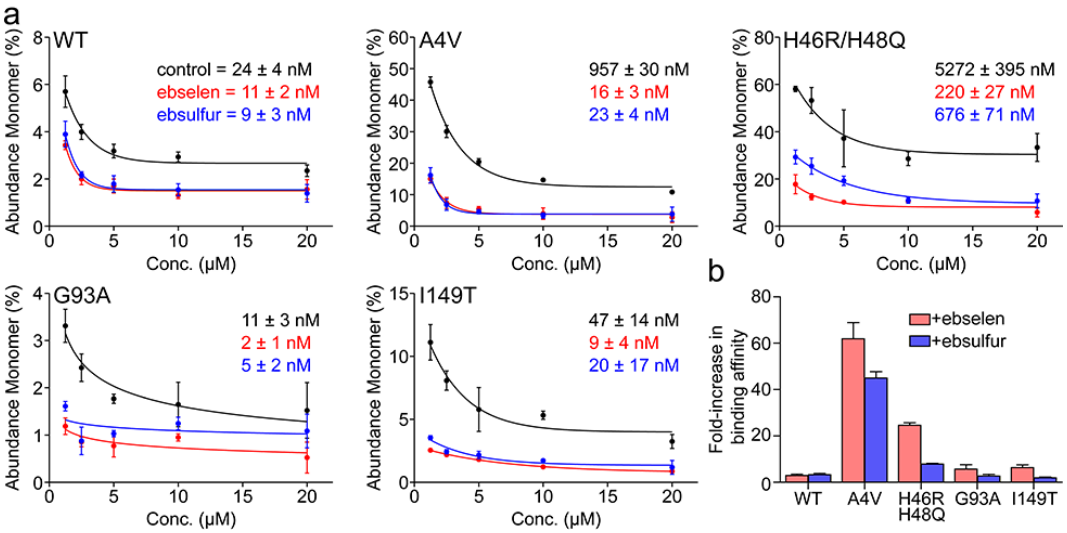

Fig. 2: Conjugation of ebselen and ebsulphur to SOD1 variants increases the binding affinity of the dimer. (**a**) SOD1 variants (wild-type, A4V, H46R/H48Q, G93A, and I149T) with ebselen (red), ebsulphur (blue), and without treatment (black) were buffer exchanged into 200 mM NH_4OAc and subject to nanoESI mass spectrometry at different protein concentrations under gentle conditions optimised to maintain non-covalent interactions. Curves show the percentage of monomer signal as a function of protein concentration with determined dimer K_D values inset for each SOD1 variant. (**b**) The fold-increase in binding affinity of each SOD1 variant when ebselen or ebsulphur is conjugated at Cys111.

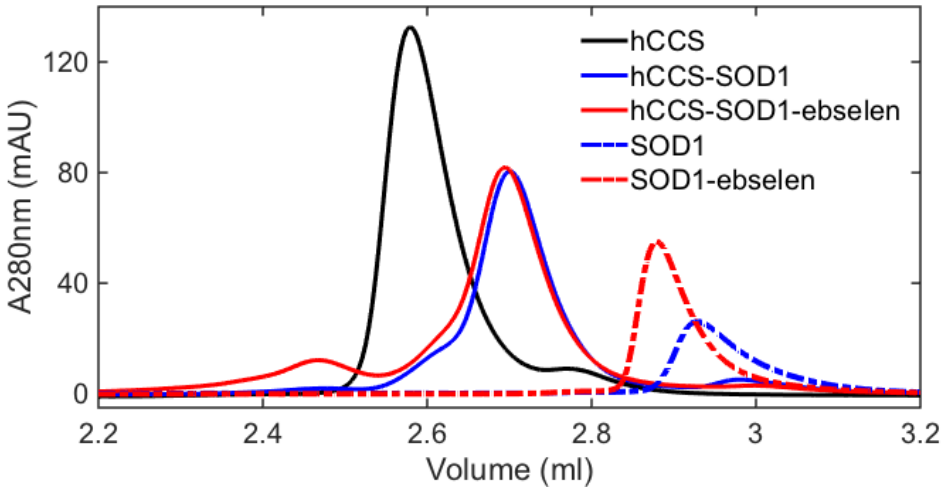

Fig. 3: Ebselen does not prevent heterodimer formation with hCCS. Size exclusion chromatograms showing how ebselen binding to C57/146A SOD1 promotes dimerization (blue dashed line to red dashed line) but does not inhibit complex formation with wild-type hCCS.

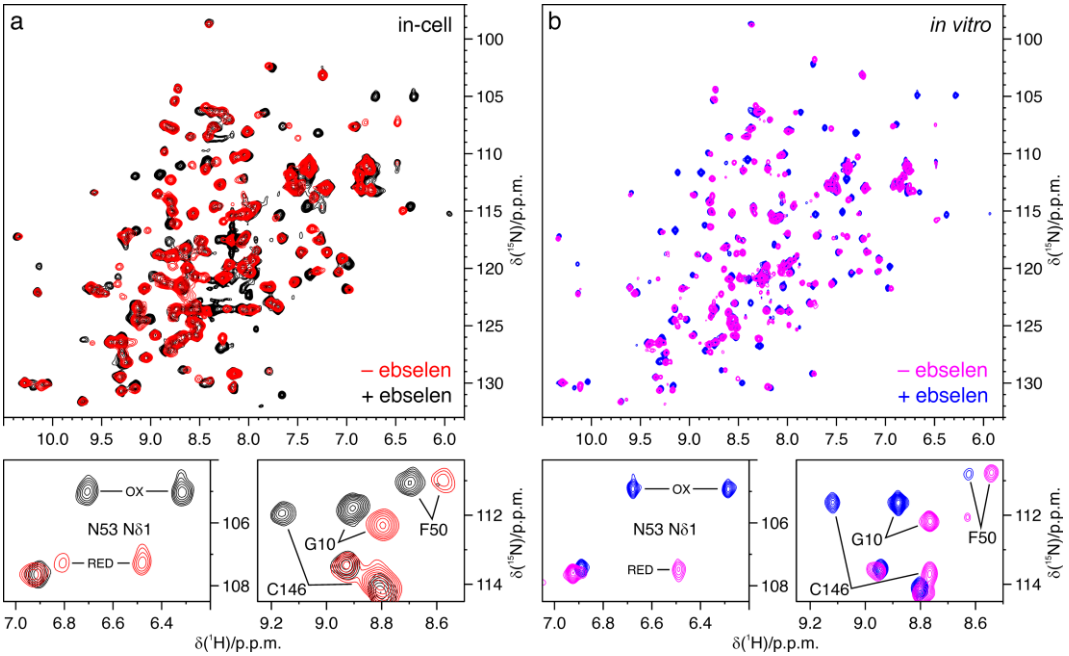

Fig. 4: Ebselen efficiently oxidizes SOD1 in living cells. (**a**) Overlay of ^{1}H-^{15}N NMR spectra acquired on human cells expressing [U-^{15}N] labelled wild-type E,Zn-SOD1 in absence (red) and in presence (black) of ebselen in the external medium. (**b**) Overlay of ^{1}H-^{15}N NMR spectra acquired on purified, disulphide-reduced [U-^{15}N] labelled wild-type E,Zn-SOD1 before (blue) and after (magenta) treatment with 1 equivalent of ebselen. Signals affected by the formation of the C57-C146 disulphide bond are labelled (bottom panels).

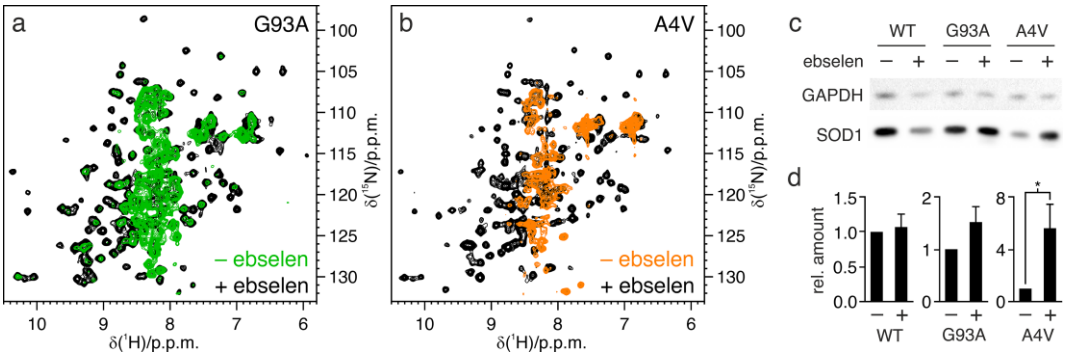

Fig. 5: Ebselen stabilizes ALS mutant SOD1 in living cells. (**a**) Overlay of ^{1}H-^{15}N NMR spectra acquired on human cells expressing [U-^{15}N] labelled SOD1 ALS mutants G93A (**a**) and A4V (**b**) in absence (green/orange) and in presence (black) of ebselen in the external medium. NMR signals clustered in the region around 8.3 p.p.m. (^{1}H) are characteristic of unstructured SOD1 species. (**c**) Western Blot analysis of cell lysates expressing wild-type and mutant SOD1 in absence and in the presence of ebselen. (**d**) expression levels of wild-type and mutant SOD1 in cell samples treated with ebselen relative to the corresponding untreated samples; error bars represent s.d. (n = 3); * indicates significant differences (ratio t-test, $p < 0.05$).

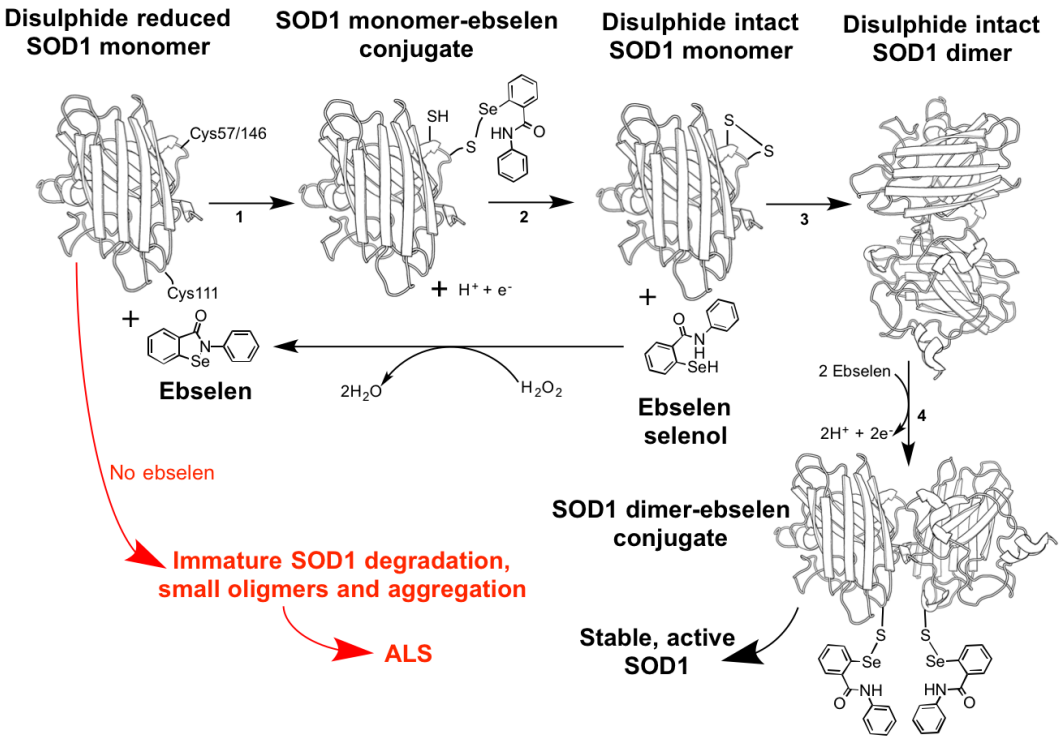

Fig. 6: Mechanism of SOD1 stabilization by ebselen. In the absence of ebselen monomeric, disulphide reduced, metal-free mutant SOD1 is highly likely to remain globally unfolded and be degraded or accumulate as small toxic oligomers or aggregates which are characteristic of ALS neural tissues (red). However, in reaction **1** ebselen forms a selenylsulphide bond with either Cys57 or Cys146 on newly translated SOD1. **2.** Selenol-disulphide exchange forms the SOD1 intra-subunit disulphide bond and frees the ebselen selenol. Reduction of hydrogen peroxide by ebselen selenol reforms the ebselen heterocycle. This recycling process indicates that relatively small amounts of ebselen could promote SOD1 maturation. **3.** SOD1 disulphide formation promotes correct folding, zinc binding and dimerization. **4.** Further modification of Cys111 by ebselen prevents monomerization by ALS mutations thus maintaining stable, active, fully metalated, homodimeric SOD1.

Table 1: Crystallographic statistics for SOD1 bound ebselen and ebsulphur structures.

	wtSOD1-ebselen	wtSOD1-ebsulphur
Data collection		
Space group	P 2_1	P 2_1
Cell dimensions		
a, *b*, *c* (Å)	38.10 67.84 51.04	38.05 67.96 51.18
α, β, γ (°)	90.00 106.35 90.00	90.00 106.73 90.00
Resolution (Å)	49.01 – 1.50 (1.52-1.50) *	67.84 – 1.30 (1.33-1.30) *
R_{merge}	11.7 (59.4)	6.4 (56.6)
$I / \sigma I$	5.9 (1.5)	7.1 (1.4)
Completeness (%)	99.9 (99.5)	98.8 (97.7)
Redundancy	3.1 (3.1)	3 (2.8)
Refinement		
No. reflections	39891	60537
R_{work} / R_{free}	16.05 / 21.24	14.53 / 18.10
No. atoms		
Protein	2241	2274
Ligand/ion	46	46
Water	309	311
B-factors		
Protein	12.35	15.45
Ligand/ion	10.32	15.47
Water	29.27	35.38
R.M.S. deviations		
Bond lengths (Å)	0.013	0.015
Bond angles (°)	1.607	1.683

*Values in parentheses are for highest-resolution shell.

2.3. Sample preparation: towards protein interacting systems by in-cell NMR

2.3.1. Solution in-cell NMR meets solid state NMR

Despite the fact that in-cell NMR is a powerful technique to study protein structures and dynamic inside cells, the nature of the investigated protein and the complexity of the intracellular environment can considerably impact on the possibility of detecting the NMR signals for the protein of interest. In fact, the protein experiences interactions of various nature that might affect its relaxation properties: from specific direct interaction with physiological partners to weak and non-specific ones with molecular assemblies or cellular components (nucleic acids, cellular membranes, protein complexes) that slow down the average molecular tumbling rate and increase relaxation rates and signal broadening [60, 61, 62, 63].

We hypothesized that soluble proteins that experience intermolecular interactions so strong that their lines are broadened beyond detection in solution could, at least in part, behave as a solid within the cells. For these systems, solid state NMR could be a suitable technique to overcome the limitations of solution in-cell NMR.

When the molecular tumbling is abolished, one can imagine that the protein will be observed as it was “frozen” in a set of orientations with respect to the magnetic field. In this regime, each molecule senses a different value for all the nuclear spin interactions, which are anisotropic in nature, instead of rapidly interconverting among different values. In a static sample, therefore, each nuclear signal intensity would be spread over a frequency range larger than a single line. To average out these effects, Magic Angle Spinning (MAS) condition is applied to

the sample. In the MAS condition the sample is tilted by a specific angle (54.74°) respect to the external magnetic field direction that averages out the dipolar interaction, and it undergoes a fast spinning to mimic molecular tumbling in solution. In the last years, MAS ssNMR was successfully used to investigate molecules inside native membranes or to characterize proteins involved in high molecular-weight complexes within the cytoplasm. [64, 65]. In these examples, the protein of interest was either extracted by isolating the native membranes, or the whole cell preparation was analyzed at sub-freezing temperatures. Here, we investigated the possibility of applying room-temperature MAS ssNMR to investigate proteins which are invisible in the cell, due to their interactions with cellular components.

2.3.1.1. Protein models

Cytochrome c (Cyt c) is a conserved globular hemeprotein of 104 amino acid residues in mammals that shows multiple functions in the cell: it is essential in electron transfer in the mitochondrial respiratory chain in the IMS, and has a pivotal role in triggering cell apoptotic pathways [66]. In the IMS, Cyt c also exerts a peroxidase cardiolipin activity [67], it is involved in the mitochondrial oxidative protein folding machinery [68], and functions as radical scavenger [69]. It has been selected as a case study for cellular solid state NMR trials because it is one of those soluble proteins that are not detectable by solution in-cell NMR and it might has a solid-like behavior since it has been reported to interact and to bind the anionic phospholipid cardiolipin [66]. Indeed, it was previously shown that Cyt c expressed in bacteria cannot be detected by solution NMR, also upon cell lysis, due to strong interactions of its surface lysine residues with the bacterial membrane, or with negatively charged macromolecules [70].

Human Profilin 1 (PFN1) is a ubiquitously expressed 139-residues globular

protein involved in a complex network of molecular interactions [71]. Recently mutations on the PFN1 gene have been linked to familial ALS. Three single-amino acid mutants have been found to be pathogenic for fALS inducing PFN1 aggregation, C71G, M114T and G118V, and a fourth mutant, E117G, has been proposed to be a risk factor for developing ALS [73]. To date, little is known about the mechanisms through which PFN1 is involved in ALS pathogenesis. It has been shown that PFN1 pathological mutants display aggregation propensities, display functional differences compared with the wild-type protein, such as a lower bound actin level, inhibition of axonal outgrowth and dynamics [REF71]. The effect of these mutations on PFN1 protein stability and structure revealed that mutants create a cleft that extend into the interior of PFN1 destabilizing the native protein's conformation [74]. Among the reported profilin 1 mutants, M114T was selected as a case study for cellular solid state NMR trials, as it was found to form insoluble aggregates, which are expected to have a solid-like behavior, when overexpressed in bacteria.

The human Menkes 6 (MNK6) protein is the sixth soluble domain of the ATP7A protein presented in (Protein model system 2.5.2.1). It is also not detectable by solution in-cell NMR, and therefore it was selected as it benefits from in cell SSNMR characterization.

2.3.1.2. Results

We first assessed whether intracellular soluble proteins could be sedimented under MAS conditions at room temperature. To this aim, we focused on the soluble protein SOD1, which was already characterized by solution in-cell NMR, expressed in bacteria. SOD1 was overexpressed in *E. coli* grown in [^{15}N, ^{13}C] enriched minimal medium M9 (Methods 4.2.1.1). The signals observed in the monodimentional experiments (^{1}H-^{13}C INEPT) indicated that a fraction of the

labelled molecules of the cell is mobile. Simultaneously, the ^{13}C-^{13}C DARR [75] spectrum, Fig. 2, contained signals likely arising from an immobilized protein fraction inside the cells. Unfortunately, the low labeling specificity and the low resolution of the signals did not allow us to identify unambiguously signals belonging to SOD1. Therefore, further tests were focused on more suitable proteins, which were expected to behave as solids within the cells, either due to strong interactions with other cellular components or to the propensity to form insoluble aggregates.

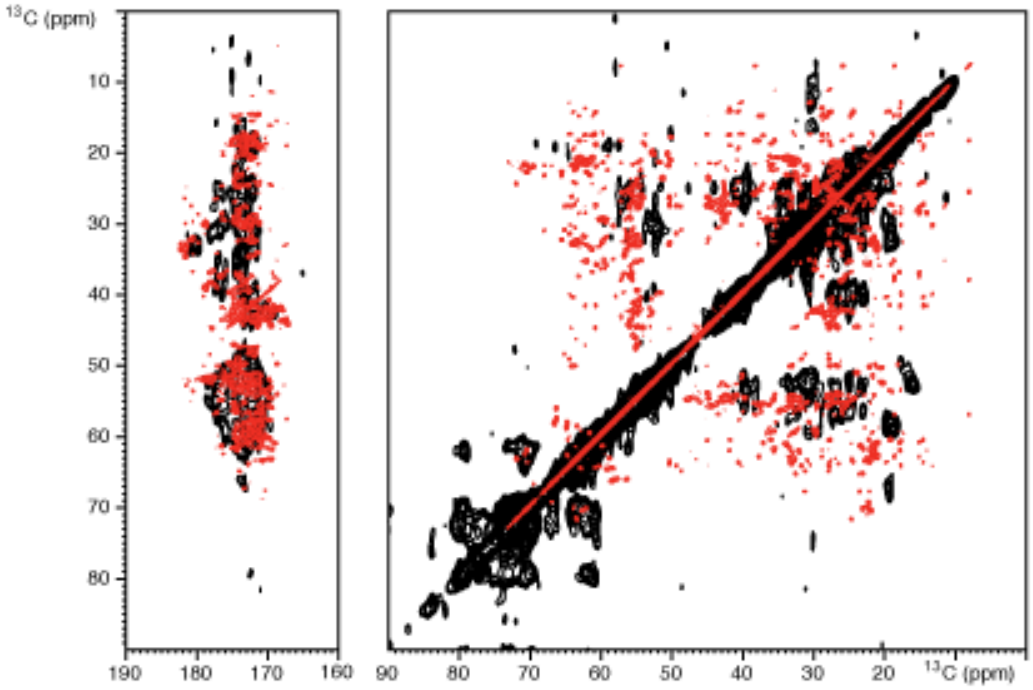

Figure 2. 2D ^{13}C-^{13}C DARR in-cell solid state NMR spectra: *E. coli* cells expressing SOD1 (black) superimposed to a reference NMR spectrum of SOD1 in vitro (red). The spectra are recorded at 700 MHz, 14 kHz, τ mix= 50 ms, rotor 3.2 mm, T=276 K (effective sample temperature).

The first candidate protein not detectable by solution in-cell NMR investigated was human cytochrome c (Cyt c). The protein was overexpressed in *E. coli* grown in [^{15}N ^{13}C] enriched minimal medium M9 (H_2O) (Methods 4.2.1.2). The ^{13}C-^{13}C DARR spectrum of Cyt c in *E.coli,* shown in Fig 3, presented unresolved peaks. This might be due to the sample low labeling

selectivity: in fact, the cytochrome c expression protocol requires three days of protein expression in [^{15}N ^{13}C] enriched media. In order to assess the contribution of Cyt c to the spectra, we repeated the same NMR experiments on a 'blank' *E. coli* sample not overexpressing any protein, prepared with the same expression protocol (Methods 4.2.1.2). Ideally, subtraction of the 'blank' spectrum would allow to better discriminate which peaks belong to the protein of interest. Despite the low spectral resolution and the presence of artifacts did not allow a proper subtraction, qualitative comparison of the two ^{13}C-^{13}C DARR spectra suggests that no resolved signals of Cyt c are present in the first spectrum (Figure 3).

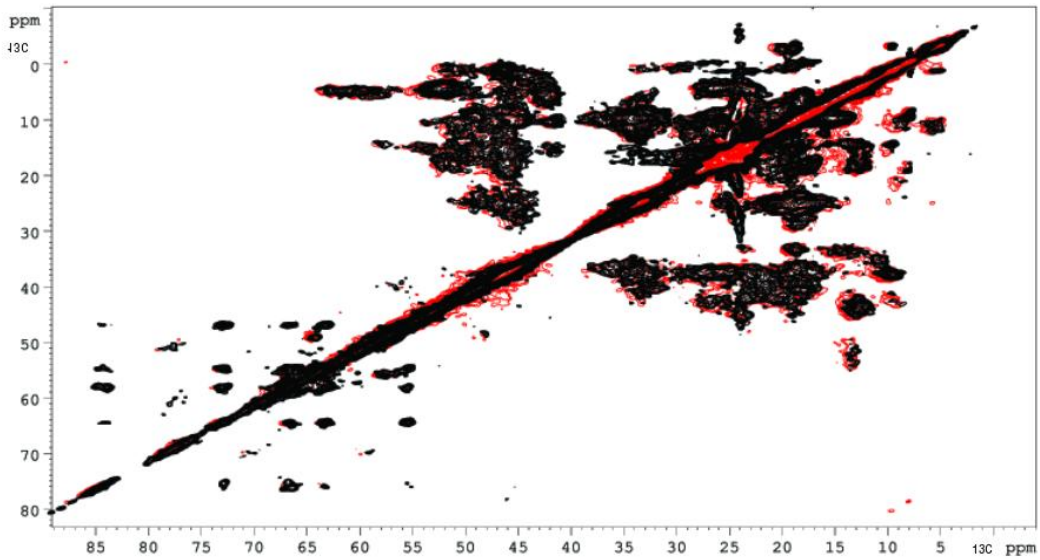

Figure 3. 2D ^{13}C-^{13}C DARR in-cell solid state NMR in black the spectrum of *E. coli* expressing cytochrome c. In red the superimposition of a 'blank': in cell spectrum of *E. coli* not expressing cytochrome c. The spectra are recorded at 700 MHz, 11 kHz, τ mix= 50 ms, rotor 4 mm, T=284 K (effective sample temperature).

Overall, these spectra show that the non-specific labeling of all cellular components greatly limits the ability to obtain well-resolved signals of the protein of interest.

In an attempt to improve both the resolution and the selectivity of the NMR experiment towards the signals of interest, we exploited heteronuclear correlation experiments, namely NCA double cross-polarization [76]. In parallel, partial

deuteration of the expressed protein was tested. To this aim, we set up a protein overexpression protocol in minimal medium containing ≈ 98% D_2O (Methods 4.2.1.3) without previous adaptation. In this protocol [^{1}H,^{13}C] glucose was used as carbon source, resulting in side chain deuteration mostly at the α and partially at the β position [77]. With this labeling protocol, partially deuterated, [^{13}C,^{15}N]-labeled insoluble mutant of PFN1, M114T, was expressed.

The NCA spectra recorded, shown in Fig 4, present low resolution in the nitrogen dimension. Nevertheless, there are some resolved peaks in the Cα region, and some glycine signals can be distinguished (~ 43 ppm ^{13}C).

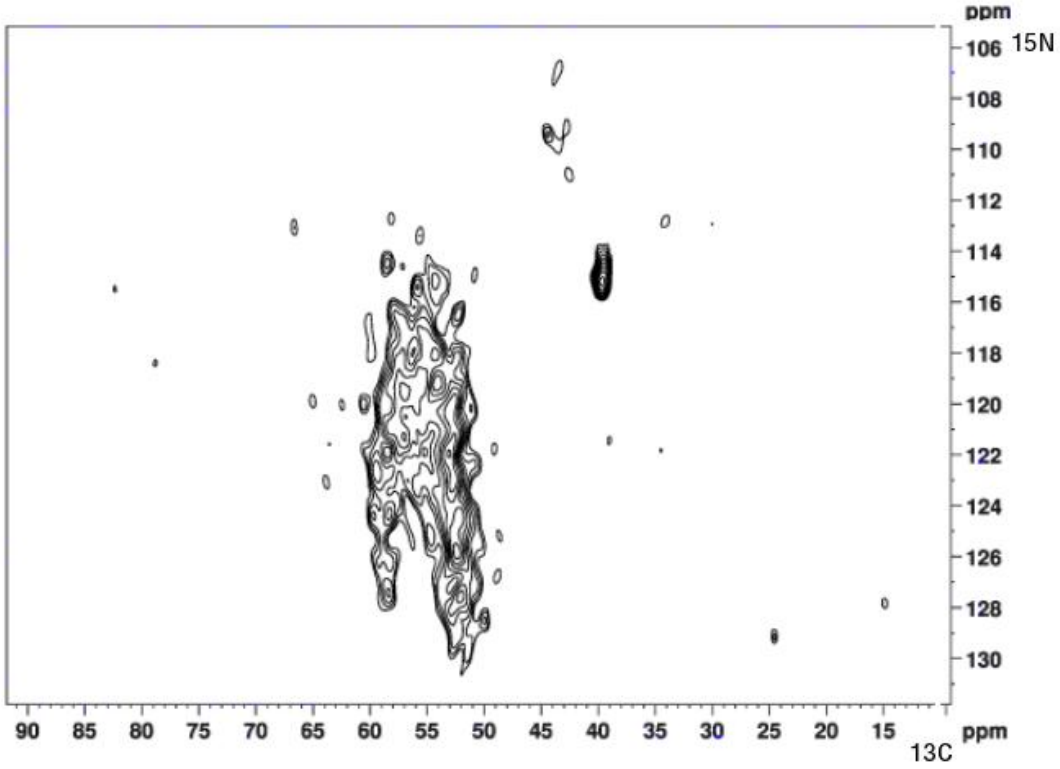

Figure 4. 2D ^{15}N-^{13}C NCA in-cell solid state NMR spectrum Profilin mutant M114T overexpressed in *E. coli* grown in ≈98% D_2O**.** The spectra are recorded at 850 MHz, 14 kHz, 3.2 mm, NCA contact time=3 ms, T=303K (effective sample temperature).

Such low resolution might still be due to the cellular background arising from non-specific labeling or, more likely, to the fact that the protein forms amorphous aggregates where multiple protein conformations spread the resonances in the ssNMR spectra.

Finally, we assessed whether chemical cross-linking could stabilize the immobilized conformation of the cellular components, producing a more solid-like cell sample, despite sacrificing cell viability. To this aim, we incubated bacterial cells overexpressing MNK6 with Paraformaldehyde (PFA) (Methods 4.2.1.4). In addition, CP-NOE pulse sequences were applied to better monitor the changes in intensity of the mobile part of the sample [78]. In the spectra shown in A Fig. 5, we observed a general signal decrease suggesting that PFA fixation decreased the amount of mobile cellular components to some extent. Despite this, the ^{13}C-^{13}C DARR ssNMR on the fixed cells sample presented in B Fig. 5, showed signals with low intensity and low resolution. Alternative cellular fixation procedures with different percentage of PFA and/or diverse fixative compounds might be investigated in order to further decrease the internal protein mobility.

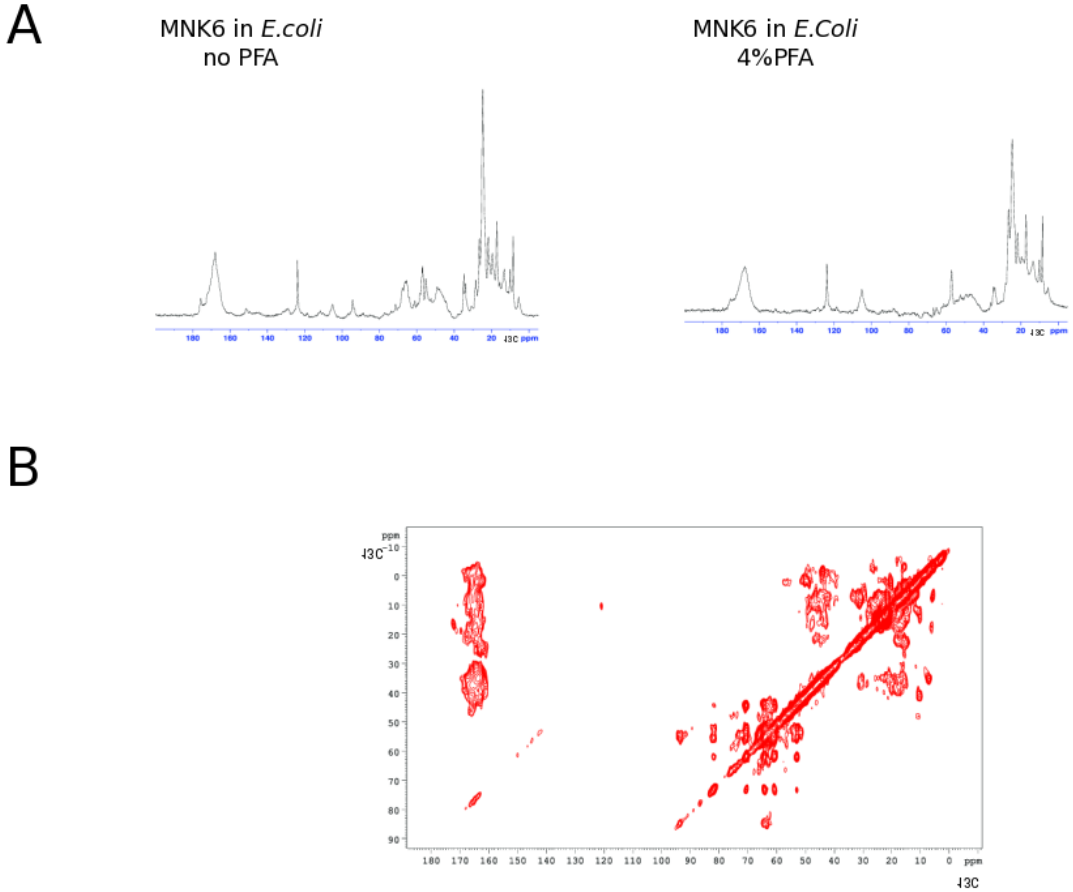

Figure 5. Solid state NMR of *E. coli* overexpressing MNK6 in A) comparison between PFA treated and untreated cells with ^{1}H-^{13}C CP-NOE recorded at 700 MHz, 14 kHz, τ mix= 2.2 s, rotor 3.2 mm, T = 284 K (effective sample temperature) in B) 2D ^{13}C-^{13}C DARR in-cell solid state NMR recorded at 700 MHz, 14 kHz, τ mix= 2.2 s, rotor 3.2 mm, T = 284 K (effective sample temperature).

2.3.2. Merging DNA transfection and protein delivery electroporation

The approach for in-cell NMR in human cells recently developed in our laboratory relies on transient transfection and protein overexpression of human HEK293T cells, and allows stable isotope labeling of one or more proteins of interest. Using this protocol, metal and chaperone dependent maturation processes were successfully characterized for several proteins involved in copper homeostasis and redox regulation [13, 14]. In order to expand the strategies for sample production, the aim of this activity within my PhD project was to combine protein transfection with protein delivery techniques to characterize intracellular protein-protein interactions at atomic resolution. For such purpose, the ability to actively deliver isotope-labeled recombinant proteins by electroporation opens up many possibilities, such as greatly reducing the cellular background resulting from non-specific isotope incorporation, therefore gaining selectivity. Moreover, electroporation would allow the production of in-cell protein samples with various labeling strategies (e.g. selective modification of individual protein residues, fluorescent or paramagnetic tagging).

2.3.2.1. Protein model system

Copper is an essential trace metal central to eukaryotes life [79]. While it operates as cofactor for a wide range of catalytic functions, it can be potentially toxic for cells if its redox reactivity is not strictly controlled. Therefore, copper trafficking and homeostasis always occur throughout tightly regulated pathways involving copper transporting proteins [80]. Among the known copper-binding proteins, we focused on ATP7A, a major regulator of copper homeostasis in human cells. ATP7A, also called Menkes protein (MNK), is a P-type transmembrane ATPase involved in the maturation of secreted copper proteins. It is responsible for transferring copper from the cytosol to the Golgi lumen by receiving Cu(I) from

the cytosolic chaperone HAH1. ATP7A is also involved in the export of excess copper through fusion of ATP7A-enriched vesicles with the plasma membrane. Mutations in ATP7A lead to a dysfunction in copper transport across membranes that results in a fatal X-linked copper deficiency syndrome, the Menkes disease [81, 82]. ATP7A is constituted of four major regions: the transmembrane domain, the ATP-binding domain, the phosphatase domain and the cytosolic copper binding domain. The N-terminal copper-binding cytosolic region contains six folded domains, which share similar sequence, structure and a conserved Cu(I) binding motif (GMXCXXC) [83, 84]. The mechanism through which the metallochaperone HAH1 delivers Cu(I) to MNK cytosolic domains has been extensively detailed by *in vitro*, also by solution NMR [85, 86]. To achieve our purpose of expanding the sample preparation methods for in-cell NMR, we selected as a case study the metal-mediated transient complex formed between the first cytosolic domain of ATP7A (MNK1) and the copper chaperone HAH1.

2.3.2.2. Results

The first experimental step was the check of MNK1 suitability to be overexpressed in HEK293T cells and to be detectable by in-cell NMR experiments. As Fig. 6 shows in A, unfortunately HEK293T cells transiently transfected with a synthetic gene encoding MNK1 presented almost no signals belonging to a folded protein. Despite MNK1 being present in the sample, as confirmed by SDS-PAGE analysis, no signals related to MNK1 were detected as well in the spectrum of the cell lysate. This result might be related to non specific interactions occurring between MNK1 and other cellular components, that are still preserved when the cells are broken and the NMR experiments are run on the lysate.

We also performed in-cell NMR experiments on HAH1-transfected

HEK293T cells and, as it is reported in Fig. 6 B, we obtained a high-quality spectrum showing well resolved peaks where the signals arising from the HAH1 folded protein are clearly identified.

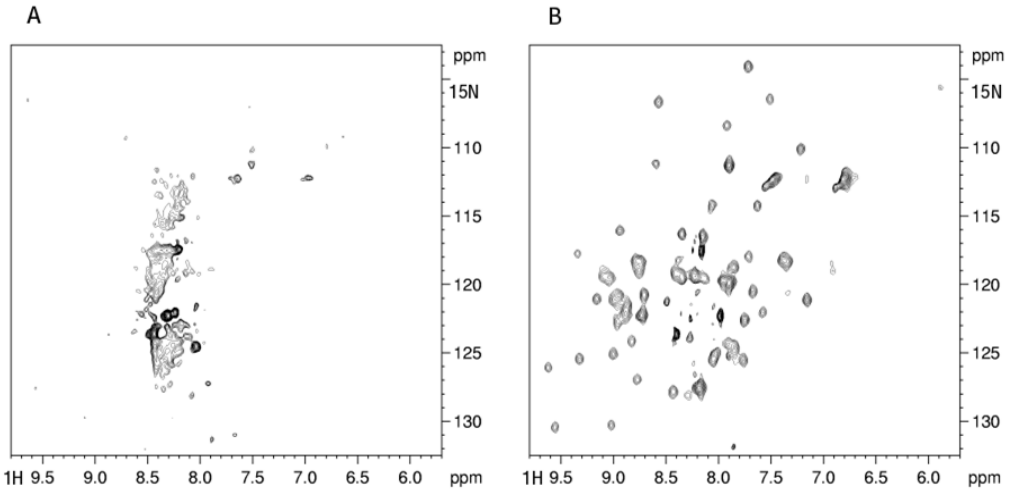

Figure 6. 2D ^{1}H-^{15}N SOFAST-HMQC in-cell *NMR* spectra of HEK293T cells in A) overexpressing wild type MNK1 protein; in B) overexpressing wild type HAH1 protein.

In light of these results, we changed our strategy and we aimed to express HAH1 in cells and subsequently incorporate, through electroporation, Cu(I)-loaded MNK1.

We performed *in vitro* NMR tests to verify that protein-protein interactions and complex formation occur upon titration of Cu-MNK1 with apo-HAH1, as this would be the reverse of what is known to occur *in vivo*, where HAH1 is the physiological metallo-chaperone that transfers copper to MNK1.

We followed the complex formation between ^{15}N Cu(I) MNK1 and apo-HAH1 via NMR titration starting with a Cu(I)MNK1 concentration of 70 µM. As shown in Fig. 7, some of the signals corresponding to residues in the proximity of the binding interface between MNK1 and HAH1 protein are shifted or broadened (E15, T25, Q28, G70), while other signals closer to the binding site disappear (T18, S21, C22).

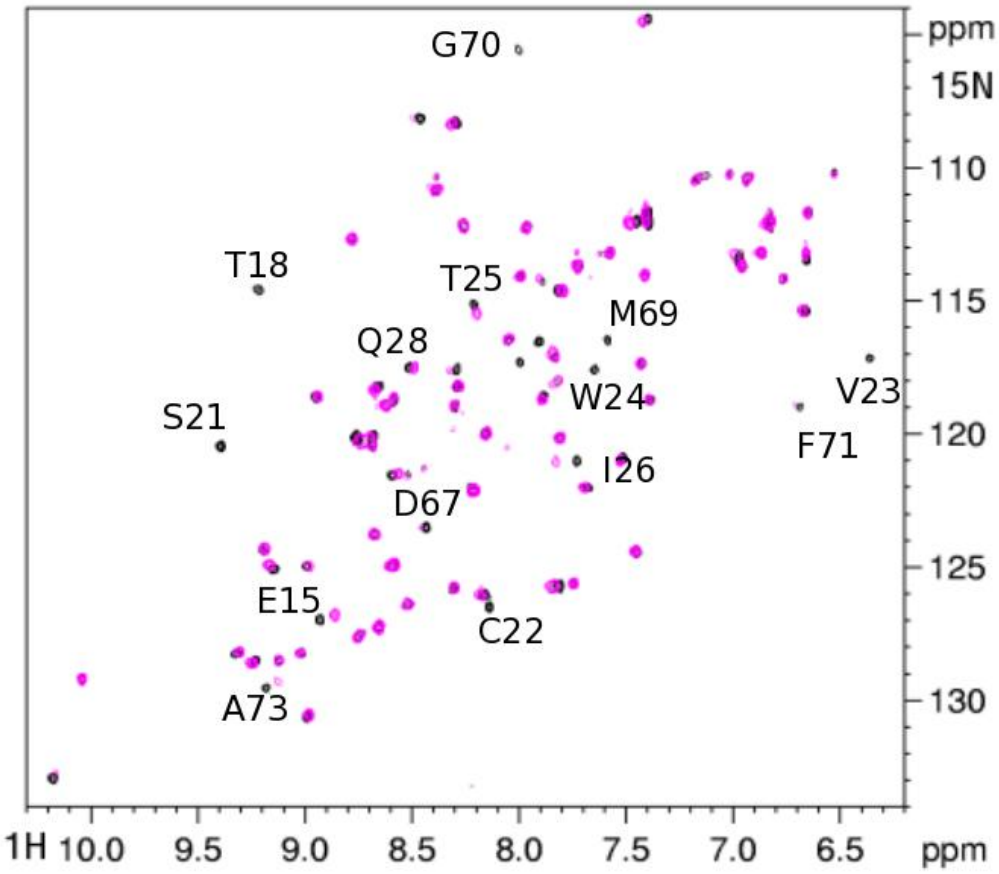

Figure 7. 2D ^{1}H-^{15}N SOFAST-HMQC *in vitro* NMR spectra comparison superimposition the spectrum of Cu(I)MNK1 protein, in black, and the complex Cu(I)MNK1-HAH1 formed, in purple.

In order to determine the percentage of MNK1 involved in the complex with HAH1, we performed ^{15}N NMR relaxation experiments to calculate the average molecular tumbling rate (τ) in a sample of MNK1:HAH1 in 1:1 molar ratio and for a protein concentration of 75μM each, in conditions comparable to the previous *in vitro* titrations. The data analysis of the ^{15}N relaxation rates reveals that ~50% of the 15N-Cu(I)MNK1 protein is complexed with HAH1.

We also tested the stability of the formed complex when it is inside a cellular lysate. From the NMR data, as is shown in Fig. 8, we can see that the spectrum maintain the characteristics of the complex formed and the peaks related to the Cu(I)MNK1 protein alone do not appear.

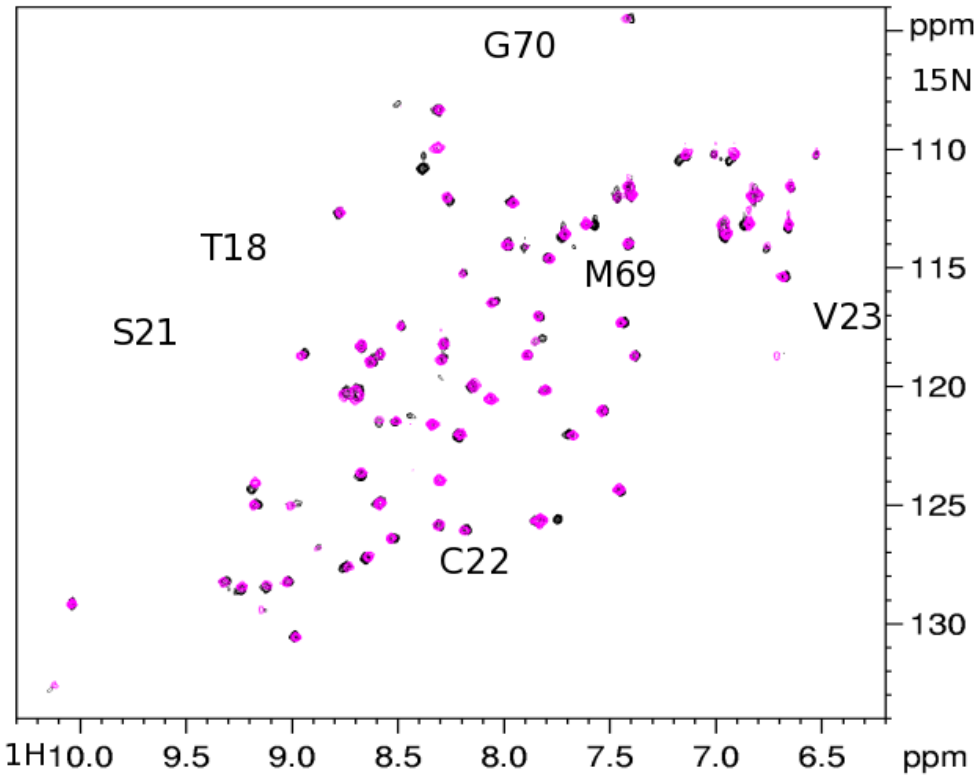

Figure 8. ^{1}H-^{15}N SOFAST-HMQC spectra comparison: in black the spectrum of Cu(I)MNK1-HAH1 complex in vitro 70 µM , in purple Cu(I)MNK1-HAH1 70 µM complex inside a HEK293T cellular lysate.

Having been able to detect by NMR the complex and its stability over the NMR experimental time in a cellular lysate, we were encouraged to start working on setting up the procedures for protein delivery. A series of 'small scale' electroporation trials in HEK293T cells were performed using purified Cu(I)MNK1 as protein to be delivered. The electroporation set up was followed according to [11]. Different electroporation conditions were tested and the protein insertion efficiency was followed and analyzed via Western Blot. The conditions that allowed higher levels of delivered protein were selected (METHODS 4.7.1).

Immunocytochemistry (ICC) analysis was performed in order to determine the delivered protein localization, after setting the best condition for cell adherence and fixation. Several florescence microscopy tests on the primary antibody against MNK1 revealed that it is not suitable for Fluorescence analysis because of a nonspecific cytosolic binding behavior of the primary antibody.

Viability tests had shown a 25-30% survival after the electroporation procedure in HEK293T cells.

A HEK293T-derived cell line stably overexpressing HAH1, previously obtained in our laboratory [87], was selected as an additional cellular system to perform delivery trials. From the characterization pursued by Western Blot and ICC analysis on this stable cell line, HAH1 protein expression levels and HAH1 localization were obtained (Methods 4.7.3). From the ICC data comparison between HEK293T cells transiently transfected with HAH1 and those stably expressing HAH1, the presence of HAH1 in the cytoplasm appears to be much more uniform in expression level and in distribution inside the stable cell line (METHODS 4.5). Therefore, the stable cell line for HAH1 was chosen as first operative system for MNK1 electroporation trials.

Before producing a 'full scale' in-cell NMR sample, in the first place we tested the MNK1 protein behavior at very low concentration in a cellular extract, mimicking at best the real cellular contest either for HEK293T cells or for the stable cell line for HAH1. Firstly, we tested some lysis conditions; the best ones resulted to be: a wash in PBS and 6 cycles of freeze and thaw. The total protein concentration of all the crude cell extracts was then determined by the Bradford assay. For the in-lysate NMR experiments, lysate of both HEK293T cells and of stable cell line for HAH1 were used. The total protein concentration was measured as 24mg/ml, pH 7.2. The Cu(I)MNK1 final concentration was 10 μM.

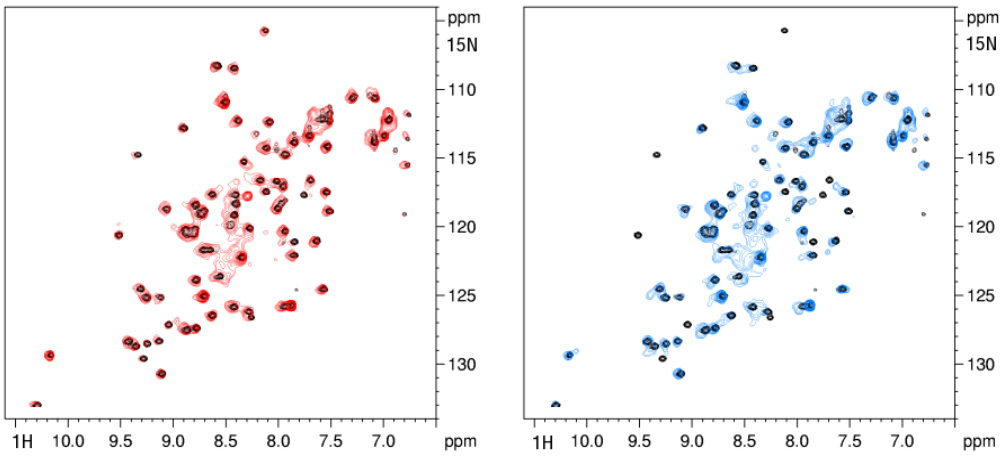

Figure 9. ^{1}H-^{15}N SOFAST-HMQC *in lysate* NMR spectra A) in red, 10 µM Cu(I)MNK1 in HEK293T cell crude extract B) in light blue, 10 µM Cu(I)MNK1 in stable HAH1 cell line crude extract; in both cases, superimposed on the *in vitro* reference spectrum of 20 µM Cu(I)MNK1, in black. The spectra are recorded at pH 7.2 T=293.8 K.

From the spectra reported in Fig. 9, it appears that the majority of the MNK1 signals are present also in a close-to-cellular context. The disappearance of a few signals might be due to some interactions with cellular components. The two spectra differ for the presence (B) or absence (A) of the partner protein HAH1. Interestingly, the pattern of signals disappearance presents some differences between the two spectra A and B. Only the spectrum of cells containing also the partner HAH1 presents signals shifts and signal disappearances that are diagnostic of the complex formation, such as C22, G70, M69 as presented in Fig. 10:

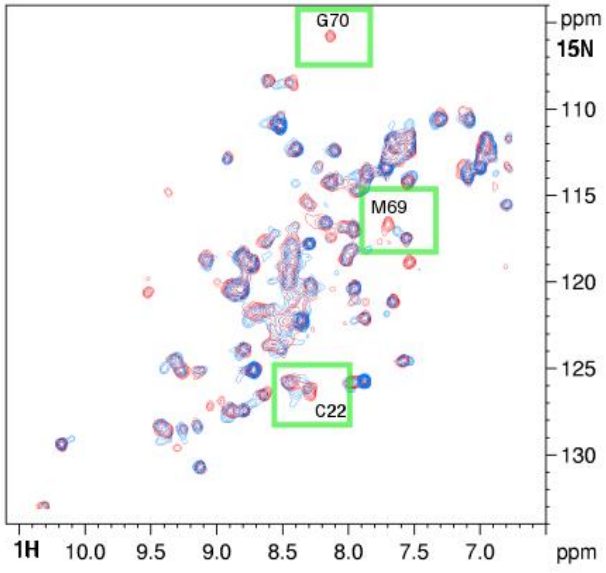

Figure 10. Superimposition of 2D ^{1}H-^{15}N SOFAST-HMQC *in lysate* NMR spectra: spectrum of 10 µM Cu(I)MNK1 in HEK293T cell crude extract in red, compared to 10 µM Cu(I)MNK1 in stable HAH1 cell line crude extract, in light blue.

This might suggest that the complex formation is possibly taking place together with interactions with unknown cellular components. Prompted by these encouraging results, we went on setting up the 'full scale' in-cell NMR sample. In Fig. 11, the spectra showing both HEK293T and stable cells expressing HAH1 electroporated with ^{15}N Cu(I)MNK1 are reported

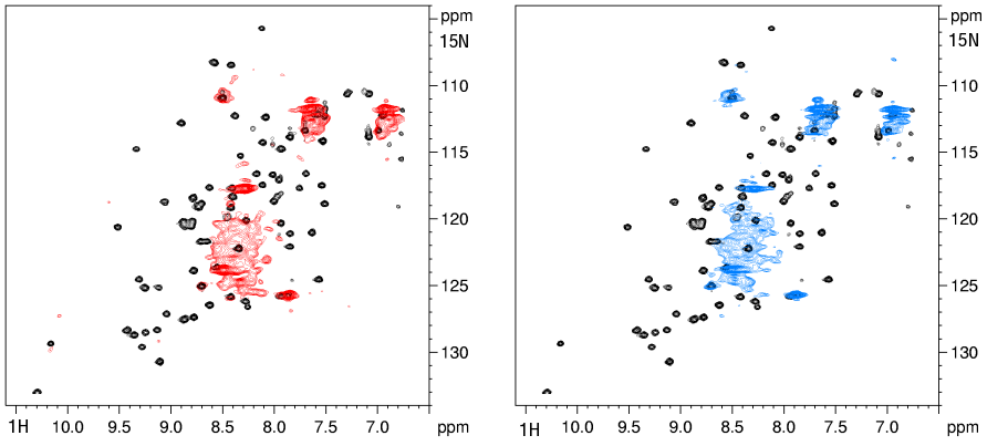

Figure 11. 2D ^{1}H-^{15}N SOFAST-HMQC *in-cell NMR*: in A) in red, delivered Cu(I)MNK1 in HEK293T cells B) in light blue, Cu(I)MNK1 in stable HAH1 cell line; in both cases, superimposed on the *in vitro* reference spectrum of 20 µM Cu(I)MNK1, in black. Spectra are recorded at pH 7.2 T=293.8K.

Almost no signals were detected in the spectra of either HEK293T cells or of the stable cell line for HAH1, except two broad peaks in the glutamine region that could arise from the ^{15}N natural abundance asparagine/glutamine in the medium. Some broad signals are observed, clustered in the region of the amide protons (around 8.3 ppm). The position and the shape of the peaks might be attributable to MNK1 in an unfolded state. Alternatively, they could arise from the ^{15}N natural abundance of the cellular background. Western blot analysis confirmed the presence of MNK1 inside the cell samples, in particular in the soluble fraction (Methods 4.7.2). Based on these results, we might speculate that the electroporation procedure itself caused an unfolding of MNK1. Such effect, likely protein-dependent, would impose some limitations to the electroporation approach, and needs to be investigated further.

3. CONCLUSIONS AND PERSPECTIVES

In this doctorate project, the in-cell NMR approach was applied to detail proteins redox state inside different cellular environments. The oxidation state and the folding of disulfide-containing proteins (human Cox17, Mia40 and SOD1) were investigated inside human and bacterial cells. Our findings showed that the glutathione redox potential of the cytoplasm cellular compartment alone does not determine the redox state of a given protein. Indeed, in human cells, co-expression of redox-regulating protein partners altered the distribution of redox states, whereas in bacterial cells, despite the less reducing environment, the absence of the disulfide reduction pathways (in Origami B cells) caused the predominance of the oxidized state of each protein. From the methodological point of view, in-cell NMR proved to be a suitable method for the non invasive direct observation of protein redox states inside living cells.

Furthermore, in-cell NMR was successfully applied to characterize the interaction of the small antioxidant molecule ebselen with disease-related SOD1 mutants inside human cells. The data obtained complemented the *in vitro* observations, and showed that ebselen facilitates the correct folding of destabilized SOD1 mutants by promoting the proper maturation pathway, inducing the disulfide bond formation and the zinc binding. Ebselen might therefore be considered a true pharmacological chaperone for SOD1. These positive effects represent a promising starting point for future SOD1-ALS drug development.

In this doctorate project, an effort to increase the applicability of in-cell NMR was undertaken in two main directions, focusing on new sample preparation

approaches.

A first direction aimed at enabling in-cell NMR investigations of those soluble proteins that experience interactions within the cells that negatively impact their relaxation properties, broadening signals beyond detection. To this aim, solid state NMR was chosen as a technique to overcome the limitations of solution in-cell NMR. The results deriving from the investigation on various proteins, diverse sample preparation and different NMR experiments highlighted several issues linked to the experimental setup, which need to be further addressed for future development. Most critical is the need of an efficient and selective protein labeling strategy, in order to distinguish the signals belonging to the protein of interest from the background arising from other cellular components. Further, our data showed that many proteins, undetectable by solution NMR, could not be detected also when investigated through MAS solid state NMR, as if they were not behaving as a “true solid”. Such need for a more solid-like sample could possibly be addressed by pursuing alternative chemical cross-linking approaches, in order to immobilize the conformation of the cellular components and of the protein of interest. Such approach would sacrifice cell viability (and lose the status of ‘NMR in living cells’) in favor of improved sample preservation and longer experimental times.

The second direction aimed at enabling the characterization by solution in-cell NMR of intracellular protein-protein interactions, through a combination of protein transfection techniques with a versatile protein delivery strategy, electroporation. From the data obtained, the electroporation procedure itself seems to have a negative effect on the protein folding state. The observed protein unfolding, which might be driven by local changes in electrostatic potential or temperature, prevented additional studies on the investigated protein system.

Further developments should focus on this adverse effect of the electroporation procedure, in order to understand its protein-dependence and to devise milder electroporation conditions.

4. METHODS

4.1. Recombinant protein production

4.1.1. Human ATP7A domain 1 (MNK1)

A culture of BL21 DE3 Rosetta pLysS transformed with the pET21 plasmid encoding his-tagged MNK1 was grown in M9 medium containing [^{15}N]ammonium sulfate at 37°C, 180 rpm. Cells were induced at OD_{600}= 0.6 with 0.5 mM Isopropil-β-D-1-tiogalattopiranoside (IPTG). Protein expression was carried on over night at 20 °C. The cells were harvested and centrifuged 20 minutes at 4500 rpm. Cell lysis was performed in 20 mM Na_2HPO_4 buffer, 0.5 M NaCl, 5 mM imidazole, pH 8 through sonication. The lysate was centrifuged at 40000 rpm for 30 minutes, and the soluble fraction was separated from the pellet. The soluble fraction was loaded on a HisTrap affinity Ni-column equilibrated with binding buffer: 20mM Na_2HPO_4, 0.5 M NaCl, 20 mM imidazole, pH 8, and washed with 20 mM Na_2HPO_4, 1 M NH_4Cl, 20 mM imidazole, pH 8. The protein was eluted in 20mM Na_2HPO_4 buffer, 0.5 M NaCl, 5 mM imidazole, 20 mM EDTA, pH 8. Cleavage of Histag was obtained by incubating overnight with Factor Xa. Cu(I) binding was performed anaerobically inside a glovebox (Coy Laboratory) filled with N_2, to preserve the copper oxidation state. Copper(I) was added to samples adding an acetonitrile solution of tetrakis(acetonitrile)copper(I) hexafluorophosphate ($[(CH_3CN)_4\ Cu]PF_6$) in the presence of 1 mM dithiothreitol.

4.1.2. Human HAH1

A culture of BL21 DE3 Gold transformed with the pET15 plasmid encoding his-tagged HAH1 was grown in M9 medium containing (either unlabeled or [^{15}N]) ammonium sulfate at 37°C, 180 rpm. Cells were induced at OD_{600}= 0.6 with 0.5mM IPTG. Protein expression was carried on for 5 hours at 37 °C. The cells were harvested and centrifuged 20 minutes at 4500 rpm. Cell lysis was performed in 20mM Na_2HPO_4 buffer, 0.5 M NaCl, 5 mM imidazole, pH 8 through sonication. The lysate was centrifuged at 40000 rpm for 30 minutes, and the soluble fraction was separated from the pellet. The soluble fraction was loaded on a HisTrap affinity Ni-column equilibrated with binding buffer: 20mM Na_2HPO_4, 0.5 M NaCl, 20 mM imidazole, pH 8, and washed with 20 mM Na_2HPO_4, 1 M NH_4Cl, 20 mM imidazole, pH 8. The protein was eluted in 20mM Na_2HPO_4 buffer, 0.5 M NaCl, 5 mM imidazole, 20 mM EDTA, pH 8. A Size-exclusion column chromatography Superdex75 16/60 in buffer Tris Buffer 20 mM, NaCl 100 mM was run.

4.2. In cell solid-state NMR sample preparation

4.2.1. Bacterial cells

4.2.1.1. SOD1

A culture of 250 mL of *E.coli* BL21 gold expressing wild type SOD1 in pET28 was grown in M9 medium containing [^{13}C]glucose and [^{15}N]ammonium sulfate. Induction was performed with 0.5 IPTG, Protein expression was carried on for 4 hours at 30°C, 180 rpm. Cell were harvested and washed twice with M9. The cell pellet was used to fill a 3.2 mm rotor to perform solid-state NMR experiments. The viability of the sample before and after the NMR experiments was tested via

plating test, none gave positive results.

4.2.1.2. Cytochrome c

A culture of 250 mL of *E.coli* BL21(DE3)C41 expressing human cytochrome c in pET21 plasmid was grown in M9 medium containing [^{13}C]glucose and [^{15}N]ammonium sulfate. The culture was grown at 30°C at 60 rpm up to OD > 1, then protein expression was induced with 0.5 mM IPTG. The cofactors Sodium 2-mercaptoethanesulfonate (MESNA) and delta-aminolevulinic acid (∂-ALA) were added together with $FeSO_4$ at the time of induction. Protein expression was then carried on for 3 days at 30°C and 60 rpm. Cell were harvested and washed twice with M9. The pellet was used to fill a 4 mm rotor to perform solid-state NMR experiments. The viability of the sample after the NMR experiments was tested via plating test but none gave positive results.

4.2.1.3. Profilin mutant M114T

The aggregation-prone profilin mutant M114T was chosen as a candidate protein to set up a deuteration protocol. Several expression tests changing growing volumes (2 mL, 4mL, 50mL) and growth temperature (25°C and 37°C) were performed on *E.coli* BL21 gold. Expression tests revealed by SDS-PAGE that the protein is mainly in the insoluble fraction and that 37°C is the eligible temperature for the higher protein overexpression, shown in Fig. 12.

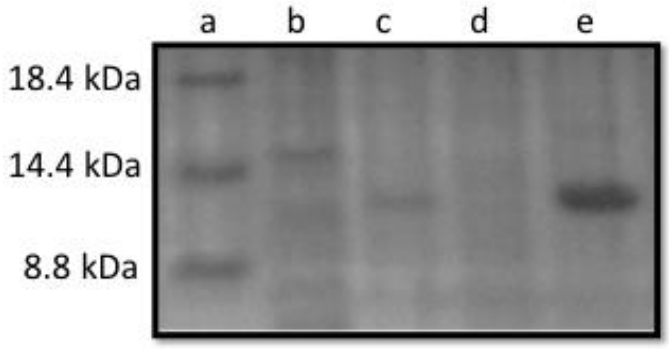

Figure 12. SDS-PAGE on gradient precast gel 4-20% Profilin mutant M114T. a) unstained protein marker; b)soluble fraction and c) insoluble fraction of , *E.coli* expressing M114T at 25°C; d) soluble fraction and e) insoluble fraction of *E.coli* expressing M114T at 37°C.

Freshly transformed colony were grown in minimal medium containing≈98% D_2O in aerated shaker at 37°C and 275 rpm. The precoltures reaching $O.D._{600}$=0.8 were selected. Cells were spun down at 2900g for 20 minutes at 4°C, washed once with fresh D_2O M9 1x and resuspended in D_2O M9 1x supplemented with antibiotics and vitamins. Induction with 0.5 mM IPTG was followed by 4 hours expression. Cell were harvested and washed once with M9. The pellet was used to fill the 3.2 mm rotor to perform solid-state NMR experiments. The viability of the sample after the NMR experiments was tested via plating test but none gave positive results.

4.2.1.4. MNK6

A culture of 250 mL of *E.coli* BL21 Rosetta pLysS expressing ATP7A sixth soluble domain (MNK6) in the pET21 was grown in M9 medium containing [^{13}C]glucose and [^{15}N]ammonium sulfate. Induction took place with 0.5 IPTG, protein expression was carried on for 4 hours at 30°C 180 rpm. Cell were harvested and washed twice with M9. The cell sample was splitted in two equal amounts, one was used to fill up the 3.2 mm rotor to perform monodimentional solid-state NMR experiments, while the other one was treated with 4% Paraformaldehyde (PFA) for 20 minutes and used to fill up the 3.2 mm rotor to perform solid-state NMR experiments. The viability of the sample after the NMR experiments was tested via plating test but none gave positive results.

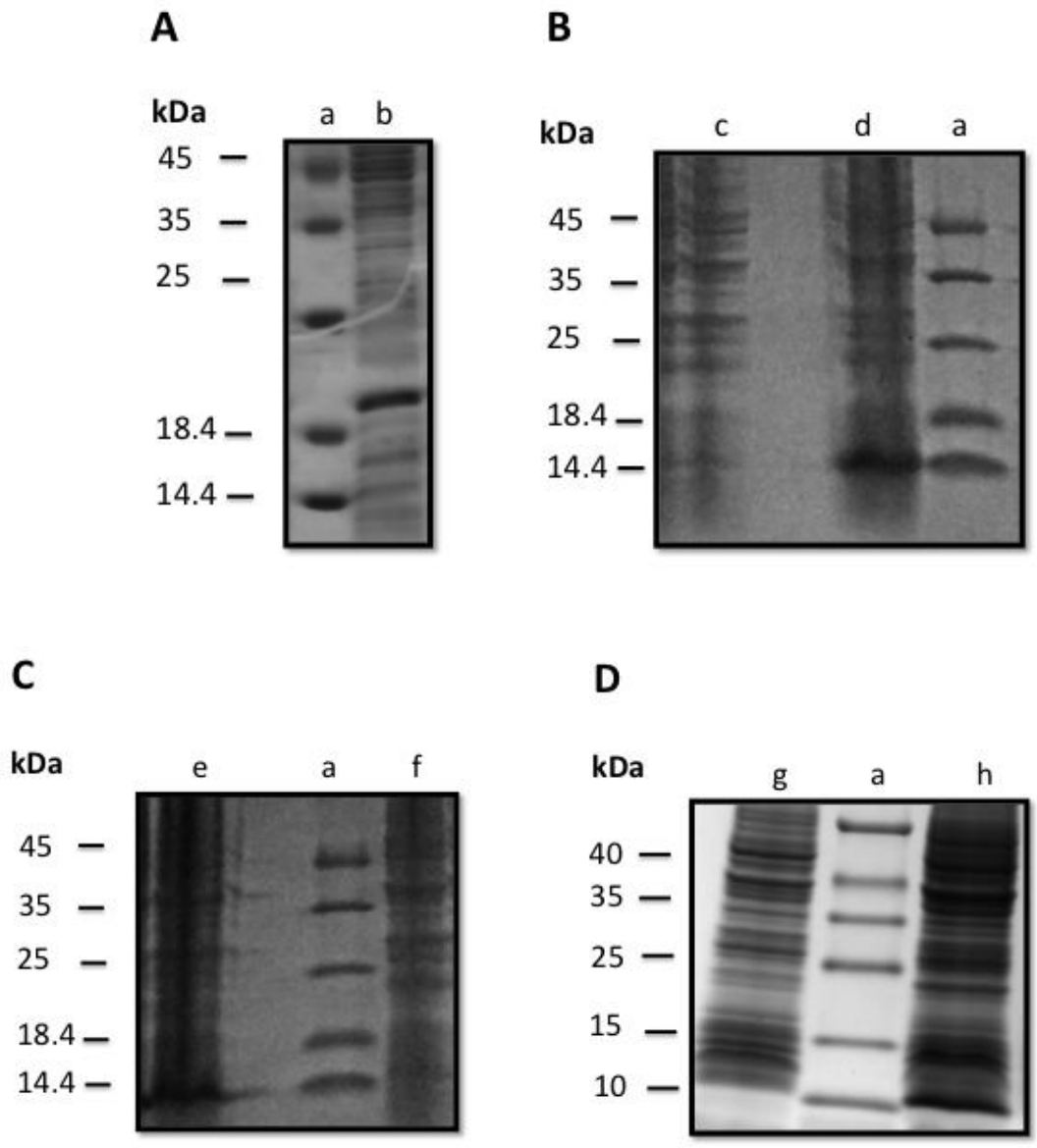

Figure 13: 4-20% gradient SDS-PAGE protein expression check on bacterial samples for solid state NMR experiments: A) in a the unstained protein marker, in b E.coli BL21 gold expressing SOD1; B) in a the unstained protein marker, in c *E.coli* BL21 C41 grown following cytochrome c expression protocol but without induction, in d *E.coli* BL21C41 expressing cytochrome c; C) in a the unstained protein marker, in e *E.coli* BL21 gold grown in ~100% D_2O expressing M114T Profilin mutant, in f *E.coli* BL21 gold grown in ~100% D_2O without induction, D) in a the unstained protein marker, in g of *E.coli* BL21 Rosetta pLysS grown following MNK6 expression protocol but without induction, in h *E.coli* BL21 Rosetta pLysS expressing MNK6.

4.3. Protein delivery sample preparation: electroporation

HEK293T cells at low passage number were prepared by seeding 2×10^6cells/flask, culturing the cells for two days in complete medium, low-glucose Dulbecco's modified Eagle medium (DMEM, Gibco), supplemented with 10% fetal bovine serum (FBS, Gibco) until 80% confluence was reached. Cells were harvested by being exposed to 0.25% trypsin/EDTA (Sigma-Aldrich) for 5 min at 37°C. Trypsin was neutralized by 5-fold dilution with complete medium. Cells were pelleted by centrifugation at 800g for 5 min at 25°C and washed with 15 mL of PBS. The number of cells was determined by a automatic cell counter TC20 (Bio-Rad). A protein electroporation mixture was prepared by diluting purified [^{15}N]-labelled Cu(I)MNK1 to a final concentration of 500 μM with sterile filtered, freshly prepared electroporation buffer (50% 100mM sodium phosphate (pH 7.0), 5 mM KCl, 15 mM $MgCl_2$,15 mM HEPES, 5 mM ATP, 5 mM reduced glutathione). 100μL of the protein electroporation mixture was added to dense cells pellet and gently mixed. The 100−200μL cell suspension was transferred into electroporation cuvettes (Lonza). Protein electroporation was performed with an Amaxa Nucleo-fector (Lonza) by using the pulse program B-28 [88]. Cells were pulsed twice while being gently mixed between pulses. Directly after electroporation, 1 mL of pre-warmed (37°C) and CO_2-saturated complete medium was added to each cuvette, the samples were transferred into cell flasks and were returned to 5% CO_2 incubators. After recovery had proceeded for 4-5 h, non-adherent cells were removed. Cultures were washed once with PBS (5 mL) and harvested by using 0.25% trypsin/EDTA for 5 min, at 37°C. Trypsin was neutralized by 5-fold dilution with complete medium, and cells were pelleted by centrifugation at 800 g for 5 min at 25°C and washed once with 1 mL of PBS. Cell pellets were resuspended in NMR buffer (Leibovitz's L-15 medium

supplemented with 10% FBS) containing 10 % D_2O. Cell suspensions were transferred into 4mm diameter Shigemi tubes (Shigemi) for NMR analysis.

4.4. In-cell NMR sample preparation: transient transfection

HEK293T cells were transiently transfected with the pHLsec plasmid containing either the gene of HAH1 or MNK1 through endocytosis mediated by branched polyethylenimine (PEI), Sigma. During protein expression, commercial DMEM medium was used to prepare unlabeled in-cell NMR samples; the expression media were supplemented with 2% FBS and antibiotics. Cells for in-cell NMR samples were collected as follows: cells from a 75 cm^2 flask were detached by trypsin treatment and suspended in one cell pellet volume of DMEM medium supplemented with 90 mM glucose, 70 mM HEPES buffer and 20% D_2O. The cell suspension was transferred to a 3 mm Shigemi tube (Shigemi); cells were spun down at the bottom of the tube. Cell viability before and after NMR experiments remained above 90%, as determined by trypan blue staining. Cleared cell lysates were prepared as follows: cells were suspended in one pellet volume of PBS buffer supplemented with 0.5 mM EDTA and 4-(2-aminoethyl)-benzenesulfonyl fluoride hydrochloride (AEBSF, Sigma) and lysed by freeze-thaw cycles with liquid N_2 and warm water. The cell lysate was centrifuged (60 min at 16000g, 4°C) and the cleared supernatant was recovered for NMR analysis in a 3 mm standard tube.

4.5. Cell sample preparation for microscopy

4.5.1. Immunocytochemistry (ICC)

Human HEK cells were seeded on coated glass coverslips and transfected with the pHLsec plasmid containing either the gene of HAH1 or MNK1 through

endocytosis mediated by branched polyethylenimine (PEI). After 48 hours expression were washed with PBS and fixed with 4% Paraformaldehyde (PFA) for 15 minutes at room temperature.

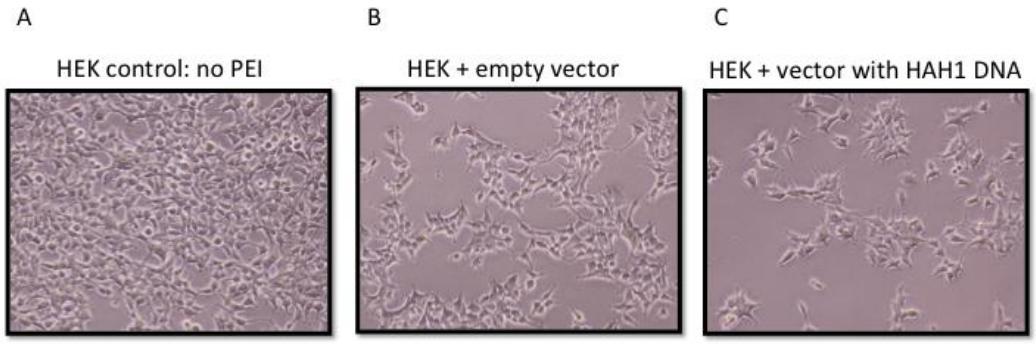

Figure 14. Optical microscopy on HEK293T cells seeded with the same concentration, upon transfection with linear PEI: A) untreated cells; B) cells transiently transfected with HAH1-containing expression vector C) cells trasiently transfected with EMPTY expression vector as a control. There is an effect of linear PEI-mediated transfection treatment that decreases cells viability not depending on the DNA vector.

For ICC staining, the cells were permeabilized using a PBS buffer containing 0.1% (v/v) Triton-X. After three washes in PBS, coverslips were blocked with blocking buffer 0.13% (v/v) of cold fish skin gelatin in PBS for one hour. Meanwhile, a dilution of primary antibody (against either HAH1 or MNK1) was made in blocking buffer, in a dilution 1:200. Coverslips were incubated for 2 hours at RT with the primary antibody, washed thrice with PBS for 5 minutes, then incubated with a 1:1000 dilution of the secondary antibody in blocking buffer (I used Atto647-coupled anti-Mouse or Atto488-coupled anti-Mouse antibodies). adding phalloidin for the actin staining. Cells were incubated with secondary antibody and phalloidin for 1 hour, in the dark. Coverslips were washed trice with PBS for 5 minutes and then incubated with 2.5 ug/mL DAPI in PBS for 5 minutes to stain the nuclei. Coverslips were washed twice with PBS and placed on a drop of ImmuMount mountant solution facing down, avoiding trapping air bubbles.

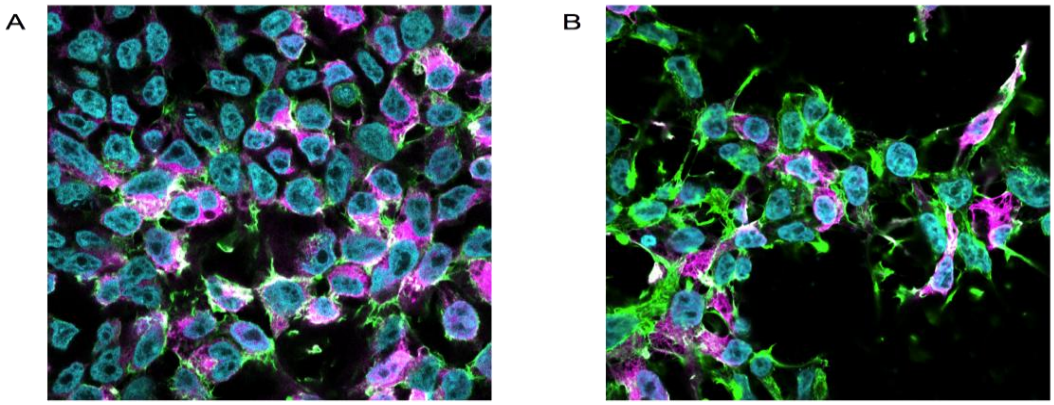

Figure 15. Confocal immages of HEK cells. In Cyan DAPI staining for nuclei, in Magenta anti-HAH1 protein selective antibody, in green Actin staining. A) H22 stable cell line overexpressing HAH1 protein; B) HEK293T PEI mediated transient transfected with HAH1-contining expression vector.

Fluorescence microscopy imaging was performed at Confocal LSM710-ConfoCor3 system and Confocal LSM780 system, Zeiss.

4.6. Polyacrylamide gel electrophoresis (PAGE)

PAGE is a method that allows the separation of biological macromolecules depending on their electrophoretic motility, which is due to their length, conformation and charge. It is frequent to treat protein samples with a denaturant (sodium dodecyl sulfate, SDS) that makes proteins motility only dependent on their length and mass-to-charge ratio. SDS is a anionic detergent able to make complexes with proteins resulting in a negative charge that are proportional to the protein mass. When exposed to an electric field, the negatively charged polypeptides migrate to the anode according to their motility. SDS-PAGE allows proteins separation according to their molecular weight. The use of a protein marker (prestained or unstained) enable to see the proteins motility in the gel and by molecular weight comparison to identify the protein of interest. The polyacrylamide gel is consituted of an acrylamide gradient in terms of pH and acrylamide concentration. Gradient gels 4-20% mini-PROTEAN® TGX™precast protein gels, BIORAD, were used. The electrophoresis buffer was 25 mM Tris,

192 mM glycine, 0.1% SDS, pH 8.3. The run took place in mini-PROTEAN® vertical electrophoresis chamber, BIORAD.

4.7. Western blot (WB)

Western Blot is a widely used semi-quantitative analytical technique that allows the identification and the study of proteins in a matrix throughout specific antibodies containing specific epitopes against the protein of interest. Firstly, are denatured and separated by size through SDS-PAGE. Secondly, proteins undergo an electrotransfer onto a membrane made of nitrocellulose or polyvinylidene (PVDF) in order to be accessible to antibody detection. A trans-Blot Turbo, BIORAD and PVDF membranes by BIORAD were used for this step. Thirdly, blocking of any non-specific binding is achieved by membrane incubation with a diluted protein solution, 5% of non fat dry milk in Tris-buffered saline (TBS), with a very small percentage of detergent, 0.005% of Tween-20 in TBS 1x. It runs 1 hour at room temperature (RT) or at 4°C overnight. Fourthly, there is a series of incubation steps with a primary antibody and then with a secondary antibody. Usually the monoclonal primary antibody incubation lasts two hours, followed by three 10-minutes washes with TBS 1x. Then, the peroxidase-coniugated secondary antibody incubation goes on for one hour at RT. There is a washing step with TBS 1x as previously and finally we have a detection and visualization step. A chemiluminescent reaction allows detecting the protein-antibody conjugates; EUROCLONE detection Kit was used. The reaction is observed at a ChemiDocTMXRS. Chemiluminescence signal intensities were quantified using ImageLab software in reference to a calibration curve obtained with recombinant protein standards. Equal sample loading was confirmed via GAPDH control.

4.7.1. Small scale electroporation

Small scale electroporation trials tested how starting with different protein concentration in the electroporation buffer affected the delivery efficiency inside HEK293T cells. In terms of protein concentration in the EP buffer, the plateau is reached when the protein is concentrated 0.5 mM and the resulting intracellular Cu(I)MNK1 uptake is around 70 µM , as shown in Fig. 16.

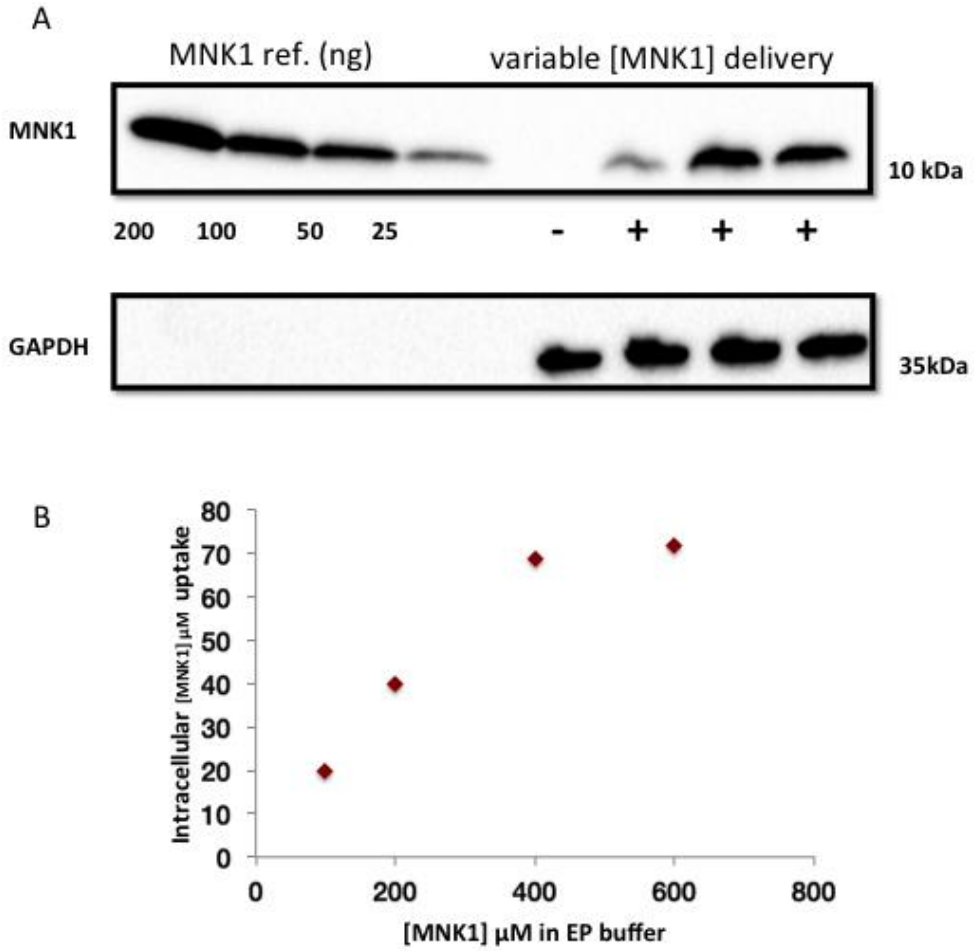

Figure 16. Studies of protein delivery in HEK293T cells with electroporation: in A) WB of protein Cu(I)MNK1 delivered varying the Cu(I)MNK1 concentration inside the electroporation buffer EP buffer (0.2 mM, 0.4 mM, 0.5mM), a non-pulsed sample named (-) as pulse effect control, GAPDH was used as a loading control and Cu(I)MNK1 purified recombinant protein as standard reference; in B) evaluation of [Cu(I)MNK1] uptake inside HEK293T cells respect to the starting concentration of Cu(I)MNK1 in the EP buffer, between 0.4mM and 0.6mM the uptake reaches a plateau.

Empirical data collected over years in Selenko lab showed that the 'effective' concentration detected inside an in-cell sample by NMR is around 10 times less than the value obtained by WB. According to these data, the in-lysate NMR trials

were tuned on the putative 'effective' MNK1 concentration, which is around 10 μM.

4.7.2. In-cell NMR sample: proteins quantification

The WB quantification of the in-cell NMR sample Cu(I)MNK1 uptake inside the cells showed that Cu(I)MNK1 concentration is 67 ±10 μM. In parallel, the quantification of HAH1 in the in-cell NMR sample with the stable cell line for HAH1 is 110 ±20 μM. Furthermore, after the in-cell NMR sample lysis, I analysed separately the soluble fraction from the pellet by WB. The majority of the delivered MNK1 was distributed in the soluble fraction.

4.7.3. HEK293T cells stably transfected with the HAH1 gene: protein quantification

WB was also used to quantify HAH1 concentration inside HEK293T cells stably transfected with the HAH1 gene. As shown in Fig. 17, the value obtained is 100±30 μM.

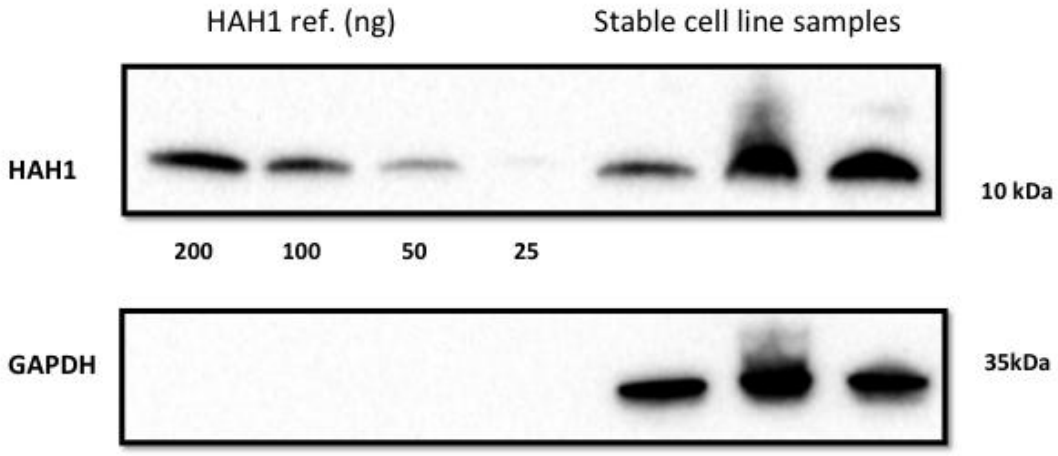

Figure 17. Protein quantification inside the stable HEK293T cell line transfected for human HAH1. WB of stable HEK293T cell line transfected for human HAH1 analysing different amount of cells. GAPDH was used as a loading control and HAH1 purified recombinant protein as standard reference.

4.8. Solution NMR experiments

NMR experiments on human cells and their lysates were acquired at a 950 MHz Bruker Avance III spectrometer equipped with a TCI CryoProbe. NMR experiments on lysates from electroporated cells were acquired at a 900 MHz Bruker Avance spectrometer equipped with a TCI Cryoprobe. 1D ^{1}H and 2D ^{1}H-^{15}N SOFAST HMQC [89] spectra were acquired at 308 K. The supernatant of each cell sample was checked in the same experimental conditions to exclude the presence of any signal arising from protein leaked out of the cells. The same NMR spectra were also acquired on the cell lysates. The total acquisition time for each cell sample was ~1 h for transiently transfected cells, ~12 h for electroporated cell lysates.

NMR experiments on thick cell lysates and electroporated cell samples were acquired at 600 MHz Bruker spectrometer equipped with a TCI CryoProbe. 1D ^{1}H and 2D ^{1}H-^{15}N SOFAST HMQC spectra were acquired at 293.8K. The total acquisition time for each cell sample was ~16 h.

In vitro NMR experiments on Cu(I)MNK1 and the Cu(I)MNK1-HAH1 complex were acquired at a 700 MHz Bruker spectrometer equipped with a TCI CryoProbe. The NMR spectra were processed with Bruker Topspin software.

4.9. Solid state NMR experiments

E. coli cells were packed into 3.2 mm and 4 mm rotors in order to perform solid state NMR experiments. The spectra were recorded on a Bruker Avance 700 MHz and on a Bruker Avance II 850 MHz wide-bore spectrometers. Standard ^{13}C-detected solid state NMR spectra were acquired at MAS frequency of 14 kHz or 11 kHz using the pulse sequences reported in the literature [75]. DCP-NCA solid state NMR spectra were acquired at MAS frequency of 14 kHz using the pulse

sequences reported in the literature [76]. The ^{1}H-^{13}C CP NOE solid state NMR spectra were acquired at MAS frequency of 14 kHz using the pulse sequences reported in the literature [78].

REFERENCES

[1] Luchinat, E., Barbieri, L., Rubino, J.T., Kozyreva, T., Cantini, F., Banci, L., "In-cell NMR reveals potential precursor of toxic species from SOD1 fALS mutants," *Nature Communications* (2014), 5:5502.

[2] Burz, D.S., Shekhtman, A., "The STINT-NMR Method for Studying In-cell Protein-Protein Interactions," *Current Protocols In Protein Science* (2010), 17–11.

[3] Banci, L., Barbieri, L., Bertini, I., Cantini, F., Luchinat, E., "In-cell NMR in *E. coli* to monitor maturation steps of hSOD1," *PLoS One* (2011), 6:e23561.

[4] Xie, J., Thapa, R., Reverdatto, S., Burz, D.S., Shekhtman, A., "Screening of small molecule interactor library by using in-cell NMR spectroscopy (SMILI-NMR)," *Journal of Medicinal Chemistry* (2009), 52:3516–3522.

[5] Ito, Y., Selenko, P., "Cellular structural biology," *Current Opinion in Structural Biology* (2010), 20:640–648.

[6] Luchinat, E., Banci, L., "In-cell NMR: a topical review," *IUCrJ* (2017), 4.2:108–118.

[7] Bertrand, K., Reverdatto, S., Burz, D.S., Zitomer, R., Shekhtman, A., "Structure of Proteins in Eukaryotic Compartments," *Journal of the American Chemical Society* (2012) 134:12798–12806.

[8] Selenko, P., Frueh, D.P., Elsaesser, S.J., Haas, W., Gygi, S.P., Wagner, G., "*In situ* observation of protein phosphorylation by high-resolution NMR spectroscopy," *Nature Structural & Molecular Biology* (2008), 15(3):321–329.

[9] Inomata, K., Ohno, A., Tochio, H., Isogai, S., Tenno, T., Nakase, I., Shirakawa, M., "High-resolution multi-dimensional NMR spectroscopy of proteins in human cells," *Nature* (2009), 458(7234):106.

[10] Ogino, S., Kubo, S., Umemoto, R., Huang, S., Nishida, N., Shimada, I., "Observation of NMR signals from proteins introduced into living mammalian cells by reversible membrane permeabilization using a pore-forming toxin, streptolysin O," *Journal of the American Chemical Society* (2009), *131*(31):10834–10835.

[11] Theillet, F.X., Binolfi, A., Bekei, B., Martorana, A., Rose, H.M., Stuiver, M., Verzini, S., Lorenz, D., van Rossum, M., Goldfarb, D., Selenko, P., "Structural disorder of monomeric alpha-synuclein persists in mammalian cells," *Nature* (2016), 530:45–50.

[12] Majumder, S., Xue, J., DeMott, C.M., Reverdatto, S., Burz, D.S., Shekhtman, A., "Probing protein quinary interactions by in-cell nuclear magnetic resonance spectroscopy," *Biochemistry* (2015), 54:2727–2738.

[13] Barbieri, L., Luchinat, E., Banci, L., "Characterization of proteins by in-cell NMR spectroscopy in cultured mammalian cells," *Nature Protocols* (2016), 11(6):1101–11.

[14] Banci, L., Barbieri, L., Bertini, I., Luchinat, E., Secci, E., Zhao, Y., Aricescu,

R., “Atomic-resolution monitoring of protein maturation in live human cells by NMR,” *Nature Chemical Biology* (2013), 9:297–299.

[15] Barbieri, L., Luchinat, E., Banci, L., “Structural insight of proteins in sub-cellular compartments: in-mitochondria NMR,” *Biochimica et Biophysica Acta* (2014), 11:2492–2496.

[16] Müntener, T., Häussinger, D., Selenko, P., Theillet, F.X., “In-Cell Protein Structure from 2D NMR Experiments,” *Journal of Physical Chemistry Letters* (2016), 21;7(14):2821–5.

[17] Pan, B.B., Yang, F., Ye, Y., Wu, Q., Li, C., Huber, T., Su, X.C., “3D structure determination of a protein in living cells using paramagnetic NMR spectroscopy,” *Chemical Communications* (2016), *52*(67):10237–10240.

[18] Renault, M., Pawsey, S., Bos, P.M., Koers, E.J., Nand, D., Tommassen-van Boxtel, R., Rosay, M., Tommassen, J., Maas, W.E., Baldus, M., “Solid-State NMR Spectroscopy on Cellular Preparations Enhanced by Dynamic Nuclear Polarization,” *Angewandte Chemie International Edition* (2012), 51:2998–3001.

[19] Brigelius-Flohé, R., Flohé, L., “Basic principles and emerging concepts in the redox control of transcription factors,” *Antioxidants & Redox Signaling* (2011), 15:2335–2381.

[20] Loi, V.V., Rossius, M., Antelmann, H., “Redox regulation by reversible protein S-thiolation in bacteria,” *Frontiers in Microbiology* (2015), 6:187.

[21] Luo, M., Zhang, J., He, H., Su, D., Chen, Q., Gross, M.L., Kelley, M.R. Georgiadis, M.M., “Characterization of the redox activity and disulfide bond formation in apurinic/apyrimidinic endonuclease,” *Biochemistry* (2012), 51(2): 695–705.

[22] Hamdane, D., Kiger, L., Dewilde, S., Green, B.N., Pesce, A., Uzan, J., Burmester, T., Hankeln, T., Bolognesi, M., Moens, L., Marden, M.C., “The redox state of the cell regulates the ligand binding affinity of human neuroglobin and cytoglobin,” *Journal of Biological Chemistry* (2003), 278:51713–51721.

[23] Gupta, N., Ragsdale, S.W., “Thiol-disulfide redox dependence of heme binding and heme ligand switching in nuclear hormone receptor rev-erb{beta},” *Journal of Biological Chemistry* (2011), 286(6):4392–4403.

[24] Kemp, M., Go, Y.M., Jones, D.P., “Nonequilibrium thermodynamics of thiol/disulfide redox systems: a perspective on redox systems biology,” *Free Radical Biology & Medicine* (2008), 44:921–937.

[25] Yoshikawa, T., Naito Y., “What is oxidative stress?” *Journal of the Japan Medical Association* (2002), 45:271–276.

[26] Del Rio, L.A., “ROS and RNS in plant physiology: an overview,” *Journal of Experimental Botany* (2015), 66:2827–2837.

[27] Giles, G.I., Tasker, K.M., Jacob, C., “Hypothesis: the role of reactive sulfur species in oxidative stress,” *Free Radical Biology & Medicine* (2001), 31:1279–1283.

[28] Zhang, A.Y., Yi, F., Jin, S., Xia, M., Chen, Q.Z., Gulbins, E., Li, P.L., “Acid sphingomyelinase and its redox amplification in formation of lipid raft redox signaling platforms in endothelial cells,” *Antioxidants & Redox Signaling*

(2007), 9:817–828.

[29] Finkel, T., “Redox-dependent signal transduction,” *FEBS Letters* (2000), 476(1–2):52–54.

[30] Storz, P., “Reactive oxygen species in tumour progression,” *Frontiers in Bioscience* (2005), 10:1881–1896.

[31] Mishra, S., Imlay, J., “Why do bacteria use so many enzymes to scavenge hydrogen peroxide?” *Archives of Biochemistry and Biophysics* (2012), 525:145–60.

[32] Sies, H., “Strategies of antioxidant defense,” *European Journal of Biochemistry* (1993), 215:213–219.

[33] Barber, S.C., Shaw, P.J., “Oxidative stress in ALS: key role in motor neuron injury and therapeutic target,” *Free Radical Biology & Medicine* (2010), 48:629–641.

[34] Berndt, C., Lillig, C.H., Flohe, L., “Redox regulation by glutathione needs enzymes,” *Frontiers in Pharmacology* (2014), 5:168.

[35] Sharma, R., Yang, Y., Sharma, A., Awasthi, S., Awasthi, Y. C. “Antioxidant role of glutathione S-transferases: protection against oxidant toxicity and regulation of stress-mediated apoptosis,” *Antioxidants & Redox Signaling* (2004), 6(2):289–300.

[36] Schafer, F.Q., Buettner, G.R., “Redox environment of the cell as viewed through the redox state of the glutathione disulfide/glutathione couple,” *Free Radical Biology & Medicine* (2001), 30(11):1191–1212.

[37] Hwang, C., Sinskey, A.J., Lodish, H.F., “Oxidized redox state of glutathione in the endoplasmic reticulum,” *Science* (1992), 257:1496–1502.

[38] Begas, P., Liedgens, L., Moseler, A., Meyer, A.J., Deponte, M., “Glutaredoxin catalysis requires two distinct glutathione interaction sites,” *Nature communications* (2017), 8:14835.

[39] Braymer, J.J., Lill, R., “Iron–sulfur cluster biogenesis and trafficking in mitochondria,” *The Journal of Biological Chemistry* (2017), 292(31):12754–12763.

[40] Lu, J., Holmgren, A., “The thioredoxin antioxidant system,” *Free Radical Biology & Medicine* (2014), 66:75–87.

[41] Holmgren, A., “Thioredoxin structure and mechanism: conformational changes on oxidation of the active-site sulfhydryls to a disulfide,” *Structure* (1995), 3:239–243.

[42] Arner, E.S., Holmgren, A., “Physiological functions of thioredoxin and thioredoxin reductase,” *European Journal of Biochemistry* (2000), 267(20):6102–6109.

[43] Mustacich, D., Powis, G., “Thioredoxin reductase,” *Biochemical Journal* (2000), 346,1–8.

[44] Banci, L., Barbieri, L., Luchinat, E., Secci, E., “Visualization of redox-controlled protein fold in living cells,” *Chemistry & Biology* (2013), 20(6):747–752.

[45] Banci, L., Bertini, I., Ciofi-Baffoni, S., Janicka A., Martinelli, M., Kozlowski, H., Palumaa, P., “A structural-dynamical characterization of human Cox17,”

The Journal of Biological Chemistry (2008), 283:7912–7920.

[46] Tsang, C.K., Liu, Y., Thomas, J., Zhang, Y., Zheng, X.F., "Superoxide dismutase 1 acts as a nuclear transcription factor to regulate oxidative stress resistance," *Nature Communications* (2014), 5:3446.

[47] Banci, L., Barbieri, L., Bertini, I., Luchinat, E., Secci, E., Zhao, Y., Aricescu, A.R., "Atomic-resolution monitoring of protein maturation in live human cells by NMR, " *Nature Chemical Biology* (2013), *9*(5):297–299.

[48] Banci, L., Bertini, I., Cantini, F., Kozyreva, T., Massagni, C., Palumaa, P., Rubino, J., Zovo, K. "Human superoxide dismutase 1 (hSOD1) maturation through interaction with human copper chaperone for SOD1 (hCCS)," *Proceedings of the National Academy of Sciences* (2012), *109*(34):13555–13560.

[49] Rosen, D. R., Siddiquef, T., Patterson, D., Figlewicz, D. A., Sapp, P., Hentatif, A., Gaston, S.M., "Mutations in Cu/Zn superoxide dismutase gene are associated with familial amyotrophic lateral sclerosis," *Nature* (1993), 362:59–62.

[50] Valentine, J.S., Doucette, P.A., Potter, S.Z., "Copper-zinc superoxide dismutase and amyotrophic lateral sclerosis," *Annual Review of Biochemistry* (2005), 74:563−593.

[51] Bruijn, L. I., Houseweart, M.K., Kato, S., Anderson, K.L., Anderson, S.D., Ohama, E., Cleveland, D. W, "Aggregation and motor neuron toxicity of an ALS-linked SOD1 mutant independent from wild-type SOD1," *Science* (1998), 281:1851–1854.

[52] Banci, L., Bertini, I., Boca, M., Girotto, S., Martinelli, M., Valentine, J.S., Vieru, M., "SOD1 and Amyotrophic Lateral Sclerosis: Mutations and Oligomerization," *PLoS One* (2008), 3:e1677.

[53] Bosco, D.A., Morfini, G., Karabacak, N.M., Song, Y., Gros-Louis, F., Pasinelli, P., Frosch, M.P. Bosco, D.A, "Wild-type and mutant SOD1 share an aberrant conformation and a common pathogenic pathway in ALS," *Nature Neuroscience* (2010), 13(11):1396–1403.

[54] Graffmo, K.S, Forsberg, K., Bergh, J., Birve, A., Zetterstrom, P., Andersen, P.M., Marklund, S.L., Brannstrom, T., "Expression of wild-type human superoxide dismutase-1 in mice causes amyotrophic lateral sclerosis," *Human Molecular Genetics* (2013), 22(1):51–60.

[55] Ding, F., Dokholyan, N.V., "Dynamical roles of metal ions and the disulfide bond in Cu, Zn superoxide dismutase folding and aggregation," *Proceedings of the National Academy of Sciences of the United States of America* (2008), 105(50):19696–19701.

[56] Teilum, K., Smith, M.H., Schulz, E., Christensen, L.C., Solomentsev, G., Oliveberg, M., Akke, M., "Transient structural distortion of metal-free Cu/Zn superoxide dismutase triggers aberrant oligomerization," *Proceedings of the National Academy of Sciences of the United States of America* (2009), 106(43):18273–18278.

[57] Banci, L., Bertini, I., Durazo, A., Girotto, S., Gralla, E. B., Martinelli, M., Whitelegge, J. P, "Metal-free superoxide dismutase forms soluble oligomers under physiological conditions: a possible general mechanism for familial ALS," *PNAS,* (2007), 104(27):11263–11267.

[58] Blokhuis, A.M., Groen, E.J.N., Koppers, M., Van Den Berg, L.H., Pasterkamp, R.J., "Protein aggregation in amyotrophic lateral sclerosis," *Acta Neuropathologica* (2013), 125:777–794.

[59] Saccon, R.A., Bunton-Stasyshyn, R.K.A., Fisher, E.M.C., Fratta, P., "Is SOD1 loss of function involved in amyotrophic lateral sclerosis?" *Brain* (2013), 136:2342–2358.

[60] Barnes, C.O., Monteith, W.B., Pielak, G.J., "Internal and global protein motion assessed with a fusion construct and in-cell NMR spectroscopy," *ChemBioChem* (2011), 12**:**390–391.

[61] Wang, Q., Zhuravleva, A., Gierasch, L.M., "Exploring weak, transient protein-protein interactions in crowded *in vivo* environments by in-cell nuclear magnetic resonance spectroscopy," *Biochemistry* (2011), 50:9225–9236.

[62] Crowley, P. B., Chow, E., Papkovskaia, T., "Protein interactions in the Escherichia coli cytosol: an impediment to in-cell NMR spectroscopy," *ChemBioChem* (2011), 12:1043–1048.

[63] Barbieri, L., Luchinat, E., Banci, L., "Protein interaction patterns in different cellular environments are revealed by in-cell NMR," *Scientific Reports* (2015), 5:1–9.

[64] Renault, M., Pawsey, S., Bos, P.M., Koers, E.J., Nand, D., Tommassen-van Boxtel, R., Rosay, M., Tommassen, J., Maas, W.E., Baldus, M., "Solid-State NMR Spectroscopy on Cellular Preparations Enhanced by Dynamic Nuclear Polarization," *Angewandte Chemie International Edition* (2012), 51:2998–3001.

[65] Reckel, S., Lopez, J.J., Lohr, F., Glaubitz, C., Dotsch, V., "In-cell Solid-State NMR as a tool to study proteins in large complexes," *ChemBioChem* (2012), 13:534–537.

[66] Huttemann, M., Pecina, P., Rainbolt, M., Sanderson, T.H., Kagan, V.E., Samavati, L., Doan, J.W., Lee, I., "The multiple functions of cytochrome c and their regulation in life and death decisions of the mammalian cell: From respiration to apoptosis," *Mitochondrion* (2011), 11:369−381.

[67] Kagan, V.E., Bayir, H., Belikova, N.A., Kapralov, A., Tyurina, Y.Y., Tyurin, V.A., Jiang, J., Stoyanovsky, D., Wipf, P., Kochanek, P.M., Borisenko, G.G., Greenberger, J.S., Shvedova, A.A., Borisenko, G., "Cytochrome c/cardiolipin relations in mitochondria: a kiss of death," *Free Radical Biology & Medicine* (2009), 46(11):1439–1453.

[68] Diekert, K., de Kroon, A.I.M., Ahting, U., Niggemeyer, B., Neupert, W., de Kruijff, B., Lill, R., "Apocytochrome *c* requires the TOM complex for translocation across the mitochondrial outer membrane," *EMBO Journal* (2001), 15 (20):5626–5635.

[69] Wang, Z.B., Li, M., Zhao, Y., Xu, J.X., "Cytochrome C is a hydrogen peroxide scavenger in mitochondria," *Protein and Peptide Letters* (2003), 10(3):247–253.

[70] Crowley, P. B., Chow, E., Papkovskaia, T., "Protein interactions in the Escherichia coli cytosol: an impediment to in-cell NMR spectroscopy," *ChemBioChem* (2011), 12:1043–1048.

[71] Yarmola, E.G., Bubb, M.R., "Profilin: emerging concepts and lingering misconceptions," *Trends in Biochemical Sciences* (2006), 31:197–205.

[72] Paavilainen, V.O., Bertling, E., Falck, S., Lappalainen, P., "Regulation of cytoskeletal dynamics by actin-monomer-binding proteins," *Trends in Cell Biology* (2004), 14:386–394.

[73] Wu, C. H., Fallini, C., Ticozzi, N., Keagle, P. J., Sapp, P. C., Piotrowska, K., Kost, J. E.., "Mutations in the profilin 1 gene cause familial amyotrophic lateral sclerosis," *Nature* (2012), 488:499–503.

[74] Boopathy, S., Silvas, T.V., Tischbein, M., Jansen, S., Shandily, S.M., Zitzewitz, J.A., Landers, L.E., Goode, B.L., Schiffer, C.A., Bosco, D.A., "Structural basis for mutation-induced destabilization of profilin 1 in ALS," *PNAS* (2015), 112(26):7984–7989.

[75] Takegoshi, K., Nakamura, S., Terao, T., "13C–1H dipolar-driven 13C–13C recoupling without 13C rf irradiation in nuclear magnetic resonance of rotating solids," *Journal of Chemical Physics* (2003), 118(5):2325–2341.

[76] Loening, N.M., Bjerring, M., Nielsen, N.C., Oschkinat, H., "A Comparison of NCO and NCA Transfer Methods for Biological Solid-State NMR Spectroscopy," *Journal of Magnetic Resonance* (2012), 214(1):81–90.

[77] Otten, R., et al. "Comprehensive and cost-effective NMR spectroscopy of methyl groups in large proteins," *Journal of the American Chemical Society* (2010), 132(9):2952–2960.

[78] Zhang, R., Mroue, K.H., Ramamoorthy, A., "Hybridizing cross-polarization with NOE or refocused-INEPT enhances the sensitivity of MAS NMR spectroscopy," *Journal of Magnetic Resonance* (2016), 266:59–66.

[79] Linder, M.C., "Biochemistry of copper," (1991), Plenum Press: New York.

[80] Harrison, M.D., Jones, C.E., Solioz, M., Dameron, C.T., "Intracellular copper routing: the role of copper chaperones," *Trends in Biochemical Sciences* (2000), 25:29–32.

[81] Vulpe, C., Levinson, B., Whitney, S., Packman, S., Gitschier, J., "Isolation of a candidate gene for Menkes disease and evidence that it encodes a copper–transporting ATPase," (1993) *Nature Genetics*, *3*(1), 7-13.

[82] Kaler, S.G., "ATP7A-related copper transport diseases: emerging concepts and future trends," *Nature Reviews Neurology* (2011), 7:15–29.

[83] Banci, L., Bertini, I., Cantini, F., Migliardi, M., Rosato, A., Wang, S., "An atomic-level investigation of the disease-causing A629P mutant of the Menkes protein, ATP7A," (2005) *Journal of Molecular Biology*, *352*(2), 409-417.

[84] Banci, L., Bertini, I., Cantini, F., Della Malva, N., Herrmann, T., Rosato, A., Wüthrich, K., "Solution structure and intermolecular interactions of the third metal-binding domain of ATP7A, the Menkes disease protein" (2006) *Journal of Biological Chemistry*, *281*(39), 29141-29147.

[85] Banci, L., Bertini, I., Cantini, F., Della Malva, N., Migliardi, M., Rosato A., "The different intermolecular interactions of the soluble copper-binding domains of the Menkes protein, ATP7A," *The Journal of Biological Chemistry*. (2007), 282(32):23140-23146.

[86] Banci, L., Bertini, I., Calderone, V., Della Malva, N., Felli, I.C., Neri, S., Pavelkova, A., Rosato, A., "Copper(I)-mediated protein-protein interactions result from suboptimal interaction surfaces," *Biochemical Journal* (2009) 422:37–42.

[87] Luchinat, E., Secci, E., Cencetti, F., Bruni, P., “Sequential protein expression and selective labeling for in-cell NMR in human cells,” *Biochimica et Biophysica Acta* (2016) 1860:527–533.

[88] Bekei, B., Rose, H.M., Herzig, M., Dose, A., Schwarzer, D., Selenko, P., “In-cell NMR in mammalian cells: part 1,” *Intrinsically Disordered Protein Analysis: Volume 1, Methods and Experimental Tools* (2012), 43–54.

[89] Schanda, P., Brutscher, B., “Very fast two-dimensional NMR spectroscopy for real-time investigation of dynamic events in proteins on the time scale of seconds,” *Journal of the American Chemical Society* (2005), 127(22):8014–8015.